

© Copyright by
Jennifer Kristin Hill
2005

PROTON TRANSPORT IN AND OUT OF HAIR BUNDLES: THE ROLES OF
PLASMA MEMBRANE CALCIUM-ADENOSINE TRIPHOSPHATASE 2W/A
AND SODIUM-PROTON EXCHANGERS 6 AND 9

by
Jennifer Kristin Hill

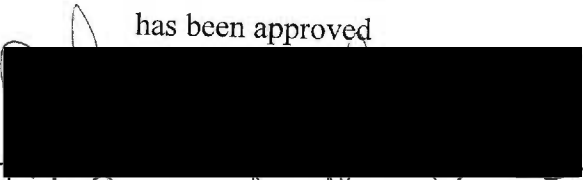
A DISSERTATION

Presented to the Program in Neuroscience
and the Oregon Health & Science University
School of Medicine
in partial fulfillment of
the requirements for the degree of
Doctor of Philosophy
April 21, 2005


School of Medicine
Oregon Health & Science University

CERTIFICATE OF APPROVAL

This is to certify that the Ph.D. dissertation of
Jennifer Kristin Hill
has been approved




Advisor




Member



Member



Member



Member

*Dedicated to Bailey,
who taught me to go for what I love
disregarding discomfort and adversity.*

CONTENTS

<u>LIST OF FIGURES</u>	<u>VI</u>
<u>LIST OF TABLES</u>	<u>IX</u>
<u>LIST OF ABBREVIATIONS</u>	<u>X</u>
<u>ACKNOWLEDGEMENTS</u>	<u>XIII</u>
<u>ABSTRACT</u>	<u>XV</u>
<u>INTRODUCTION</u>	<u>1</u>
THE INNER EAR	1
HAIR BUNDLES	12
MECHANOTRANSDUCTION	20
POTASSIUM RECYCLING	26
ADAPTATION	29
COCHLEAR AMPLIFIER	33
PLASMA-MEMBRANE Ca^{2+} -ATPASE	37
PROTON TRANSPORT	43
<u>RESEARCH OBJECTIVES</u>	<u>46</u>

<u>MATERIALS AND METHODS I</u>	47
GENERATING ANTIBODIES AGAINST PMCA2A VARIANTS	47
CONSTRUCTING PMCA2A-VARIANT EXPRESSION VECTORS	48
PREPARING MICROSOMES EXPRESSING PMCA2A VARIANTS	50
SDS-PAGE AND IMMUNOBLOTTING	51
IMMUNOFLUORESCENCE	51
CULTURING AND TRANSFECTING SENSORY EPITHELIA	53
<u>MATERIALS AND METHODS II</u>	55
HAIR-CELL ISOLATION	55
LOADING HAIR CELLS WITH PH SENSITIVE DYES	55
CONFOCAL MICROSCOPY	57
IMAGE ANALYSIS	58
PHARMACOLOGICAL MANIPULATION	59
CDNA SYNTHESIS FROM THE MOUSE INNER EAR	60
AMPLIFYING NHEs FROM THE MOUSE INNER EAR	60
CLONING MNHE6 AND MNHE9	61
GENERATING A POLYCLONAL NHE9 ANTIBODY	63
IMMUNOFLUORESCENCE	63
ANTIGENIC PEPTIDE COMPETITION	65
IMMUNOPRECIPITATION	65
FROG HAIR-BUNDLE ISOLATION	65
COS-7 CELL LYSATES	67

RAT HAIR-BUNDLE ISOLATION	68
PREPARING MICROSOMES EXPRESSING NHEs	68
SDS-PAGE AND IMMUNOBLOTTING	69
MOLECULAR WEIGHT MARKERS	70
MEMBRANE FRACTIONATION FROM MOUSE BRAIN	70
AMINO-ACID ALIGNMENTS	71
ANTIBODIES	71
ANIMALS	72
ACKNOWLEDGEMENTS FOR METHODS	72
<u>RESULTS I</u>	<u>73</u>
GENERATION OF ANTIBODIES SPECIFIC TO PMCA2 _A SPLICE A VARIANTS	73
LOCALIZATION OF PMCA2 _W IN THE RAT INNER EAR	78
EXPRESSION OF PMCA SPLICE A VARIANTS IN THE RAT INNER EAR	82
<u>DISCUSSION I</u>	<u>91</u>
ROLE OF SPLICE SITE C IN REGULATION AND TARGETING OF PMCA	91
SPLICE SITE A IS NECESSARY FOR APICAL TARGETING	91
IS SPLICE SITE A SUFFICIENT FOR APICAL TARGETING?	92
ROLE OF SPLICE SITE A IN REGULATION OF PMCA ACTIVITY	93

RESULTS II	95
PMCA ACTIVATION INCREASES HAIR BUNDLE H^+ -LOAD	95
HAIR BUNDLES AND SOMATA HAVE INDEPENDENT H^+ TRANSPORTERS	95
Na^+/H^+ EXCHANGERS ARE EXPRESSED IN THE MOUSE INNER EAR	104
PROTEIN-IMMUNOBLOT AND IMMUNOPRECIPITATION ANALYSES OF hNHE6 AND MNHE9	110
MNHE6 AND MNHE9 ARE EXPRESSED ON THE PLASMA MEMBRANE OF COS-7 CELLS	117
NHE6 IS EXPRESSED IN RAT HAIR CELLS	118
NHE6 IS EXPRESSED ON THE PLASMA MEMBRANE OF BULLFROG HAIR CELLS	118
NHE6 IS EXPRESSED IN A SUBSET OF BULLFROG HAIR BUNDLES	119
NHE9 IS EXPRESSED IN BULLFROG HAIR BUNDLES	128
NHE9 IS EXPRESSED IN RAT AUDITORY AND VESTIBULAR HAIR CELLS	129
DISCUSSION II	144
PMCA ACTIVITY ACIDIFIES HAIR BUNDLES	147
NHE6 AND NHE9 ARE CANDIDATES FOR THE HAIR BUNDLE H^+ TRANSPORTER	148
NHE9 IS LOCALIZED TO BULLFROG SACCULAR HAIR BUNDLES	149
NHE9 IS EXPRESSED IN RAT AUDITORY AND VESTIBULAR ORGANS	150
SDS-PAGE ANALYSIS OF NHE ISOFORMS: GLYCOSYLATION AND AGGREGATION	151

CATION SELECTIVITY OF NHE9	152
USING PHARMACOLOGICAL MANIPULATIONS TO IDENTIFY THE BUNDLE H^+ TRANSPORTER	153
<u>SUMMARY AND CONCLUSIONS</u>	<u>156</u>
<u>OPEN QUESTIONS</u>	<u>158</u>
CHARACTERIZATION OF HAIR BUNDLE PMCA2w/A IN RODENT HAIR BUNDLES	158
CHARACTERIZATION OF Na^+/H^+ EXCHANGER 9	162
<u>REFERENCES</u>	<u>164</u>

LIST OF FIGURES

FIGURE 1.	THE MAMMALIAN INNER EAR.....	3
FIGURE 2.	ANATOMY OF THE EAR.....	5
FIGURE 3.	GUINEA PIG ORGAN OF CORTI	8
FIGURE 4.	BULLFROG SACculus	10
FIGURE 5.	MAMMALIAN CRISTA AMPULLARIS	12
FIGURE 6.	BULLFROG HAIR CELL	15
FIGURE 7.	HAIR CELLS FROM MOUSE, BULLFROG, AND GUINEA PIG.....	17
FIGURE 8.	HAIR BUNDLE STRUCTURE	19
FIGURE 9.	GATING-SPRING MODEL OF HAIR CELL MECHANOTRANSDUCTION.....	22
FIGURE 10.	TIP LINKS	25
FIGURE 11.	MODEL OF THE HYPOTHETICAL HAIR-CELL TRANSDUCTION APPARATUS.....	28
FIGURE 12.	MODEL OF SLOW ADAPTATION	32
FIGURE 13.	TWO COMPONENTS OF ADAPTATION	35
FIGURE 14.	SCHEMATIC OF PMCA2	40
FIGURE 15.	SPLICE SITE A VARIANTS OF PMCA2	75
FIGURE 16.	IMMUNODETECTION WITH PMCA2W-SPECIFIC ANTIBODY	77
FIGURE 17.	LOCALIZATION OF PMCA2W IN RAT ORGAN OF CORTI BY IMMUNOFLUORESCENCE	80
FIGURE 18.	LOCALIZATION OF PMCA2W IN RAT VESTIBULAR ORGANS BY IMMUNOFLUORESCENCE	82
FIGURE 19.	EXPRESSION OF PMCA2W/A-C8 IN RAT HAIR BUNDLES FOLLOWING GENE GUN TRANSFECTION	86

FIGURE 20.	EXPRESSION OF PMCA2x/A-C8 IN RAT VESTIBULAR HAIR CELLS FOLLOWING GENE GUN TRANSFECTION	88
FIGURE 21.	EXPRESSION OF PMCA2z/A-C8 IN BASOLATERAL MEMBRANES OF RAT VESTIBULAR HAIR CELLS FOLLOWING GENE GUN TRANSFECTION.....	90
FIGURE 22.	DETECTION OF pH CHANGES IN HAIR CELLS WITH SNAFL-CALCEIN	97
FIGURE 23.	DETECTION OF pH CHANGES IN HAIR CELLS WITH SNARF-5F	100
FIGURE 24.	SUMMARY OF pH RECOVERY RATES IN BUNDLES AND SOMATA	102
FIGURE 25.	ALIGNMENT OF AMINO-ACID SEQUENCE OF MOUSE NHE ISOFORMS	106
FIGURE 26.	EXPRESSION OF NHE ISOFORMS IN THE MOUSE INNER EAR	110
FIGURE 27.	CHARACTERIZATION OF NHE6 ANTIBODY	114
FIGURE 28.	CHARACTERIZATION OF NHE9 ANTIBODY	116
FIGURE 29.	IMMUNOPRECIPITATION OF NHE6 FROM BULLFROG SACculI	121
FIGURE 30.	LOCALIZATION OF NHE6 IN BULLFROG SACculUS BY IMMUNOFLOURESCENCE	123
FIGURE 31.	NHE6 EXPRESSION IN ISOLATED BULLFROG SACculAR HAIR CELLS	126
FIGURE 32.	NHE6 COLOCALIZES WITH PMCA2 AND CALRETININ.....	128
FIGURE 33.	COLOCALIZATION OF NHE9 AND PMCA IN BULLFROG SACculUS BY IMMUNOFLOURESCENCE	131
FIGURE 34.	NHE9 EXPRESSION IN ISOLATED BULLFROG SACculAR HAIR CELLS	133
FIGURE 35.	ANTIGEN COMPETITION OF NHE9 LABELING IN ISOLATED BULLFROG SACculAR HAIR CELLS	135

FIGURE 36.	LOCALIZATION OF NHE9 IN RAT ORGAN OF CORTI BY IMMUNOFLUORESCENCE	138
FIGURE 37.	ANTIGEN COMPETITION OF NHE9 LABELING IN RAT ORGAN OF CORTI.....	140
FIGURE 38.	LOCALIZATION OF NHE9 IN RAT VESTIBULAR ORGANS BY IMMUNOFLUORESCENCE	142
FIGURE 39.	ANTIGEN COMPETITION OF NHE9 LABELING IN RAT VESTIBULAR ORGANS	144
FIGURE 40.	MODEL FOR THE REGULATION OF ION FLUX IN HAIR CELLS	147
FIGURE 41.	PMCA2W/A TRANSGENIC CONSTRUCT	160

LIST OF TABLES

TABLE 1.	PRIMERS FOR GENERATING PMCA2A SPICE REGION A VARIANTS	49
TABLE 2.	IONIC COMPOSITION OF SOLUTIONS.....	56
TABLE 3.	PRIMERS FOR AMPLIFYING Na^+/H^+ EXCHANGERS	62
TABLE 4.	PERCENT SIMILARITY OF MOUSE NHE ISOFORMS	108
TABLE 5.	PHARMACOLOGICAL MANIPULATIONS FOR ASSAYING PH RECOVERY IN HAIR BUNDLES	155

LIST OF ABBREVIATIONS

aa	amino acid
ATP	adenosine triphosphate
ATPase	adenosine triphosphatase
BCA	bicinchoninic acid assay
β_{int}	intrinsic buffering capacity
bp	base pair (nucleotides)
CAPS	3-cyclohexylamino)-1-propane sulfonic acid
DEG	degenerins
DIDS	4,4'-diisothiocyanatostilbene-2,2'-disulfonic acid
Dm	<i>Drosophila melanogaster</i>
DM	n-dodecyl- β -D-maltoside
DMEM	Dulbecco's Modified Eagles' Medium
DMSO	dimethylsulfoxide
DTT	dithiothreitol
EDTA	ethylenediaminetetraacetic acid
EGFP	enhanced green fluorescent protein
EGTA	ethyleneglycol-bis(2-aminoethylether)- <i>N,N,N',N'</i> -tetraacetic acid
ENaC	epithelial sodium channel
FITC	fluorescein isothiocyanate
HEPES	N-(2-Hydroxyethyl)piperazine-N'-(2-ethanesulfonic acid)
HRP	horseradish peroxidase
hr	hour
HS	HEPES/sucrose solution

IC ₅₀	half-maximal inhibitory concentration
IgG	immunoglobulin gamma
IP	immunoprecipitation
kDa	kilodalton
k_{recover}	rate of recovery
LM	light membranes
MDCK	Madin-Darby canine kidney cells, a polarized epithelial cell
MEM	Minimum Essential Medium
MES	(2-[N-morpholino]ethanesulfonic acid) hydrate
Mohm	megaohm
min	minute
NDS	normal donkey serum
NHE	sodium-proton exchanger
NHS-PEO ₄ -Biotin	polyethylene oxide- <i>N</i> -hydroxysuccinimidobiotin
NMDG ⁺	<i>N</i> -methyl-D-glucamine
PAGE	polyacrylamide gel eletrophoresis
PAO	phenylarsine oxide
PBS	phosphate buffered saline
pH	log of hydrogen ion concentration
PIP ₂	phosphotidylinositol-4,5-bisphosphate
PMCA	plasma membrane calcium adenosine triphosphatase
PMSF	phenylmethysulfonyl fluoride
PVDF	polyvinylidene difluoride
RT-PCR	reverse transcription-polymerase chain reaction

s	second
SDS	sodium dodecyl sulfate
SNAFL-calcein	seminaphthorfluorescein-calcein
SNARF-5F	5-(and-6)-carboxylic acid seminaaphthorhodamine-5F
TRITC	tetramethylrhodamine B isothiocyanate
TRP	transient receptor potential
VDCC	voltage dependent calcium channel
vol	volume

PMCA isoforms are designated as the splice site A isoform ("v", "w", "x", "y", or "z") followed by the splice site C form ("a", "b", or "c"); for example PMCA2w/a.

ACKNOWLEDGEMENTS

Graduate school has been a long, but very fun and always fascinating adventure. I could not have survived without the friends and family who gave me intellectual and emotional support throughout the entire journey.

Foremost, this thesis would not have been possible without the assistance and guidance of my advisor, Dr. Peter Gillespie. I thank Peter for his patience and allowing me to pursue my own way. His excitement and enthusiasm for understanding hair cell function is inspiring and I appreciate the opportunity to have worked with such an elegant system.

I am indebted to Dr. Meredith LeMasurier, a wonderful mentor and friend. Meredith and I spent countless hours discussing ideas and experiments from which came several of the ideas and experiments presented here. I thank her for invaluable technical assistance (in and out of the lab). I am also grateful to her for critically reading and editing this dissertation. Thank you to Dr. Kevin Nusser, because he understands that some months it is harder to get motivated. The lab would have definitely been far less interesting without Kevin. I have appreciated all the trivia we shared and breathed a sigh of relief to find that Richard Dawson isn't dead. I would also like to thank Diane Ronan for generously dispensing advice and help when needed.

I want to thank members of my thesis committee, Drs. Ed McCleskey, Larry Trussell, and Gary Banker, for their thoughtful comments and advice on my research. I also thank Dr. John Brigande for taking an interest in my work and agreeing to sit on my examining committee.

A special thank you to Tonya Dailey, my friend since elementary school, for being a wonderful cheerleader and keeping me in touch with life outside the lab.

My appreciation goes to, my parents, Dorothy and Robert, for their support, encouragement, and love, and to my brothers Jeff and Jason, who know well the trials, tribulations, and joys of searching for your path. I am grateful to Alana for her support and to my brothers Taylor and Aidan for making sure I have stayed plugged in and have always had an escape plan.

Finally, the encouragement, understanding, and love of my fiancé, Ben, has been invaluable. You have brought much joy and laughter, and oh yes lots of cat hair into my life. The future holds many more adventures and I am excited to be sharing them with you.

ABSTRACT

The concentration of Ca^{2+} , a ubiquitous regulatory ion, must be strictly controlled to ensure appropriate signaling and cellular function in many systems. Hair cells rely on Ca^{2+} for proper hair-bundle function, such as control of adaptation and high-frequency hair-bundle twitches, possibly a manifestation of signal amplification. Plasma membrane calcium-ATPase (PMCA), an obligatory $\text{Ca}^{2+}/\text{H}^{+}$ anti-porter, plays a dominant role in Ca^{2+} regulation in the hair bundle. Several spontaneous and engineered mutations in PMCA2 suggest a critical role for this Ca^{2+} pump in hearing and balance (Kozel et al., 1998; Street et al., 1998; Takahashi and Kitamura, 1999). Because PMCA2 is highly expressed in vestibular and cochlear hair bundles (Crouch and Schulte, 1995; Yamoah et al., 1998; Dumont et al., 2001) and is critical for normal function of the inner ear, understanding its regulation and the consequences of its activity in the hair bundle is an important contribution to characterizing components of hair cell transduction.

To determine conclusively the specific bundle isoform of PMCA2a in rat hair cells, we examined the expression of splicing region A variants using immunohistochemistry and gene gun transfection. These results have allowed us to define a targeting sequence in PMCA2a necessary for hair bundle localization: the “w” sequence, which is created by alternative splicing at region A. Hair bundles of rat auditory and vestibular organs were exclusively labeled with a “w”-specific antibody. Transfected auditory and vestibular hair cells show strong bundle expression of epitope-tagged PMCA2w/a; by contrast, PMCA2z/a was targeted to the basolateral plasma membrane and PMCA2x/a was present on intracellular membranes. Together these data confirm that PMCA2w/a is the bundle isoform of PMCA in rat hair cells.

In the hair bundle, which has a large surface-volume ratio, a significant consequence of activating a $\text{Ca}^{2+}/\text{H}^{+}$ exchanger such as PMCA is quick acidification of the bundle. Although the bundle may buffer and immediately blunt the rapid decline in pH, H^{+} extrusion mechanisms must provide tighter control of pH homeostasis. We examined hair cell acidification in order to identify if the bundle allows H^{+} to diffuse to the soma or if there is a H^{+} transporter expressed in the hair bundle.

Using the standard NH_4Cl -pulse method for H^{+} loading, we compared bundle and soma responses to increases in H^{+} . We observed different behaviors for H^{+} extrusion in the soma and bundle when extracellular Na^{+} was removed. Although the soma pH recovered extremely slowly ($k_{\text{recover}} = 0.04 \pm 0.01 \text{ mM s}^{-1}$), the pH of the hair bundle quickly returned to the resting value ($k_{\text{recover}} = 0.90 \pm 0.04 \text{ mM s}^{-1}$). These results are consistent with a classic $\text{Na}^{+}/\text{H}^{+}$ exchanger acting as the primary H^{+} extruder of hair-cell somata and inconsistent with such exchanger function in the bundle, where the lack of a transmembrane Na^{+} gradient at the hair bundle precludes a Na^{+} -dependent transport mechanism.

The organellar subgroup of $\text{Na}^{+}/\text{H}^{+}$ exchangers (NHE, isoforms 6-9) can use K^{+} to drive H^{+} extrusion (Numata and Orłowski, 2001), making them viable candidates for a bundle H^{+} extruder. Two members of this class of NHEs were localized to hair bundles by immunodetection. We found robust NHE6 immunolabeling in the apical region of isolated bullfrog saccular hair cells, as well as in hair bundles in a subset of hair cells in the intact saccular epithelium. By contrast, NHE9 immunoreactivity is seen in all hair bundles of the intact saccular epithelium and isolated hair cells; moreover, NHE9 colocalizes with PMCA immunoreactivity. We propose that NHE9, and possibly NHE6 in some hair cells, mediates $\text{K}^{+}/\text{H}^{+}$ exchange to respond to the H^{+} load arising as a consequence of hair bundle PMCA activity.

INTRODUCTION

The Inner Ear

Our ability to communicate and maintain a sense of balance stems from the incessant activity of six tiny organs residing within the temporal bone. The fluid-filled membranous labyrinth comprises the coiled auditory organ, called the cochlea, and five vestibular organs. These vestibular organs are the sacculus, which detects vertical acceleration; the utricle, which detects horizontal acceleration; and three ampullae of the semi-circular canals, which are sensitive to angular accelerations about mutually perpendicular axes (Figure 1).

The cochlea is a spiral tube divided into three fluid-filled compartments, the scala vestibuli, scala media, and scala tympani. The scala media is separated from the scala vestibuli above by Reissner's membrane, and from the scala tympani below by the basilar membrane. Sound is transmitted through the vibrations of the middle ear ossicles to the oval window of the scala vestibuli; fluid is displaced to the round window of the scala tympani, eliciting a displacement of the basilar membrane and stimulating the organ of Corti within the scala media (Figure 2). The organ of Corti is comprised of four parallel rows of mechanoreceptive hair cells, tonotopically arranged along the length of the cochlea, with high frequency hair cells at the base and low frequency hair cells at the apex. There are three rows of outer hair cells, primarily endowed with efferent innervation, which are essential for signal amplification; in addition, there is a single row

Figure 1. The mammalian inner ear. A diagram of the membranous labyrinth from a mammalian ear showing three semicircular canals, the utricle, the saccule, and the cochlea (from Fain, 2003).

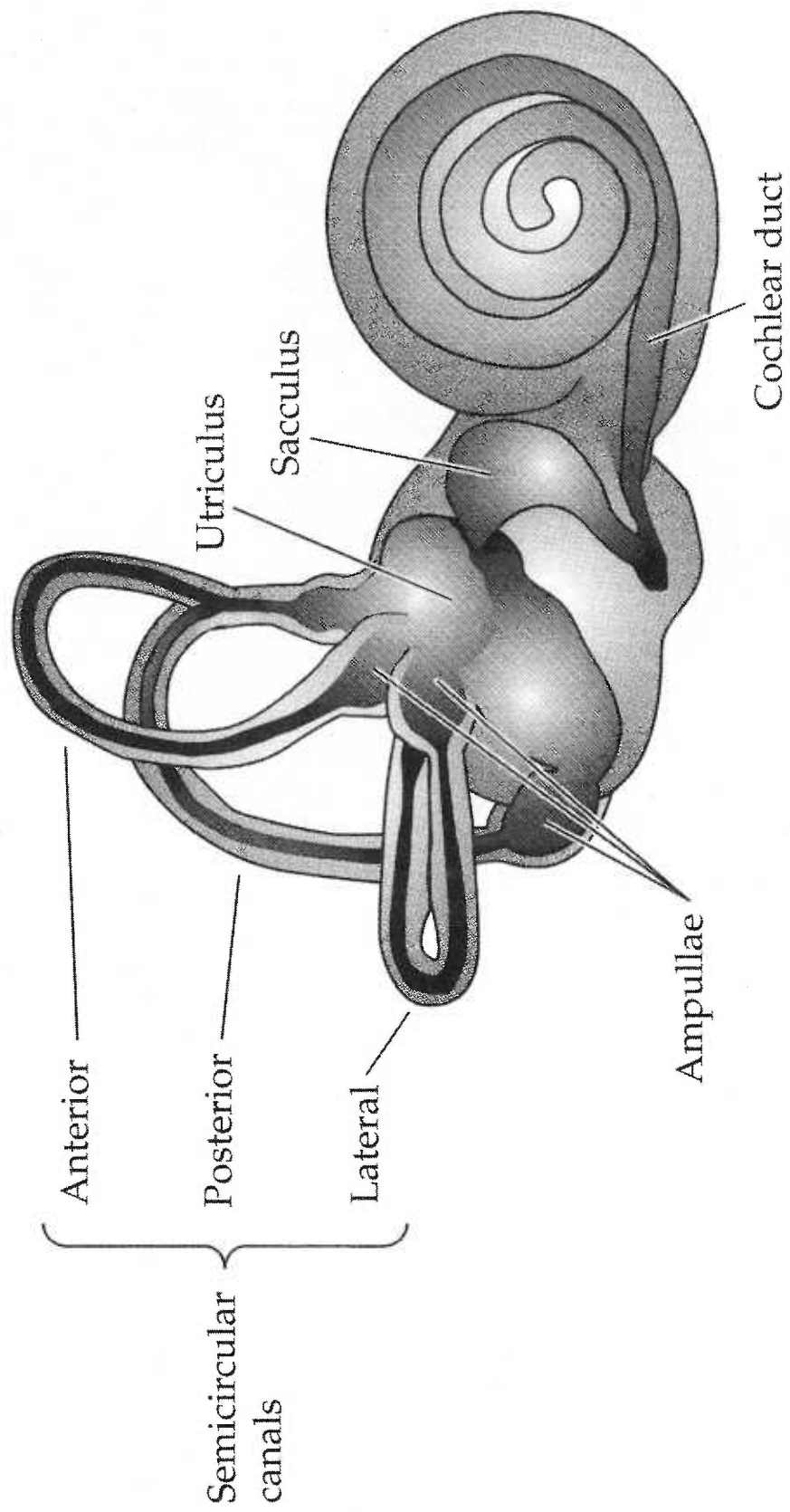
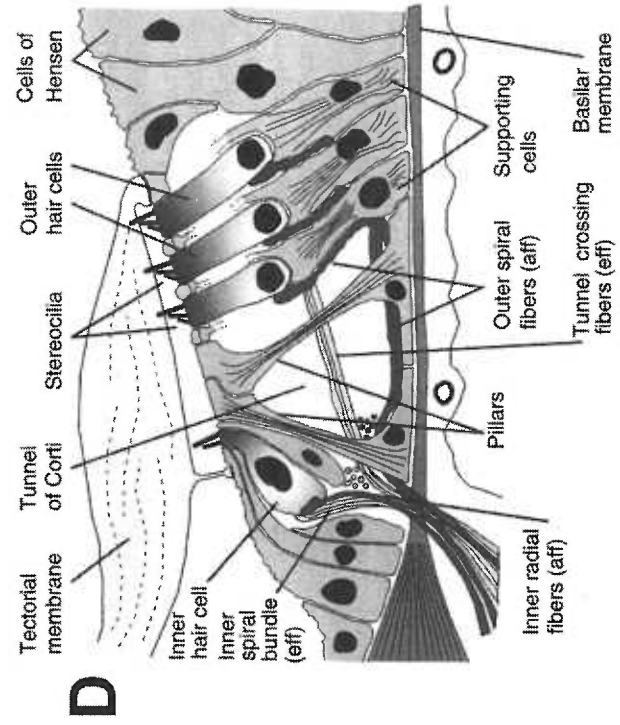
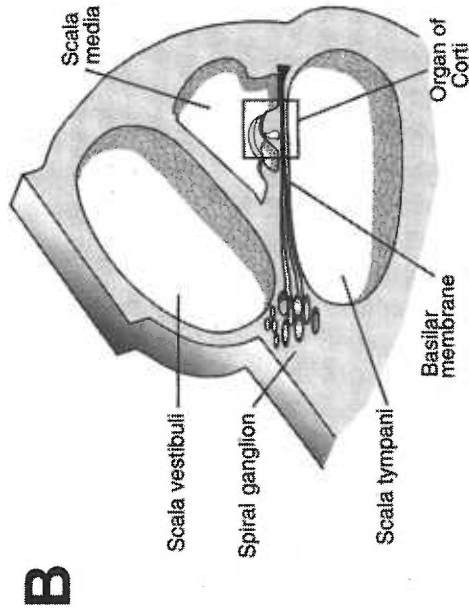
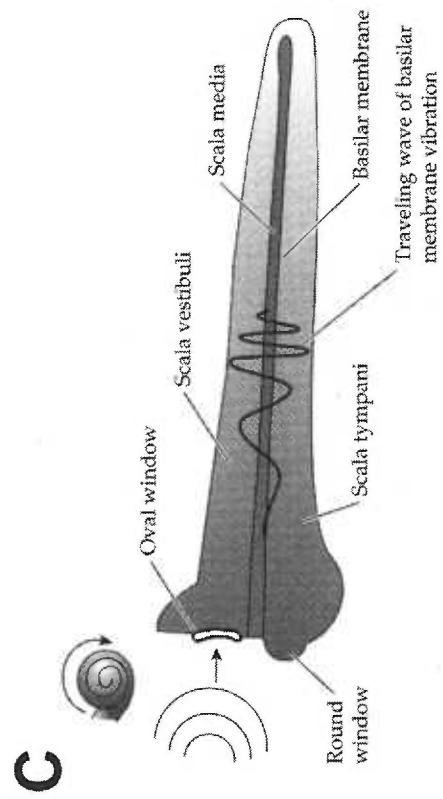
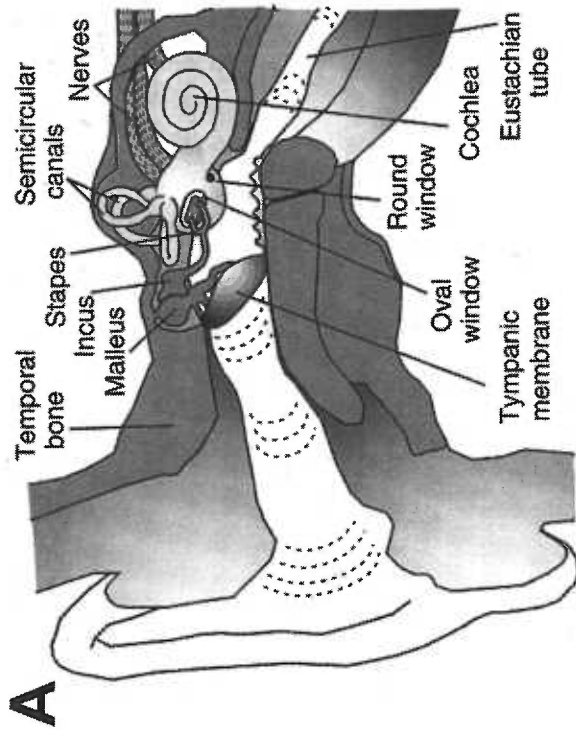


Figure 2. Anatomy of the inner ear. *A*, Sound vibrations are transmitted to the fluid-filled inner ear by the vibrations of the ossicles (malleus, incus, and stapes). *B*, Cross-section through the cochlea. The cochlea is divided into three chambers, the scala vestibuli, scala media, and scala tympani. The sensory receptors are located in the organ of Corti, which rests on the basilar membrane. *C*, The cochlea uncoiled illustrating the motion of the basilar membrane from base to apex. The vibrations of the ossicles apply pressure on the oval window, which is translated through the fluids of the scala vestibuli and scala tympani to the round window, producing a traveling wave of basilar membrane oscillation. *D*, three rows of outer hair cells and a single row of inner hair cells reside in the organ of Corti. The bundles of outer hair cells are embedded in the overlying tectorial membrane and are stimulated when basilar membrane oscillations cause the hair cells to move relative to the tectorial membrane. Inner hair cells are predominantly innervated by afferent radial fibers, whereas outer hair cells are contacted primarily by efferent fibers. Pillar cells provide structural rigidity to the organ of Corti (from Fain, 1999).



of inner hair cells, which have nearly all of the afferent innervation in the cochlea and whose primary function is to relay sensory information to the brain (Figures 2 & 3). Outer hair cells are mechanically coupled to the tectorial membrane, an acellular membrane that drapes over the organ of Corti. Displacement of the basilar membrane by fluid movement in the scala tympani causes a shearing between the tectorial membrane and the organ of Corti, which stimulates the outer hair cells. This stimulus is then transferred via fluid coupling to excitation of the inner hair cells (Figure 2).

The sacculus registers acceleration in the vertical plane. In the bullfrog, a common model used for hair cell research, the sacculus is most sensitive to the low frequencies of ground-borne vibrations (Koyama et al., 1982). The bullfrog sacculus has approximately 3000 hair cells (Hudspeth and Jacobs, 1979; Figure 4), which are coupled to an overlying otolithic membrane, upon which lie calcium carbonate crystals known as otoconia (Marmo et al., 1983). An acceleration of the head deflects the dense otoconia, causing the otolithic membrane to move and subsequently stimulates the sensory hair cells. The utricle is very similar to the sacculus, oriented in the head such that utricular hair cells are sensitive to motion in the horizontal plane.

The three semicircular canals register angular accelerations in three orthogonal planes. The ampulla is an enlarged area of the canal, which houses the crista ampullaris, a ridge of tissue where the hair cells are located. The hair cells are embedded in an overlying gelatinous mass called the cupula. Angular acceleration moves fluid within the semicircular canal leading to a deflection of the cupula and stimulating the hair cells (Rusch and Thurm, 1989; Figure 5).

Figure 3. Guinea pig organ of Corti. Scanning electron micrograph of a section from a guinea pig organ of Corti showing a single row of inner hair cells (IHC) and three rows of outer hair cells (OHC). Also shown are pillar cells (IP) and Deiter's cells (D), another type of supporting cell (from Stopp, 1983).

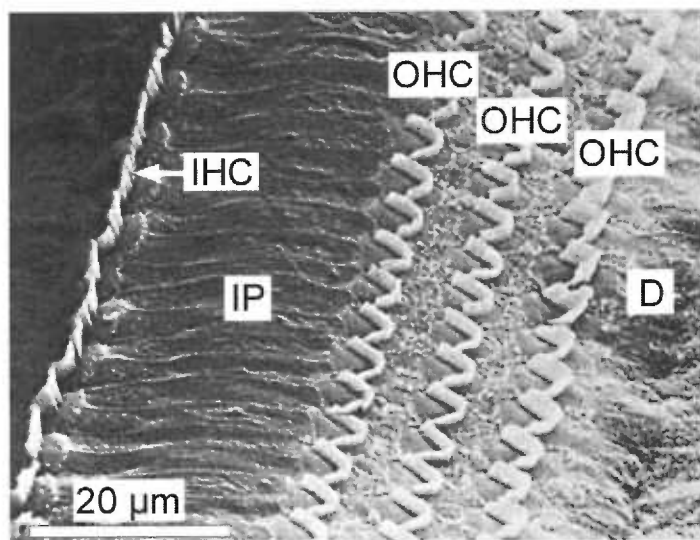


Figure 4. Bullfrog sacculus. Scanning electron micrograph of a bullfrog sacculus. The kidney shaped sensory epithelium consists of ~3,000 one hair cells. Each bright spot represents one hair bundle, which in turn comprises ~50 stereocilia and one kinocilium. The large particles seen at the periphery are clusters of the calcium carbonate crystals called otoconia (from Jacobs and Hudspeth, 1990).

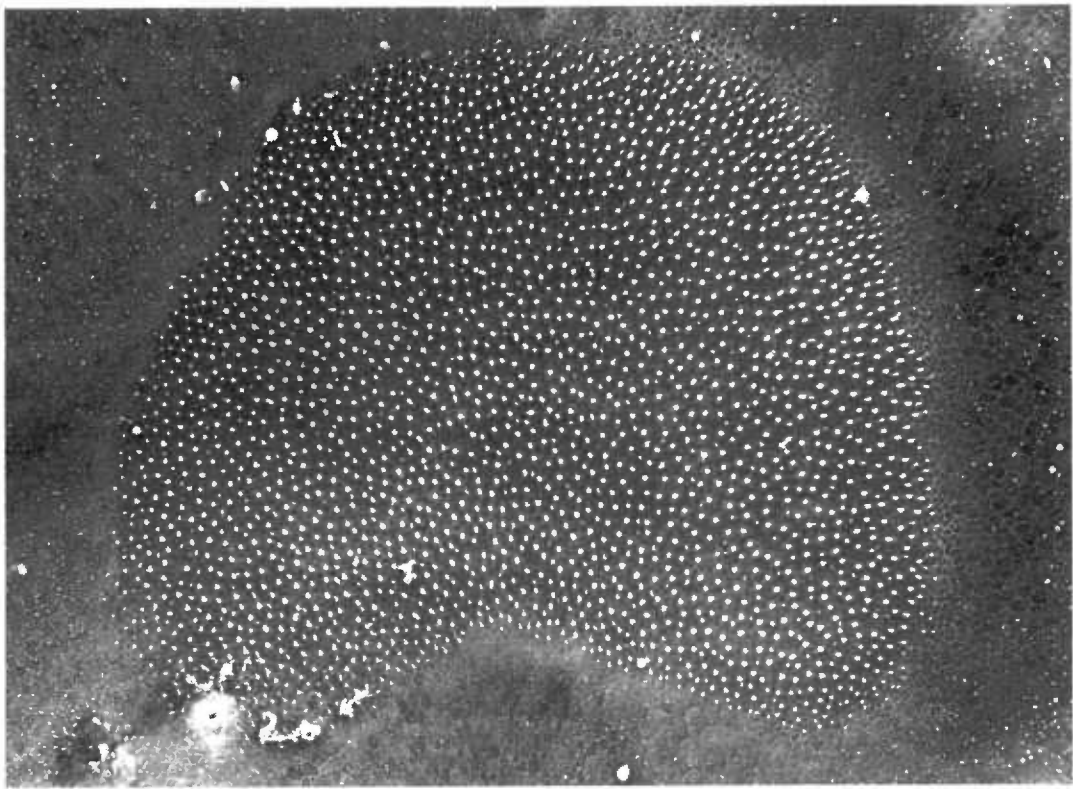
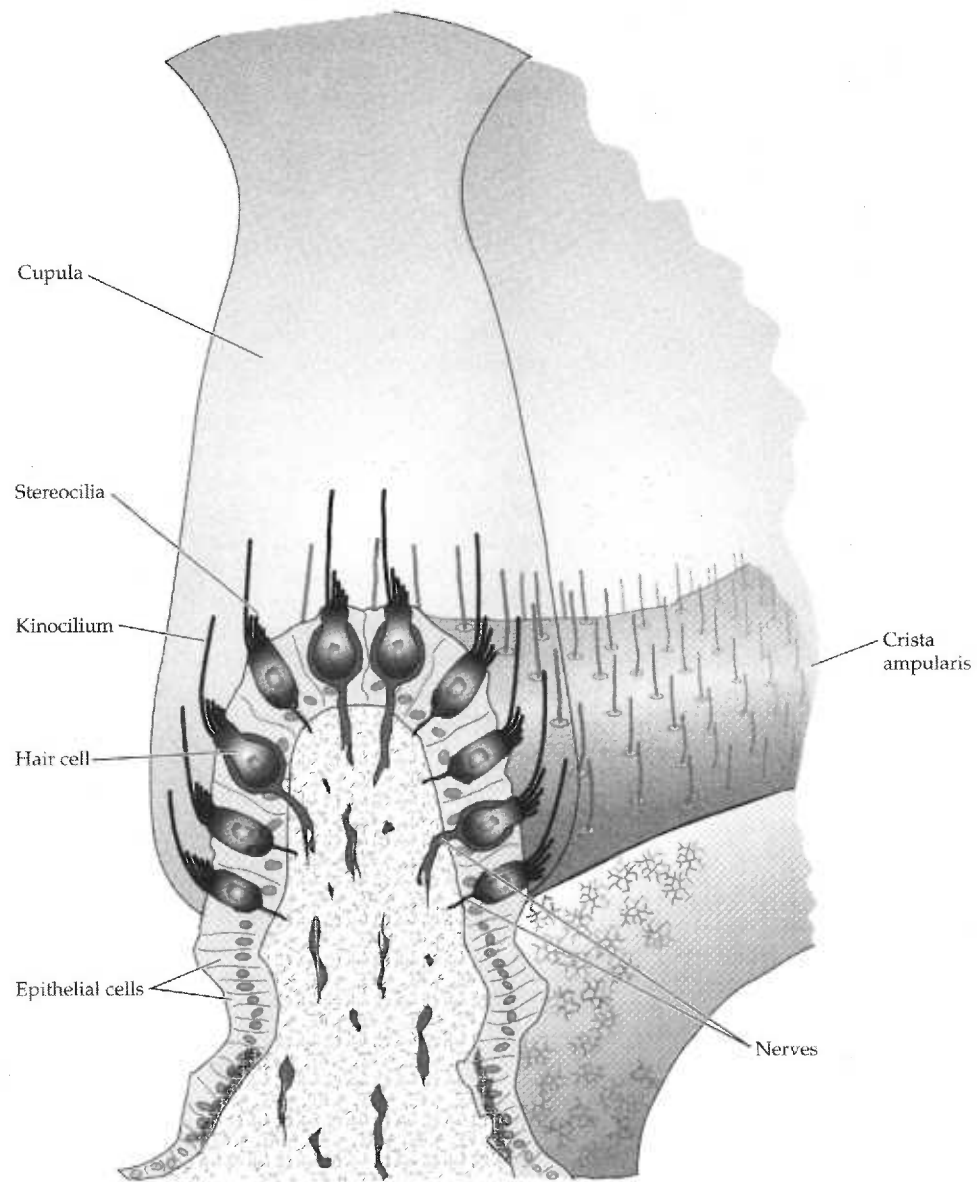


Figure 5. Mammalian crista ampullaris. Hair cells reside on a ridge within the ampulla called the crista. The stereocilia of these hair cells are embedded within the gelatinous cupula and are stimulated when fluid in the semicircular canal presses against the cupula (from Fain, 2003).



Hair Bundles

Hair cells of the auditory and vestibular systems are a complex yet elegant factory, charged with the duty of converting the slightest mechanical stimulation into an electrical signal that we detect as sound or movement. They owe their name to the shock of hair-like stereocilia that crowns each cell (Figure 6). This actin-filled array of stereocilia is the mechanosensitive hair bundle, an impressively sensitive organelle that is responsive to minute mechanical deflections (~ 0.3 nm; reviewed in Hudspeth and Gillespie, 1994). Although hair bundles vary widely among species and within each sensory organ, in general they consist of 10s-100s of stereocilia arranged in ascending height and a single true cilium, the kinocilium, which is posited to play a role in proper patterning of the hair bundle (Kelley et al., 1992; Montcouquiol et al., 2003). Although the kinocilium is present in all hair cells during development, it is not required for mechanosensitivity (Hudspeth and Jacobs, 1979). The kinocilium atrophies during the development of auditory hair cells (Figure 7).

Stereocilia are full of parallel actin filaments cross-linked by fimbrin and espin (Drenckhahn et al., 1991; Zheng et al., 2000b) and are ensheathed by plasma membrane, which is contiguous with that of the hair-cell soma. The base of the stereocilium tapers to create a rootlet that inserts into the cuticular plate, a meshwork of randomly oriented actin filaments that lies just beneath the apical surface of the hair cell (reviewed in Hudspeth, 1989). Cross-linking and tapering at the base confers rigidity along the length of the stereociliary shaft, while allowing the entire bundle to pivot at its insertion point; the constituent stereocilia move in unison sliding along one another (Figure 8).

Figure 6. Bullfrog hair cell. An isolated bullfrog saccular hair cell viewed by differential interference contrast microscopy showing the mechanosensitive hair bundle that crowns the cell (W. M. Roberts and A. J. Hudspeth, unpublished).

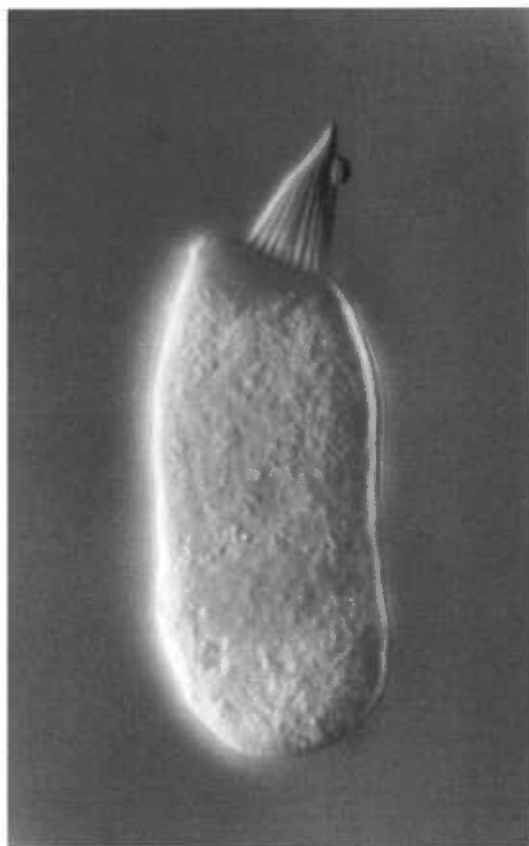


Figure 7. Hair cells from mouse, bullfrog, and guinea pig. Although they come in different shapes and sizes, in general hair bundles consist of 10s-100s of stereocilia (S), and a single kinocilium (K). Scanning electron micrographs of three hair cells. A, Mouse utricular hair bundle with a very long kinocilium (from Rzadzinska et al., 2004). B, Bullfrog saccular hair bundles facing opposite directions (J. A. Assad and D. P. Corey, unpublished). C. Guinea pig outer hair cell with its distinctive “v” or “w” shape. The kinocilium does not persist in hair bundles of auditory hair cells. The arrowhead indicates where the kinocilium was during development (from Lenoir, 1998).

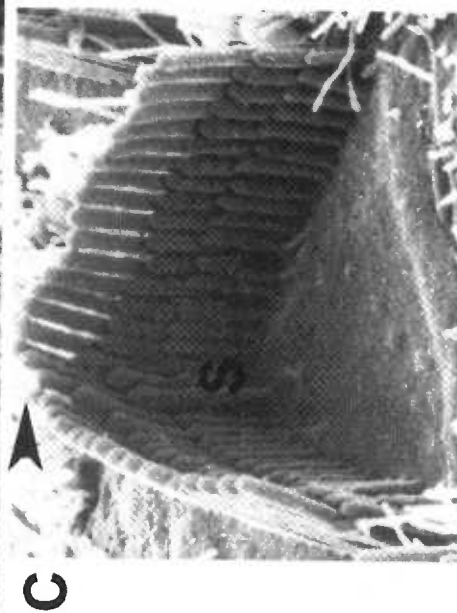
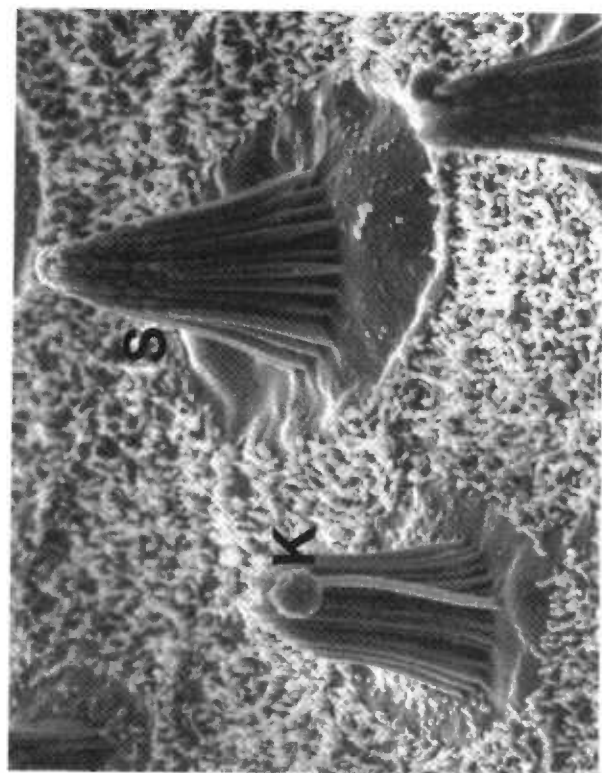
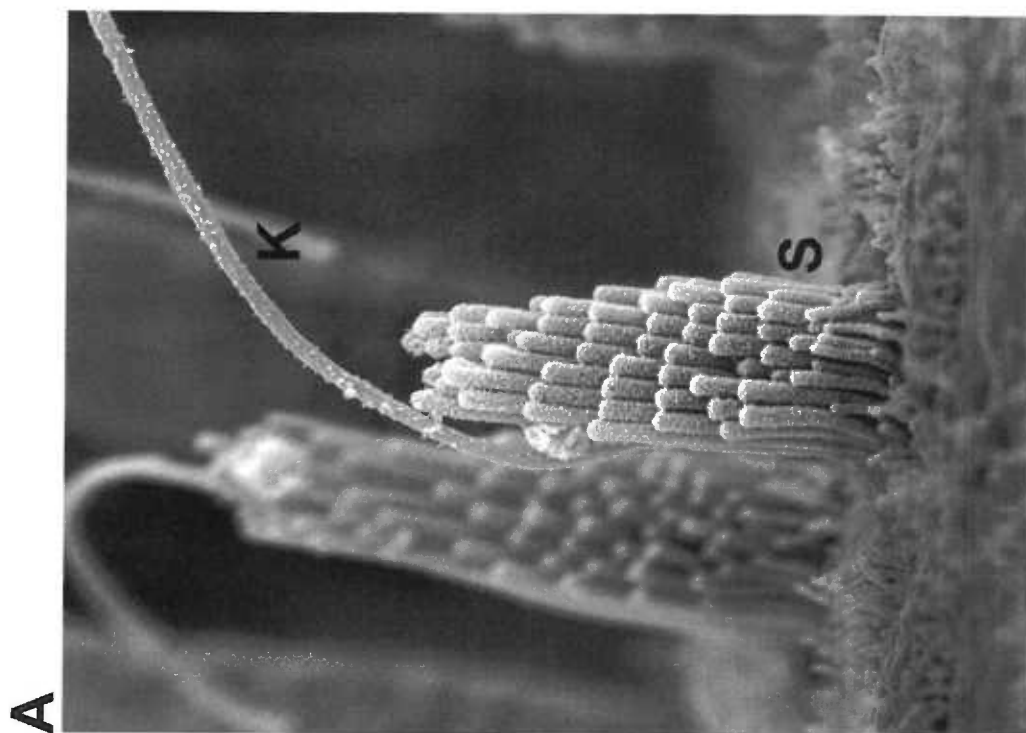
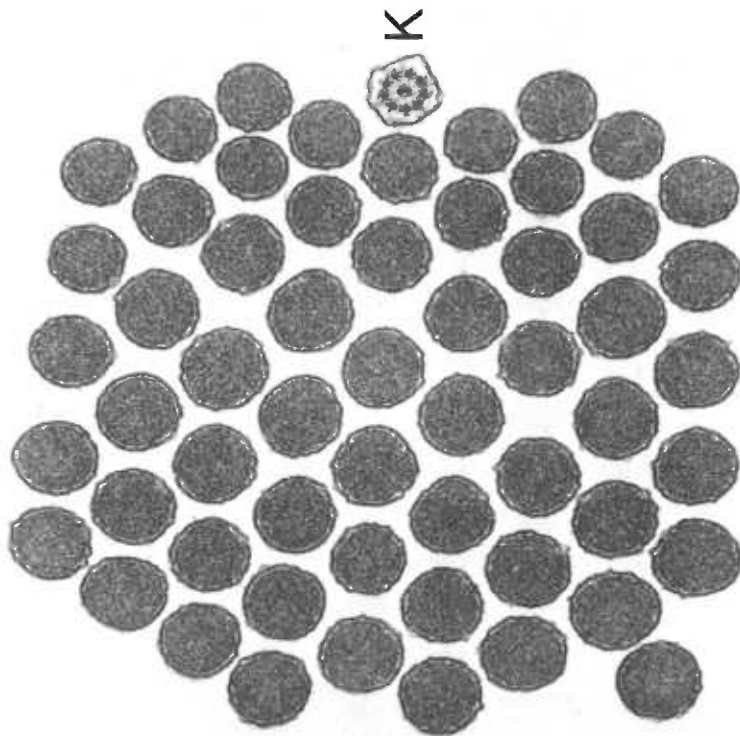
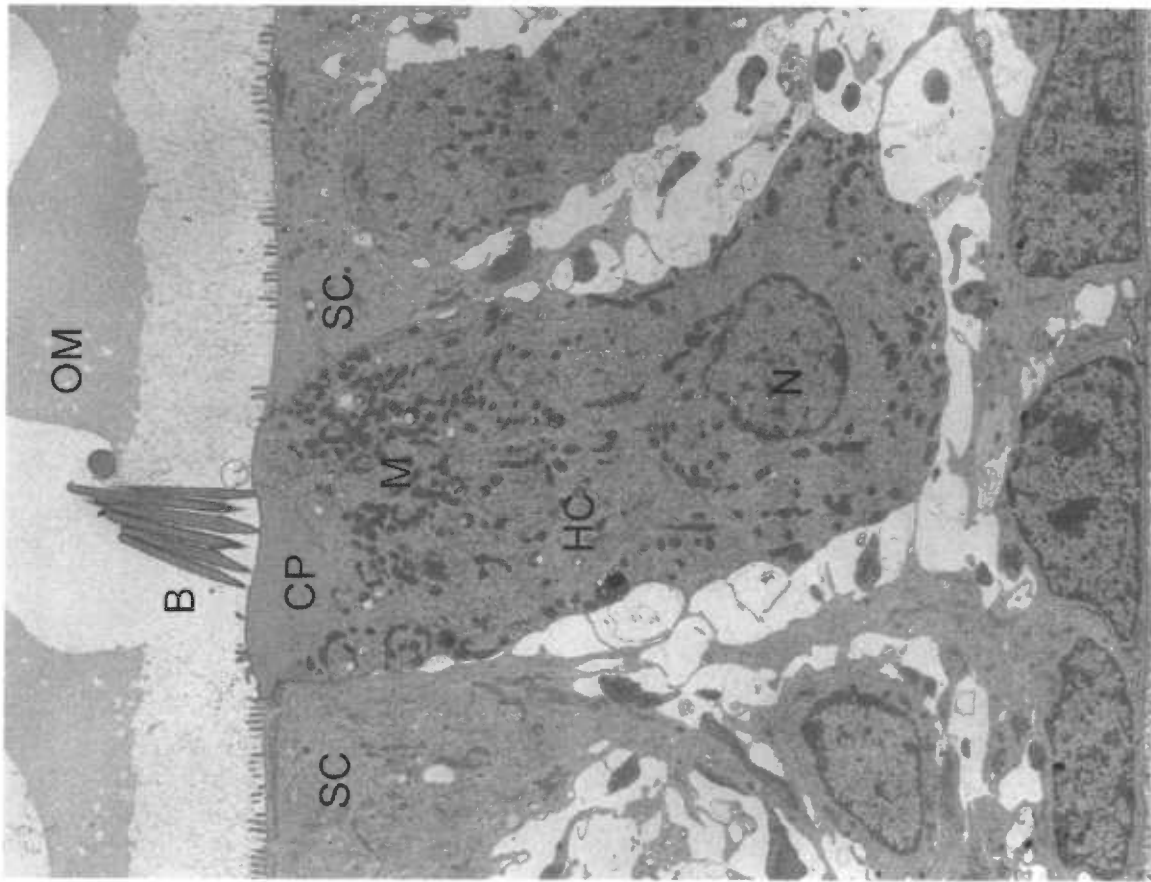


Figure 8. Hair bundle structure. Transmission electron micrograph of a bullfrog saccular hair bundle in cross section. Stereocilia are full of actin filaments and ensheathed by plasma membrane. The single kinocilium has the classic 9+2 microtubule array (K) (from Jacobs and Hudspeth, 1990). Transmission electron micrograph of a lateral section of a bullfrog saccular hair cell. The stereocilia of the bundle (B) dramatically taper as they insert into the actin meshwork of the cuticular plate (CP). (HC) hair cell; (M) mitochondria; (N) nucleus; (SC) supporting cells, (OM) otolithic membrane (R. A. Jacobs and A. J. Hudspeth, unpublished).

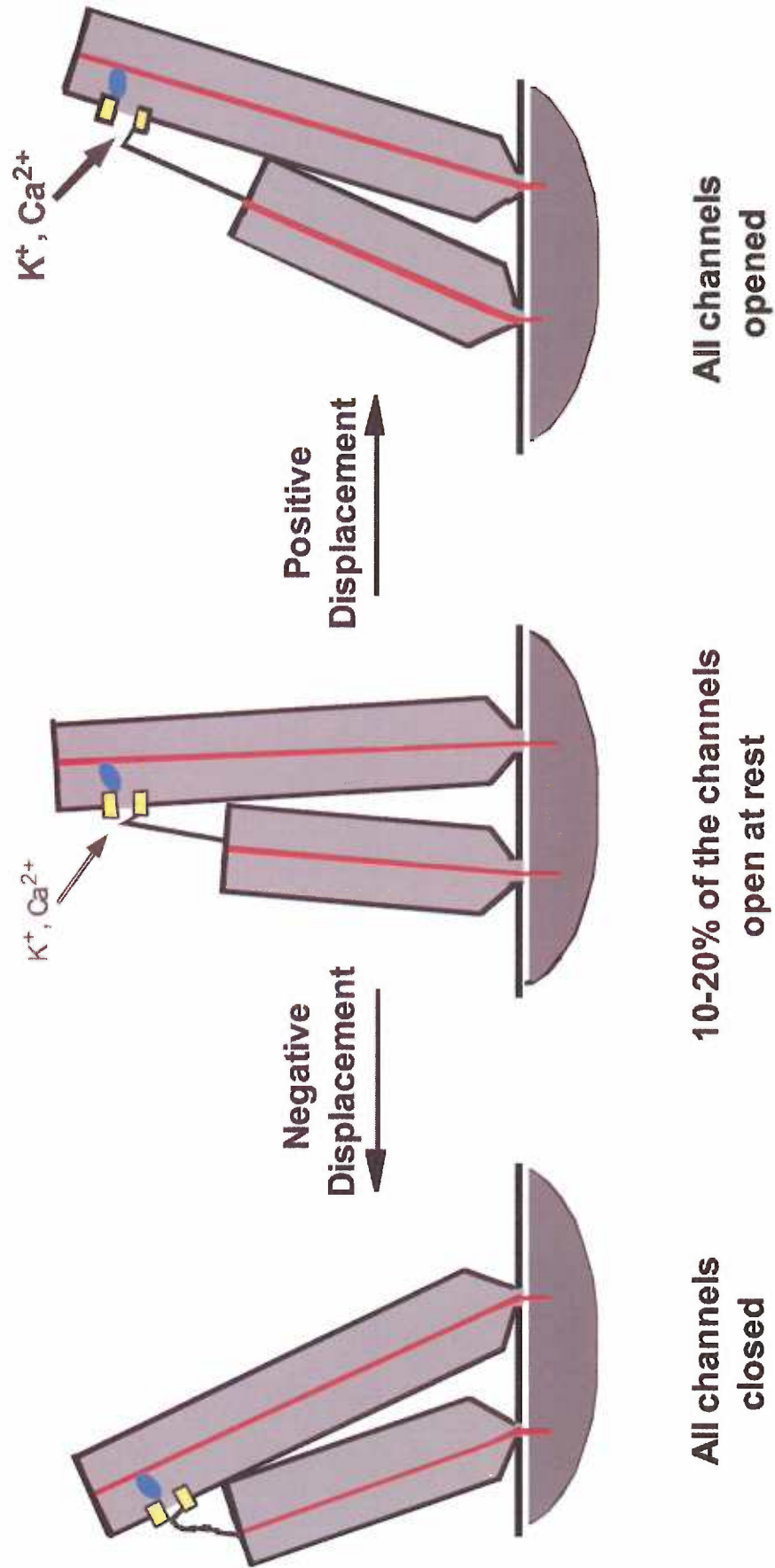


Mechanotransduction

Deflections of the hair bundle along the axis of sensitivity produce changes in membrane potential, resulting in a modulation of neurotransmitter release from the synapses at the basolateral surface of the hair cell. Movements of the bundle towards the tallest stereocilia, designated positive stimuli, open cation-selective transduction channels, which depolarize the hair cell and increase neurotransmitter release. Because 10-20% of the transduction channels are open at rest, there is a tonic release of neurotransmitter that is inhibited by negative deflections. Negative stimuli, deflections towards the shortest stereocilia, close transduction channels and prevent cation entry; the cell is hyperpolarized and hence neurotransmitter release is inhibited (Figure 9).

The speed at which hair cells respond to mechanical stimulation argues against a metabotropic cascade; the mechanism of hair cell mechanotransduction is likely ionotropic with the channels directly gated by the mechanical stimulus. The prevailing model for hair-cell transduction, the gating-spring model (Hudspeth, 1992; Pickles and Corey, 1992), postulates that deflection of the bundle in the positive direction puts tension on gating springs; this increased tension leads in turn to an increase in the open probability of the transduction channels. The positive electrical potential in the endolymphatic space created by the endolymph bathing the hair bundle drives entry of mainly K^+ , but also Ca^{2+} and Na^+ , into the hair bundle and depolarizes the hair cell. The unique properties of endolymph will be discussed further in the following section (see **Potassium Recycling**).

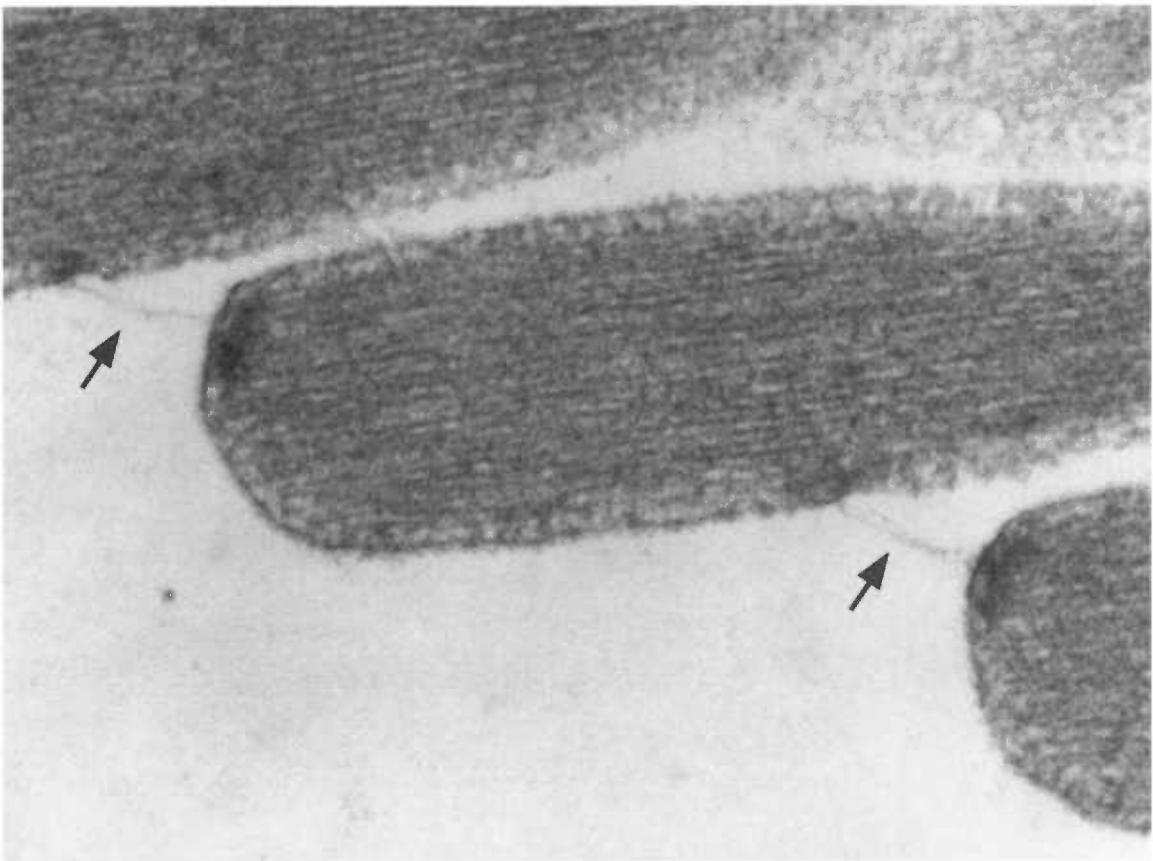
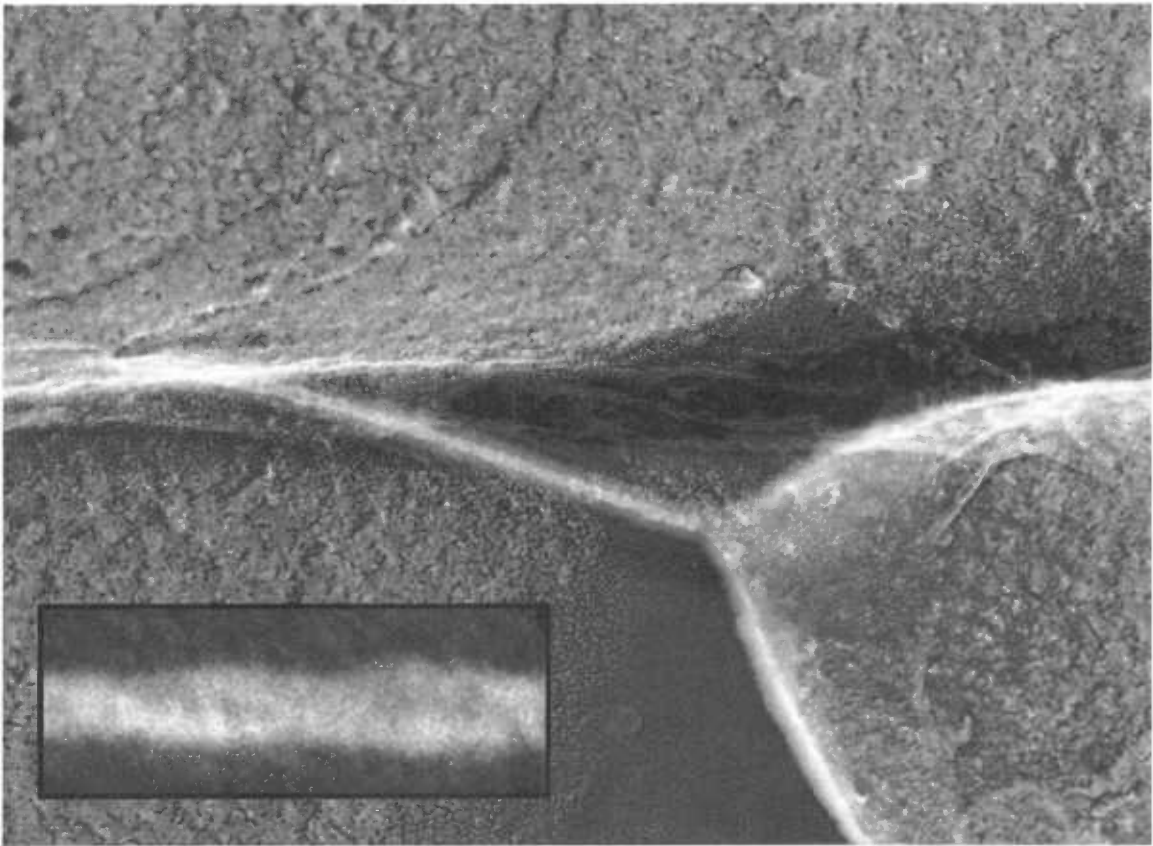
Figure 9. Gating-spring model of hair-cell mechanotransduction. For simplicity, only the cuticular plate and stereocilia are illustrated. The hair bundle is represented by a pair of stereocilia connected by a tip link. Deflection of the hair bundle toward the tallest stereocilia increases tension in the tip links that gate the transduction channels, entering K^+ , the primary charge carrier and Ca^{2+} depolarize the cell. Negative deflections slacken the tip link, which closes the 10-20% of the channels open at rest (from Gillespie, 1995).



A recent flurry of activity in hearing research has resulted in the tentative identification of two components of the transduction apparatus: the tip link and the transduction channel (Siemens et al., 2004; Sollner et al., 2004). The tip link is a helical filament that stretches from the top of each stereocilium to its taller neighbor (Pickles et al., 1984; Figure 10). Until recently, it was thought that the tip link could be the gating spring proposed in the transduction model (Assad et al., 1991). In the last few years, observations of scanning electron micrographs and mathematical models of flexural rigidity of tip links suggest that the tip link is stiffer than the modeled gating spring (Kachar et al., 2000). Just last year, cadherin 23 was put forth as a plausible candidate for the tip link (Siemens et al., 2004; Sollner et al., 2004). It is hypothesized that cadherin interacts as a dimer of dimers, forming a helix, which is consistent with the morphology observed by electron microscopy (Siemens et al., 2004; Figure 10). The gating spring is proposed to be a unique element within the bundle, connected in series with the tip link.

Another elusive component of mechanoreceptors has been the transduction channel. Large-scale genetic screens for mechanosensation in worms (Chalfie and Sulston, 1981) revealed an assortment of candidate genes that resulted in the recent identification of four members of the DEG/ENaC family required for nematode mechanotransduction (O'Hagan et al., 2005). The degenerins (DEGs), ion channels related to the vertebrate epithelial sodium channels (ENaCs) have long been the focus of mechanotransduction in other organisms as well. However, the requisite electrophysiological characteristics of the hair cell transduction channel rule out members of the DEG/ENaC family (Gillespie and Walker, 2001). *nompC*, a *Drosophila* gene essential for bristle mechanosensation, is not a member of the DEG/ENaC family but

Figure 10. Tip links. *Left*, Transmission electron micrograph of stereocilia from a bullfrog saccular hair cell (R. A. Jacobs and A. J. Hudspeth, unpublished). Tip links are indicated (arrows). *Right*, Freeze-etch scanning electron micrograph of a bullfrog tip link highlighting the helical structure (inset; from Kachar et al., 2000).

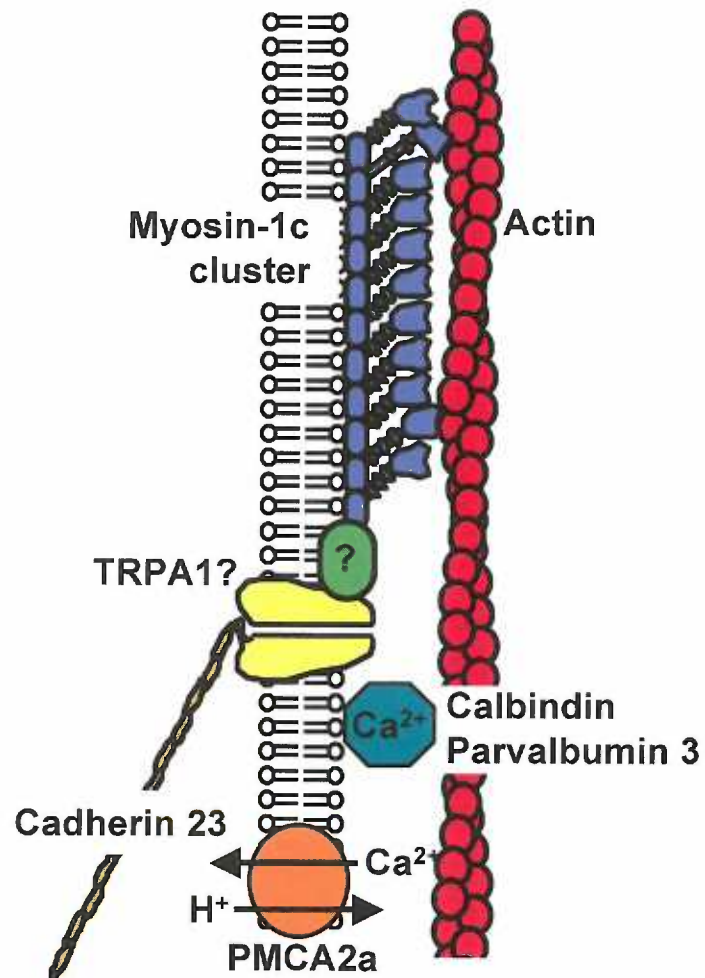


instead belongs to the transient potential receptor (TRP) family (Walker et al., 2000). Although NompC has not been definitively established as the bristle mechanotransduction channel, its identification has shifted focus to TRP channels as mediators of mechanotransduction in many systems (reviewed in Strassmaier and Gillespie, 2002). Accordingly, two TRP channel subunits (*nanchung* and *inactive*) were recently identified as components of the transduction channel in the hearing organ of flies (Kim et al., 2003; Gong et al., 2004). Moreover, Sidi et al. (2003) have shown that a homolog of *nompC* is essential for hearing in zebrafish. Although *nompC* appears to be absent from the human and mouse genomes, other mammalian TRP channels have been implicated in mechanosensation (Di Palma et al., 2002; Nauli et al., 2003). Recently, TRPA1 was offered as a candidate for the mechanotransduction channel of mammalian hair cells (Corey et al., 2004). Additionally, Corey et al. proposed that TRPA1 harbors the gating spring in its N-terminus. NompC, also called TRPN1, and TRPA1 each possess a large number of ankyrin repeats (29 and 17, respectively). Crystal structures and molecular modeling present the possibility that tandem ankyrin repeats can form a spring, satisfying the biophysical criteria of the gating spring (Corey et al., 2004; Figure 11).

Potassium Recycling

Endolymph is unlike most extracellular fluids; the unique fluid that bathes hair bundles is rich in K^+ , yet low in Na^+ and Ca^{2+} . Thus, in the inner ear it is K^+ not Na^+ that carries most of the current entering hair cells. The high K^+ concentration of the endolymph is maintained by the marginal cells in the stria vascularis of the cochlea. The

Figure 11. Model of the hypothetical hair-cell transduction apparatus. The actin core of the stereocilium (red) is the base for the entire transduction complex. Attached to this actin core is a proposed cluster of myosin-1c molecules, the adaptation motor (blue). TRPA1, the putative transduction channel (yellow), is connected in series with the tip link, cadherin 23, to the next stereocilium. The adaptation motor is proposed to be connected in series with the transduction channel through some unknown linker (green). Also shown are two mobile calcium buffers, calbindin and parvalbumin 3, and PMCA2a, which play a key role in regulating the influx of Ca^{2+} from transduction (P. G. Gillespie, unpublished).



marginal cells express a highly active $\text{Na}^+\text{-K}^+\text{-2Cl}$ cotransporter (Crouch et al., 1997; Sakaguchi et al., 1998) and a $\text{Na}^+\text{,K}^+\text{-ATPase}$ (Iwano et al., 1989; Schulte and Adams, 1989) in their basolateral membranes, which direct K^+ flowing originally from the hair cell into the marginal cells. The marginal cell apical membranes are permeable to K^+ , allowing a net flow of K^+ into the endolymph (Sakagami et al., 1991; Sunose et al., 1994; Wangemann et al., 1995). Dark cells of the vestibular system use a similar method to maintain the K^+ -rich endolymph of the vestibular organs (Wangemann, 1995). A key feature of K^+ recycling is that the hair cell is completely passive in this process; hair cells rely on the active process of the stria vascularis or dark cells to maintain the electrochemical gradient that drives transduction. For example, targeted deletion of the $\text{Na}^+\text{-K}^+\text{-2Cl}$ cotransporter gene in mice produces a collapse of the scala media, degeneration of the hair cells, and profound deafness (Delpire et al., 1999; Vetter et al., 1996; reviewed in Wangemann, 2002a).

Adaptation

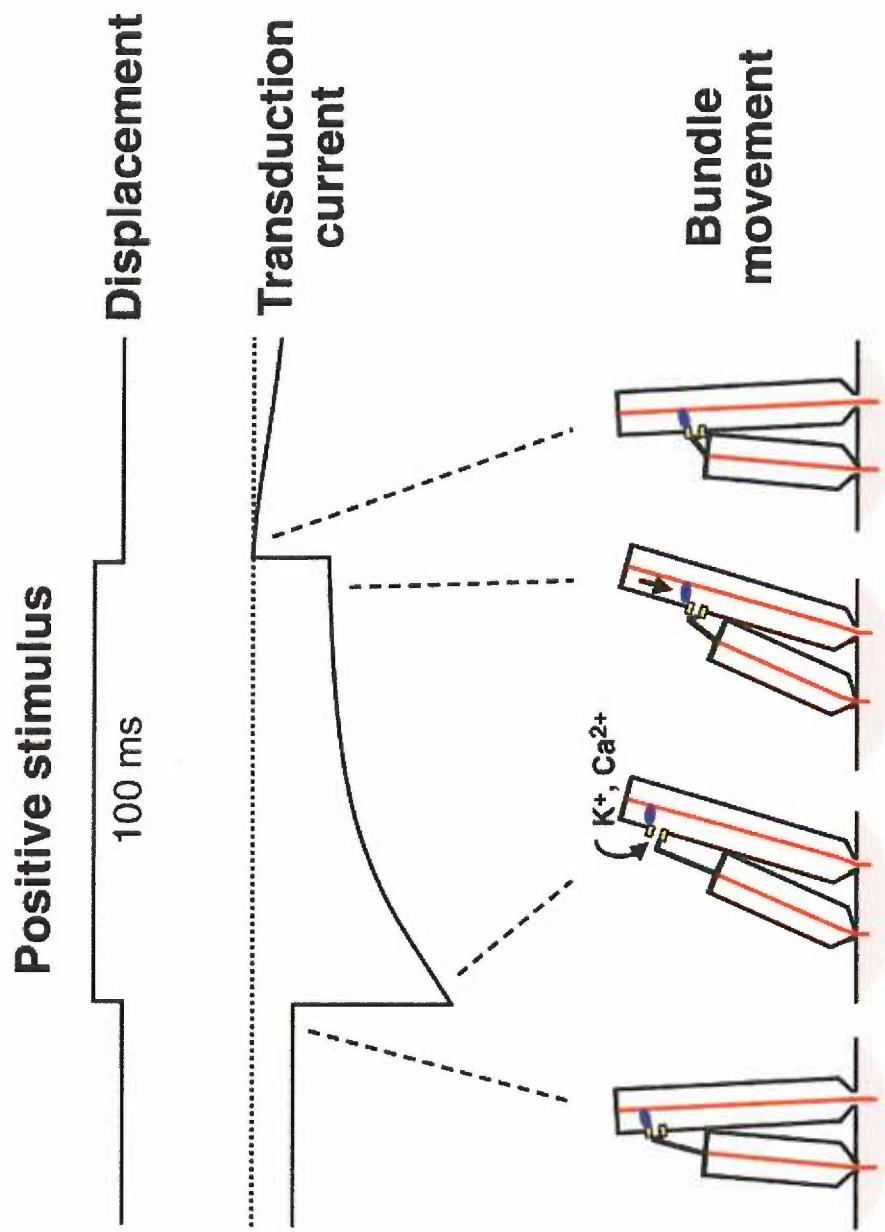
To maintain high sensitivity, hair cells must adapt to sustained stimuli. Since mechanotransduction is direct, without a regulatory second messenger, the hair cell has evolved a means of mechanically resetting the transduction apparatus to maintain sensitivity. This process is known as adaptation and is characterized by an alteration in the displacement-response curve of a hair cell, which relates bundle displacement and channel open probability. Adaptation shifts the operating range of the hair cell in the direction of the applied stimulus; however, the ability of the cell to respond to a stimulus remains unchanged (Eatock et al., 1987). Adaptation requires Ca^{2+} and has been

characterized by two time constants; changes in external or internal Ca^{2+} concentrations vary the rate of either component of adaptation (Eatock et al., 1987; Assad and Corey, 1992; Wu et al., 1999), emphasizing the importance of proper Ca^{2+} regulation to appropriate hair-cell responses.

Slow adaptation (>15 ms) is mediated by an unconventional myosin motor, myosin-1c, it is proposed that myosin-1c is linked in series with the channel and the tip link (Holt et al., 2002; for review see Gillespie, 2004). In the current model for slow adaptation, when tension in the tip links is high and transduction channels are open, the influx of Ca^{2+} modulates the force production of the myosin-1c motors; myosin-1c slips down the actin core. The slipping reduces the tension in the tip links and channels close, thereby reducing Ca^{2+} influx. The changing levels of Ca^{2+} in the hair bundle regulate the slipping and climbing of myosin-1c along the actin core, thereby controlling tension in the tip link and influencing open probability of the transduction channels (Howard and Hudspeth, 1987; Assad and Corey, 1992; Holt et al., 2002; Gillespie and Corey, 1997; Figure 12). The utility of slow adaptation seems obvious in a bullfrog sacculus, where hair cells respond to transient stimuli (movement) in the face of a saturating steady stimulus (gravity). It was not immediately obvious how adaptation would benefit the high frequency processing of auditory organs.

Fast adaptation (~ 1 ms) observed in turtle basilar papilla hair cells, and more recently in mammalian outer hair cells, may not involve an adaptation motor, yet is also dependent on Ca^{2+} flux (Ricci and Fettiplace, 1997; Ricci et al., 1998; Kennedy et al., 2003). It is posited that Ca^{2+} binding to a site associated with the transduction channel

Figure 12. Model of slow adaptation. *Top*, Prolonged positive deflection applied to hair bundles. *Middle*, Transduction currents measured for the stimulus shown above. *Bottom*, Hair bundle movement and corresponding position of the transduction apparatus of the stimulated hair cells. The decline in transduction current is coincident with the myosin-1c adaptation motor (blue) slipping down (arrow) the actin core, allowing channels to close (from Hudspeth and Gillespie, 1994).



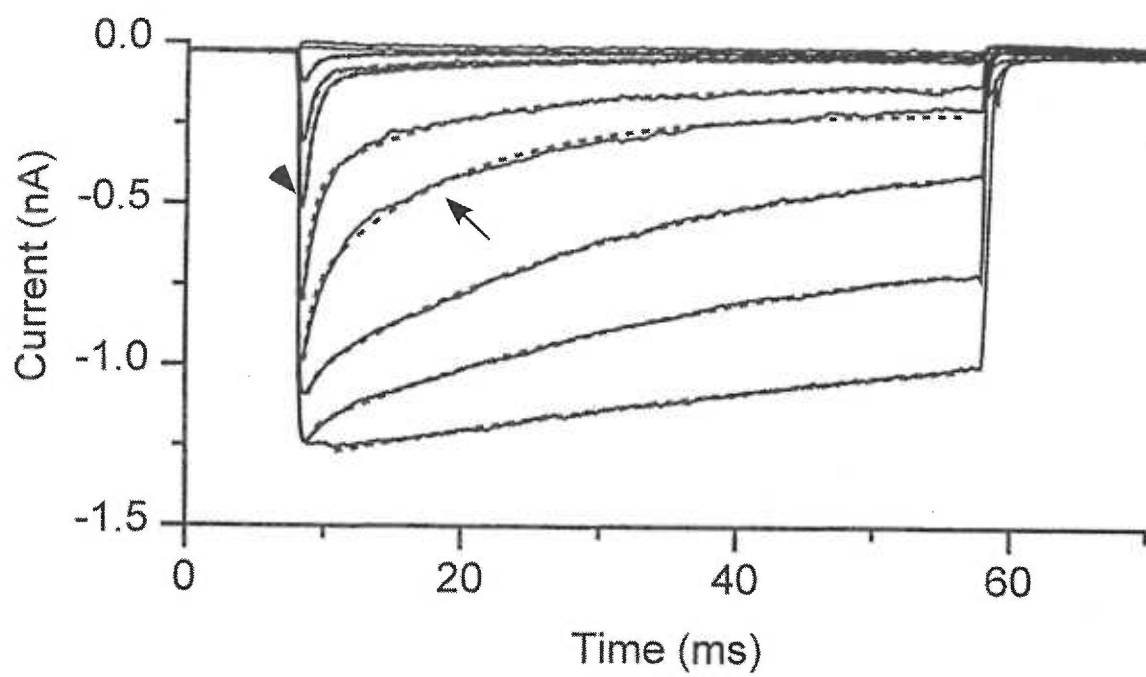
induces rapid channel closing (Wu et al., 1999; Ricci et al., 2000; Figure 13). The closing channels transfer an increase in tension to the tip-links exerting a force that causes the bundle to move in the negative direction (toward the stimulus). If the stimulus provided to the bundle is oscillatory, then when the stimulus enters the negative-going phase, the increased tip-link tension will enhance bundle movement. When channels close, Ca^{2+} influx halts, the local Ca^{2+} concentration is immediately reduced by mobile Ca^{2+} buffers, and the channel returns to a state that is sensitive to opening. The hair bundle can thus oscillate at frequencies that track auditory stimuli, suggesting that fast adaptation contributes to frequency tuning in the cochlea (Ricci et al., 2003; Ricci and Fettiplace, 1997; Ricci et al., 1998).

Cochlear Amplifier

The extraordinary sensitivity of the auditory system requires that hair cells must use some active process to overcome the dampening of incoming signals due to transmission of sound waves through the fluid in the inner ear. This active process, called the cochlear amplifier, enhances sound-stimulated basilar-membrane movement and overcomes the viscous drag of the hair-cell environment (Davis, 1983). Although the mechanism of the amplifier has yet to be identified, two models are worth discussing here.

The strongest candidate for a mammalian cochlear amplifier is a somatic-motor that controls contractility of outer hair cells in response to changes in membrane potential, such that depolarization results in the cell shortening and hyperpolarization causes the cell to elongate (Brownell et al., 1985). In the cochlea, somatic motility in

Figure 13. Two components of adaptation. Transducer currents recorded in a turtle hair cell for step deflections of its hair bundle. Prolonged positive step deflections generated inward currents that adapted. The fast (arrowhead) and slow (arrow) components of adaptation are indicated (from Wu et al., 1999).



synchrony with basilar membrane oscillations, would increase outer hair cell bundle movements, and result in amplification of the signal to inner hair cells. Recently prestin, a member of the solute-carrier family, was put forth as the outer hair cell motor (Zheng et al., 2000a; for review see Dallos and Fakler, 2002). Heterologous expression of prestin confers voltage-dependent electromotility in kidney cells. Moreover, hair cells from mice lacking prestin have no electromotility *in vitro* and their cochleae are 100-fold less sensitive than cochleae from wild-type littermates (Liberman et al., 2002). Although these compelling data suggest that somatic motility is required for function of the cochlear amplifier, outer hair cell motility falls short of satisfying all criteria for an amplifier. Most importantly, this mechanism should not work at high frequencies due to the membrane time constant, the product of the membrane resistance and capacitance. Moreover, mechanical amplification is not limited to mammals; nonmammalian vertebrates, which lack outer hair cells, also demonstrate amplification (reviewed in Hudspeth, 1997).

A second hypothesis holds that the amplification mechanism is located in the hair bundles, represented by active hair bundle movements. Hair bundles from frogs and turtles display spontaneous oscillations *in vitro*, ranging in frequency from 5-40 Hz (Crawford and Fettiplace, 1985; Martin and Hudspeth, 1999; Martin et al., 2003). When stimulated at the hair cell's characteristic frequency with a sinusoidal wave, bundles show a power gain (the output signal has a gain in energy with respect to the input signal), which is representative of amplification (Martin and Hudspeth, 1999). Another manifestation of a bundle-based active process is force generation by the bundle in response to stimulation with a flexible glass fiber (Kennedy et al., 2005; Crawford and

Fettiplace, 1985; Howard and Hudspeth, 1988; Ricci et al., 2000; Ricci et al., 2002). There are two proposed mechanisms for force generation by hair bundles. In lower vertebrates cochlear amplification appears to generate from fast adaptation. Ca^{2+} entering through the transduction channels binds to a cytoplasmic site on the channel and increases the probability of channels closing (Howard and Hudspeth, 1988). When the channels close, tension on the tip links is increased, causing the stereocilia to jerk back in the negative direction. If the increased tension in the tip-links is in phase with an oscillatory stimulus, then the tension will amplify the bundle movement. The mechanical force of these bundle movements can be harnessed on a cycle-by-cycle basis to increase cochlear sensitivity and selectivity, similar to prestin-driven motility (Ricci et al., 2000).

The second model stems from recent observations from the mammalian cochlea and predicts that a flexible molecule (perhaps myosin-1c) in series with the channel is modified by the entering Ca^{2+} , reducing tension in the tip link, and allowing further movement of the bundle driven by the stored energy in the stereocilia pivot springs (Kennedy et al., 2005). Because Ca^{2+} regulation is essential to each of these models, rapid reduction of intracellular levels of this ion may be necessary to reset the sensitivity of the hair bundle for mechanical amplification powered by the local transmembrane Ca^{2+} gradient.

Plasma-Membrane Ca^{2+} -ATPase

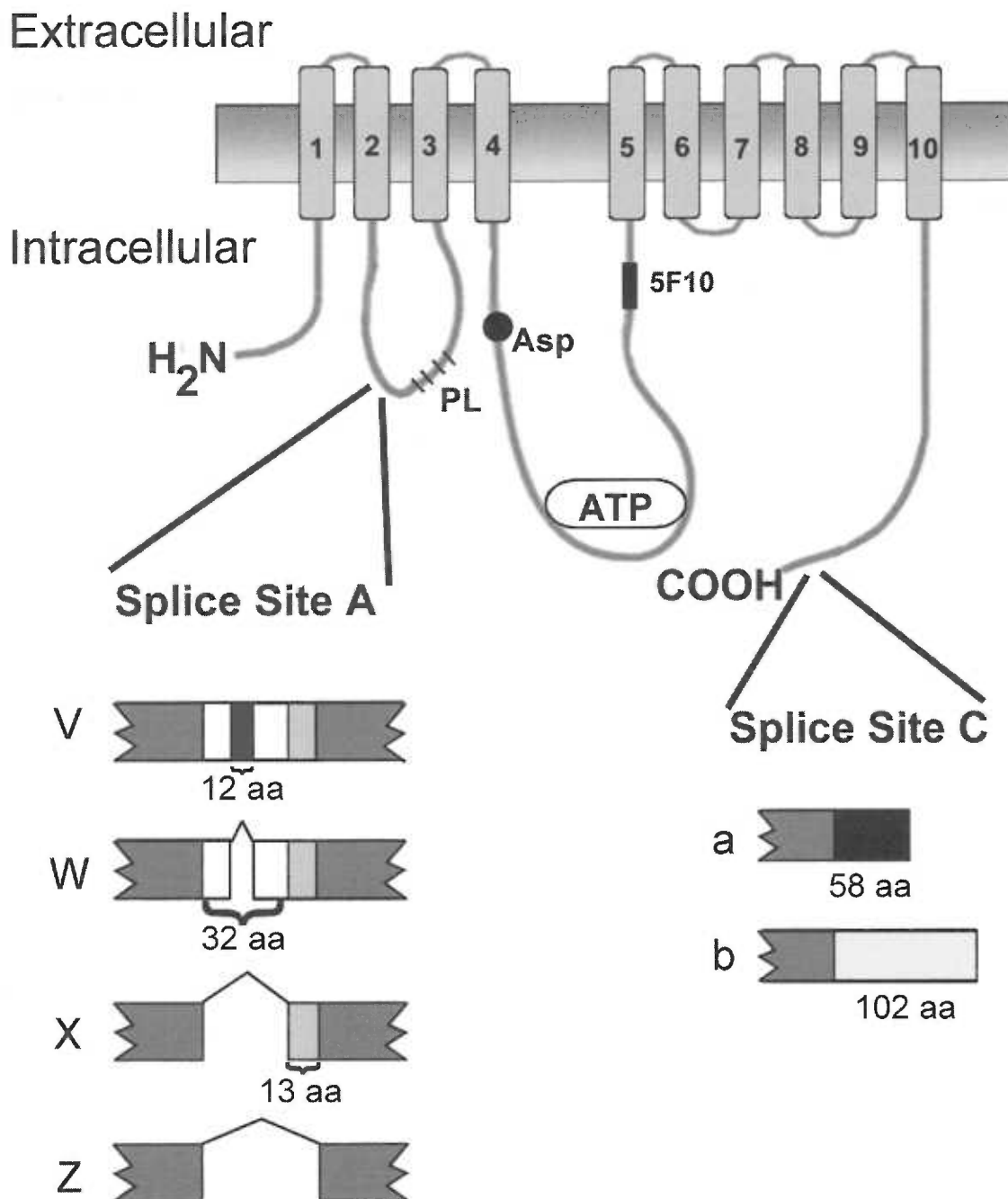
Because hair bundles are bathed in endolymph, no transmembrane ion gradient exists to support common carrier-mediated Ca^{2+} -transport mechanisms, such as the $\text{Na}^+/\text{Ca}^{2+}$ exchanger. Because stereocilia also cannot sequester Ca^{2+} , they rely instead on

two mechanisms for removing Ca^{2+} that enters during transduction, buffered diffusion and transmembrane Ca^{2+} transport (Lumpkin and Hudspeth, 1998).

The endogenous Ca^{2+} buffer of hair bundles behaves similarly to ~ 0.5 mM BAPTA (1,2-bis(*O*-aminophenoxy)ethane-*N,N,N',N'*-tetraacetic acid) (Ricci et al., 1998) and is important for reducing free Ca^{2+} immediately following transduction (Lumpkin and Hudspeth, 1995; Denk et al., 1995). The majority of Ca^{2+} in the stereocilia is not buffered, however, and must be locally extruded (Lumpkin and Hudspeth, 1998). The only known Ca^{2+} -extrusion mechanism in the hair bundle is the plasma membrane Ca^{2+} -ATPase (PMCA). This pump is highly expressed in stereocilia (Dumont et al., 2001; Yamoah et al., 1998) and is believed to remove more than three-fourths of the intracellular Ca^{2+} following transduction (Lumpkin and Hudspeth, 1998).

PMCA is a member of the P-type ATPase family. Characteristic of the P-type ATPases, PMCA forms a phosphorylated aspartate intermediate during its reaction cycle. The Ca^{2+} pump also shares the family's sensitivity to orthovanadate and La^{3+} , which potently inhibit enzymatic activity (Figure 14). PMCA is an integral membrane protein consisting of ten transmembrane domains that uses the energy from ATP hydrolysis to move Ca^{2+} up its transmembrane gradient. There are four mammalian PMCA genes (PMCA1-4), each of which has two splice regions (A and C); alternative splicing in these regions can therefore generate a variety of isoforms. PMCA1 and PMCA4 are ubiquitously expressed and are essential housekeeping pumps that regulate basal Ca^{2+} levels. PMCA2 and PMCA3 expression is restricted, which suggests more cell-type specific roles for these isozymes (Stauffer et al., 1995).

Figure 14. Schematic of PMCA2. Diagram depicting the 10 membrane-spanning domains of PMCA2 in a lipid bilayer. Key intracellular features are marked: splice sites A and C, a phospholipid-sensitive domain in the first intracellular loop near splice site A (PL), the phosphorylated aspartate, the ATP-binding pocket, and the 5F10 epitope that is common to all PMCA2s. The major PMCA2 variants are diagramed below, with amino acid differences indicated. PMCA2v has been identified only in bullfrog hair bundles (Dumont et al., 2001).



Most of the focus on alternate splicing of PMCA has been on variants generated from the C splice site, which can be “a”, “b”, or “c”; splicing in this region alters the affinity of PMCA for calmodulin (Enyedi et al., 1994) and determines the presence or absence of at least one phosphorylation site (Enyedi et al., 1997). In contrast, the functional consequences of splicing within region A, which determines the “v”, “w”, “x”, “y”, or “z” isoforms, are poorly understood.

Although all four PMCA isoforms and many splice variants are expressed in the mammalian cochlea (Crouch and Schulte, 1996; Furuta et al., 1998), engineered as well as spontaneously occurring mutations in mice have demonstrated the importance of at least one PMCA isozyme in hearing and balance. Disruption of the *Pmca2* gene (*Atp2b2*) by targeted deletion of exon 19 (Kozel et al., 1998) resulted in deaf mice with profound vestibular dysfunction, a phenotype similar to three naturally occurring mutations, *deafwaddler* (*dfw*) (Street et al., 1998), *dfw*^{2J} (Noben-Trauth et al., 1997), and *Wriggle Mouse Sagami* (*wri*) (Takahashi and Kitamura, 1999). Immunoreactivity to all PMCA isoforms was absent from hair bundles of *dfw*^{2J} and *wri* mice, implicating PMCA2 as the predominant hair-bundle isozyme (Street et al., 1998; Takahashi and Kitamura, 1999). The Gillespie lab recently showed that PMCA2 is the only PMCA expressed in hair bundles; the predominant splicing region C version of PMCA2 in rat and frog hair bundles is the “a” variant, while in frogs, the splicing region A form is the “v” variant (Figure 14; Dumont et al., 2001). We were unable to identify which splicing region A isoform is used in mammalian hair bundles, although we found by RT-PCR only the “w”, “x”, and “z” splice forms in cochlea and vestibular organs. Because a “v” form has not been identified in mammals, it has been proposed that PMCA2w/a is the bundle isoform

(Chicka and Strehler, 2003). Because the “v” sequence interrupts the “w” sequence, rat PMCA2w/a might not target to the bundle (Figure 14).

When PMCA2 was expressed in Madin-Darby canine kidney (MDCK) cells, splicing region A dictated apical versus basolateral targeting; “w” was the only region A variant to traffic to the apical membrane of this polarized-epithelial cell line (Chicka and Strehler, 2003). Although these data suggest that “w” can serve as an apical targeting signal in a heterologous system, this result does not immediately translate to *in vivo* expression. Membrane proteins are sorted to either the apical or basolateral domains by several mechanisms that vary by cell type; any one protein may be targeted by more than one mechanism. Although the sorting of plasma-membrane proteins in polarized cells is understood in general terms, the distinct molecular mechanisms controlling the specific targeting of these membrane proteins are not yet known. A relevant example is expression of the Na^+, K^+ -ATPase of retinal pigmented epithelium (RPE). The Na^+, K^+ -ATPase is typically considered a basolateral membrane protein, localizing to this membrane compartment in cell types such as the gastro-intestinal epithelia and the cochlear marginal cells. This localization is recapitulated in MDCK cells; however, the Na^+, K^+ -ATPase of RPE is targeted to the apical membrane (reviewed in Rizzolo, 1999), which suggests that there are different sorting signals between RPE and MDCK cells, perhaps also in hair cells.

Although there is very little known about how proteins specifically target to the hair bundle, PMCA is the best characterized membrane protein in the hair bundle. By determining the apical targeting sequence of PMCA, we can begin to deduce the signals required for assembling the hair cell transduction apparatus.

Proton Transport

Despite evidence for and against the electrogenicity of PMCA (reviewed in Dumont and Gillespie, 2000), the prevailing hypothesis is that every Ca^{2+} extruded by PMCA results in the entry of one H^+ (Hao et al., 1994; Salvador et al., 1998). This exchange implies that when PMCA is fully activated, H^+ entry may exceed 1 mM s^{-1} in a stereocilium (Yamoah et al., 1998). Similar to Ca^{2+} homeostasis, we suggest that hair bundles have endogenous H^+ buffers that immediately blunt pH changes; however, the presence of H^+ transporters could more tightly control the H^+ concentration. If H^+ extrusion required diffusion from the bundle to the soma, a transepithelial H^+ flux would develop, requiring a H^+ recycling mechanism to maintain endolymph pH. The presence of a H^+ transporter in the bundle would make this energy expenditure unnecessary. Although there is strong evidence demonstrating a Na^+ -dependent H^+ extruder in the outer hair-cell soma (Ikeda et al., 1992), the paucity of Na^+ in the endolymph suggests that a bundle-based H^+ extrusion mechanism will be Na^+ -independent.

Two K^+ -dependent transporters that could be employed by the bundle are the gastric and non-gastric H^+, K^+ -ATPases. These H^+ transporters are responsible for acidifying the stomach (gastric) and removing H^+ from the colon and kidney (non-gastric) (Jaisser and Beggah, 1999; Rabon and Reuben, 1990; Wingo and Cain, 1993). Since inner ear physiology has many features in common with renal physiology, examining transporters in the kidney may provide clues for candidate hair bundle proteins. Recent evidence suggests that this comparative approach may be useful. Karet et al. (1999) demonstrated that mutations in the gene for the B1 subunit (*Atp6v1b1*) of the H^+ -pumping vacuolar-ATPase (V-ATPase) produce distal renal tubular acidosis (dRTA)

with sensorineural deafness in humans. Until recently the B1 subunit was thought to be a specific kidney isoform (Puopolo et al., 1992; van Hille et al., 1994). However, immunoreactivity for this B1 subunit has also been seen in the interdental cells of the spiral limbus, which suggests that V-ATPase expression may be important for returning H^+ to the endolymph (Stankovic et al., 1997). Recently a mouse carrying a null mutation for *Atp6v1b1* showed no deficit in hearing, suggesting a compensatory mechanism in the mouse inner ear (Dou et al., 2003). The V-ATPase is a highly complex molecule made up of ~13 subunits, many with multiple isoforms; therefore other isoforms could compensate in the mouse or other subunits could be critical for hearing. A second gene mutation responsible for dRTA with sensorineural deafness in humans was recently identified in the A4 subunit; however, no data was presented showing inner ear localization (Stover et al., 2002). An isoform of the 31-kD subunit of the V-ATPase was also localized to the stria vascularis, inner hair cells, and the endolymphatic sac (Stankovic et al., 1997); there have been no deafness-associated mutations reported with this subunit, however. Although expression of the V-ATPase subunits has not been demonstrated in hair bundles, a novel bundle V-ATPase might be expressed (Hemken et al., 1992).

A hallmark of all the H^+ transporters thus far discussed is the reliance upon ATP hydrolysis. The demand for ATP in the hair bundle is predicted to be high; since PMCA activity requires the hydrolysis of one ATP for every cycle of Ca^{2+}/H^+ exchange, ATP consumption may exceed 1 mM s^{-1} (Yamoah et al., 1998). This places a heavy burden on the hair bundle to maintain a supply of ATP when the closest mitochondria is ~8 μm away below cuticular plate (Heywood et al., 1975; Figure 8). Although the question of

how the hair bundle maintains an ATP supply is not addressed in this dissertation, the problem is germane to H^+ transport.

Secondary active transporters are not coupled directly to ATP hydrolysis, but instead their driving force is derived from the electrochemical gradient established for one of the cations that drives countertransport of the other. Members of the Na^+/H^+ exchanger (NHE) family are classified as such transporters. This family is divided into two major subgroups, the plasmalemma NHEs and the intracellular NHEs. All five of the plasmalemma NHEs (NHE1-5), as their name suggests, reside on the plasma membrane and are Na^+ selective (reviewed in Orlowski and Grinstein, 2004). In contrast, the newest members of the family, the intracellular NHEs (NHE6-9), are much more promiscuous in their localization as well as cation transport. Human NHE7, NHE8 and the yeast ortholog of NHE6, *Nhx1*, can transport Na^+ or K^+ in exchange for H^+ (Brett et al., 2005b; Numata and Orlowski, 2001; Nakamura et al., 2005). NHE6 also trafficks to the plasma membrane prior to reaching its target destination of endosomal compartments (Brett et al., 2002). Furthermore, NHE8 has been localized to the apical brush-border membranes of kidney and intestine (Goyal et al., 2005; Xu et al., 2005). Our hypothesis is that the hair bundle co-opts a member of the intracellular NHEs and uses the high K^+ of the endolymph to remove H^+ from bundles. A H^+ transporter that would not rely on ATP and yet responds to the electrochemical gradient of H^+ created by the Ca^{2+}/H^+ exchange of PMCA would be an elegant and energy-efficient solution for the hair bundle to regulate pH.

RESEARCH OBJECTIVES

This dissertation reports data from two parallel projects. The first was to identify the region of PMCA2a that dictates apical targeting in hair cells. We used affinity purified PMCA2w-specific antibodies to look at endogenous PMCA2 and gene gun transfection of hair cells to monitor expression of epitope-tagged splicing region A variants. We identified PMCA2w/a as the bundle isoform of PMCA in rat vestibular and auditory hair cells.

The second project aimed to identify the mechanism by which the hair bundle regulates H^+ as a consequence of PMCA activity. To examine if hair bundles allow H^+ to diffuse to the soma or have a local transport mechanism, we combined pharmacology, cell biology, molecular biology, and biochemistry to identify two candidates for maintaining pH homeostasis in amphibian and rodent hair bundles. We propose that isoforms 6 and 9 of the Na^+/H^+ exchanger family are central to hair bundle H^+ homeostasis.

MATERIALS AND METHODS I

Generating antibodies against PMCA2a variants

Polyclonal rabbit antibodies for PMCA2w, PMCA2x, or PMCA2z splice variants were raised against synthetic peptides with an added C-terminal cysteine residue, corresponding to the splice region of human PMCA2. The three peptides 2w-GDGLQLPAADGAAASNAADS(C), 2x-DDKKGKMQDGNVDA(C), and 2z-DDKKAKQQDGAAAM(C) were synthesized in the Mayo Clinic Protein Core facility (Rochester, MN) and used to immunize two rabbits each (Cocalico Biologicals, Reamstown, PA). Antibodies were affinity purified by coupling synthetic peptides, derived from the rat sequence 2w-GDGLQLPAADGAAPANAAGS(C), 2x-KKGKMQGGG(C), 2z-DKKAKQGGG(C), to SulfoLink resin (Pierce Biotechnology, Rockford, IL) via their terminal cysteine residues (1 mg of peptide/ml of resin). Antisera were diluted with 10 vol of 25 mM Tris-HCl pH 8.0 and incubated with 0.5-1.0 ml peptide-resin overnight at 4°C. The resin was poured into a column and washed with 20 vol of 25 mM Tris-HCl, pH 8.0 and 10 vol of 500 mM NaCl/25 mM Tris-HCl, pH 8.0. Antibodies were eluted with 100 mM glycine, pH 2.5, followed by 100 mM CAPS ((3-cyclohexylamino)-1-propane sulfonic acid), pH 10.5. Eluates were neutralized, pooled, and dialyzed against PBS containing 0.02% sodium azide.

Constructing PMCA2a-variant expression vectors

The coding region of PMCA2z/a was amplified with Phusion DNA polymerase (MJ Research, Waltham, MA) from pMT2-PMCA2z/a (gift of Dr. J. Penniston), creating a 5'-XbaI site and a 3'-HindIII site (Table 1, 2z/a primers). PMCA2z/a was subcloned into the XbaI and HindIII sites of pJPA5 (gift of Dr. J. Adelman), which contained a C8 epitope tag (PRGPDRPEGIEE) downstream from the CMV promoter. The original clone we received had a single base deletion at nucleotide G1310 (numbering based on the coding sequence), causing a frameshift that resulted in a premature stop codon after transmembrane domain 4. We used site directed mutagenesis to correct this deletion and took advantage of flanking AgeI sites to cut and paste the corrected fragment into the pJPA5.C8-PMCA2z/a construct. To create PMCA2w/a and PMCA2x/a, we again used site directed mutagenesis to create a unique PacI site and an unique NheI site flanking splicing region A. Overlapping oligonucleotides were synthesized (Table 1), annealed, and amplified to create the “w” and “x” splice sequence. Briefly, the oligonucleotides were mixed together for a final total concentration of 200 μ M. Dilutions of 1:10, 1:100, or 1:1000 were used as a template for 40 cycles of amplification with Phusion DNA polymerase. Dilutions of products from this round of PCR were used as templates for a second round of 40 cycles with the two outermost primers. Resulting products of correct size were sequenced and cloned into the PacI and NheI sites of PMCA2z/a. The introduced restriction sites were then mutagenized back to the native sequence, creating PMCA2w/a and PMCA2x/a.

TABLE 1. Primers for generating PMCA2a splicing region A variants

Primer	Primer Sequence (5'-3')
2z/a For	<u>TCTAGAC</u> ATGGGTGATATGACCAACAGCGAC
2z/a Rev	<u>AAGCTT</u> CTAGCCCTGCCCAGCTGCAG
Top 1wx	<u>GCTAGC</u> GCTGGTGGTGAAGAGGAAGAGAAGAA
Top 1w	AGACAAAAAAGGCGTGAAGAAGGGCGACGGC
Top 2w	CTGCAGCTGCCCCGCCGCCGACGGCGCCGCC
Top 3w	CCGCCAACGCCGCCGGCAGCGCCAACGCCAG
Top 4w	CCTGGTGAACGGCAAGATGCAGGACGGCAGCG
Top 2wx	CCGACAGCAGCCAGAGCAAGGCCAAGCAGCAG
Top 1x	AGACAAAAAAGGCAAGATGCAGGACGGCAGCG
Bottom 1wx	GCCTTTTTTGTCTTTCTTCTCTTCCTCTT
Bottom 1w	CGGGCAGCTGCAGGCCGTCGCCCTTCTTCAC
Bottom 2w	GCGGCGTTGGCGGGGGCGGCGCCGTCGGCGG
Bottom 3w	GCCGTTACACAGGCTGGCGTTGGCGCTGCCG
Bottom 2wx	TGGCTGCTGTCGGCGCTGCCGTCCTGCATCTT
Bottom 3wx	<u>TTAATTA</u> ACCATCCTGCTGCTTGGCCTTGCTC

*Added restriction sites are underlined.

Preparing microsomes expressing PMCA2a variants

COS-7 cells were grown to ~90% confluence in 10-cm plates (Fisher Scientific) using Dulbecco's Modified Eagles' Medium (DMEM; Invitrogen, Carlsbad, CA) supplemented with 10% fetal bovine serum and penicillin/streptomycin. Cells were transfected with 17.5 μ g pJPA5-PMCA2a variant DNA using 35 μ l Fugene 6 (Roche Applied Science, Indianapolis, IN). After 48 hr, the cells were washed twice in cold phosphate buffered saline (PBS, in mM: 137 NaCl, 2.7 KCl, 4.3 Na₂HPO₄, and 1.4 KH₂PO₄ at pH 7.3) and harvested in 1 ml per 10-cm plate of PBS with protease inhibitors (0.2 mM phenylmethylsulfonyl fluoride (PMSF), 4 μ g/ml aprotinin, 1 μ g/ml leupeptin) and 1 mM EGTA. The cells were pelleted and resuspended in an ice-cold hypotonic solution (in mM: 10 Tris-HCl, pH 7.5; 1 MgCl₂; 0.5 EGTA; 0.5 dithiothreitol (DTT); 0.2 PMSF; 4 μ g/ml aprotinin; 1 μ g/ml leupeptin), incubated on ice for 15 min, gently homogenized (40 strokes with a glass dounce), and diluted with an equal volume in a sucrose solution (in mM: 500 sucrose, 300 KCl, 10 Tris-HCl, pH 7.5; 0.5 DTT). The cells were homogenized again (20 strokes) and nuclei were pelleted (3,000x g for 15 min). The supernatants were adjusted to 0.6 M KCl and 1.5 mM EDTA and the microsomes were pelleted at 150,000x g for 30 min. The final pellets were resuspended in (in mM) 250 sucrose, 150 KCl, 20 CaCl₂, 0.5 DTT, 10 Tris-HCl, pH 7.5, assayed for protein concentration by a standard Bradford assay, adjusted to 1 mg/ml with resuspension buffer, aliquoted, and stored at -80°C.

SDS-PAGE and immunoblotting

Microsomes (2.5 μ g total protein) expressing each variant of PMCA2a were run on a 10% polyacrylamide gel and transferred to polyvinylidene difluoride (PVDF; Millipore, Billerica, MA) blotting membranes in 5% methanol and 10 mM CAPS, pH 10.5, at 100 V for 1 hr with cooling. To enhance protein mobilization from the acrylamide gel, we added 0.25 mg/ml hemoglobin to the pretransfer equilibration solution (10 mM CAPS, pH 10.5 with 5% methanol), as described previously (Gillespie and Gillespie, 1997). Following a 1 hr block in 5% Liquid Block (Amersham Biosciences, Buckinghamshire, England), the membranes were incubated with either 2 μ g/ml anti-PMCA2w or NR2 (a pan-PMCA2 antibody), followed by a 1:20,000 dilution of peroxidase-conjugated donkey anti-rabbit IgG (Jackson ImmunoResearch Laboratories, West Grove, PA). The membranes were incubated for 5 min with SuperSignal West Pico chemiluminescent substrate (Pierce Biotechnology) and exposed to film (X-Omat Blue, Kodak, Rochester, NY).

Immunofluorescence

COS-7 cells were grown to ~90% confluence on a coverslip in 24-well plates (Fisher Scientific) in DMEM supplemented with 10% fetal bovine serum (FBS) and penicillin/streptomycin. Cells were transfected with 0.5 μ g pJPA5-PMCA2a variant DNA using the TransIT-COS Transfection kit (Mirus, Madison, WI). After 48 hr, the cells were washed with PBS and fixed in 3% formaldehyde (16% stock, Ted Pella, Inc, Redding, CA) in PBS for 20 min. Following another wash in PBS, the cells were permeabilized for 15 min with 0.2 % saponin in blocking solution (3% normal donkey

serum (NDS) and 10 mg/ml bovine albumin serum (BSA)), and blocked for 40 min in blocking solution without detergent. The cells were incubated for 2 hr with primary antibody diluted in blocking solution (10 μ g/ml anti-PMCA2w or 2.5 μ g/ml NR2), washed in PBS, and then incubated with a secondary antibody, 7.5 μ g/ml Cy3-conjugated donkey anti-rabbit IgG (Molecular Probes, Eugene, OR) in blocking solution for 2 hr. Cells were washed in PBS, the coverslips were mounted with Vectashield (Vector, Burlingame, CA), and viewed with a Plan Apo 60x (numerical aperture, 1.40) oil lens on a Nikon Eclipse E800 upright microscope equipped with a Photometrics CoolSnap CCD camera and Metamorph Imaging system (version 6.1r4, Molecular Devices, Sunnyvale, CA).

Auditory and vestibular organs from postnatal day 21-23 rats were dissected in Minimum Essential Medium (MEM; Invitrogen) supplemented with 25 mM HEPES, pH 7.5 (N-(2-Hydroxyethyl)piperazine-N'-(2-ethanesulfonic acid)). Tissues were fixed, permeabilized, and blocked as described for COS cells. Tissues were incubated overnight with primary antibody diluted in blocking solution (10 μ g/ml anti-PMCA2w, 1:500 5F10 (ascites), 5 μ g/ml anti-horseradish peroxidase (HRP), or 5 μ g/ml anti-C8), washed in PBS, and then incubated with secondary antibodies (7.5 μ g/ml Cy3-conjugated donkey anti-rabbit IgG and Cy5-conjugated donkey anti-mouse IgG; Molecular Probes) and 0.25 μ M FITC-phalloidin (fluorescein isothiocyanate; Sigma, St Louis, MO) in the blocking solution for 2 hr. Tissues were washed in PBS, mounted with Vectashield, and viewed with a Plan Apo 60x (numerical aperture, 1.40) oil lens on a Nikon TE 300 inverted microscope with a Bio-Rad 1024 confocal imaging system (Hercules, CA). Acquired

images were processed with ImageJ (version 1.32j) and Photoshop (version 7.0; Adobe Systems, San Jose, CA).

Culturing and transfecting sensory epithelia

Inner ear sensory epithelia were harvested from postnatal day 3-5 rat pups in DMEM/F12 (Invitrogen). The cochlea was dissected away from the modiolus, Reissner's membrane was opened, and the tectorial membrane removed. The organ of Corti was cut into 2-3 pieces. The saccule, utricle and ampulla were also harvested and the overlying otoconia and membranes removed. The sensory epithelia were cultured in 24-well plates on collagen-coated coverslips in DMEM/F12 supplemented with 10% FBS and penicillin; cultures were maintained at 37°C and 5% CO₂. Tissues were cultured for 24 hr to allow firm attachment to the collagen substrate before transfection.

A Helios gene gun (Bio-Rad, Hercules, CA) was used to transfect cultures. Bullets were prepared by precipitating plasmid DNA onto 1- μ m diameter gold microcarriers at a ratio of 2 μ g DNA per 1 mg gold particles. The inner wall of Tefzel tubing was coated with the DNA-coated gold microcarriers and cut into individual bullets containing ~1 μ g of DNA. Cartridges were loaded into the bullet chamber of the gene gun, and a blast of helium gas was used to strip the inner wall of the tubing and bombard the culture with the gold microcarriers. For each culture, one cartridge of DNA microcarriers was shot using a pressure of 140 psi. A Bio-Rad diffusion screen was affixed to the gene gun and placed directly over the culture well.

The gold microcarriers contained two plasmids, enhanced green fluorescent protein (EGFP)-actin (Clontech laboratories, Inc. Palo Alto, CA) and one of the three C8-

tagged PMCA2a expression constructs. Cultures were fixed 24 hr after transfection using 4% paraformaldehyde in PBS for 25 min, permeabilized in 0.2% saponin for 15 min, and incubated for 1 hr in blocking solution (3% NDS, and 10 mg/ml BSA). Tissues were incubated overnight in primary antibody (2.5 μ g/ml mouse monoclonal C8 in blocking solution), washed in PBS, and incubated with secondary antibody (5 μ g/ml of either Cy3- or Rhodamine Red-X-conjugated donkey anti-mouse IgG) and 0.25 μ M Alexa 633 or 660 phalloidin (Molecular Probes). Tissues were again washed in PBS, mounted in Vectashield, and viewed by confocal microscopy as described for immunofluorescence.

MATERIALS AND METHODS II

Hair-cell isolation

Experiments were performed at room temperature on bullfrog (*Rana catesbeiana*) saccular hair cells. Each internal ear was dissected in low- Ca^{2+} saline solution (Table 2), the tissue over the saccular nerve was removed and the ear was incubated for 15 min in low- Ca^{2+} saline solution containing 1 mM EGTA. The saccular maculae were then dissected and subjected to a 20 min protease treatment (50 $\mu\text{g}/\text{ml}$, Sigma protease type XXIV, Sigma) and digested for 5 min with deoxyribonuclease I (DNase I, 50 $\mu\text{g}/\text{ml}$, Worthington Biochemical Corporation, Lakewood, NJ). The otolithic membrane was peeled away, then hair cells were dissociated with an eyelash and allowed to settle on glass coverslips treated with concanavalin A (1 mg/ml , Worthington).

Loading hair cells with pH sensitive dyes

Hair cells were loaded with the acetoxymethyl ester form of the pH-sensitive ratiometric dye 5-(and-6)-carboxylic acid seminaphthorhodamine-5F (SNARF-5F, Molecular Probes). The dye was resuspended at 1 $\text{nmol}/\mu\text{l}$ in chloroform, dispensed in 20 nmol aliquots, and air-dried in the dark for 2 hr. For each experiment a fresh solution of 20% (w/v) Pluronic F-127 (Molecular Probes) in DMSO was prepared and used to make a 2 mM dye stock solution. Two SNARF-5F loading-solutions, which contained <0.4% (v/v) DMSO, were made from the stock: 6 ml of 3.33 μM SNARF-5F in low- Ca^{2+} saline

TABLE 2. Ionic composition of solutions (mM)

Solutions	Na ⁺	K ⁺	Ca ²⁺	Mg ²⁺	Cl ⁻	NH ₄ ⁺	NMDG ⁺	EGTA	Glucose	HEPES
Standard	110	2	4	2	124	0	0	0	3	10
Low-Ca ²⁺	110	2	0.1	2	116	0	0	0	3	10
20 mM K ⁺	92	20	4	2	124	0	0	0	3	10
NH ₄ ⁺	85	2	4	2	124	25	0	0	3	10
NMDG ⁺	0	2	4	2	124	0	110	0	3	10
NH ₄ ⁺ /NMDG ⁺	0	2	4	2	124	25	85	0	3	10
NH ₄ ⁺ /15 mM K ⁺ /NMDG ⁺	0	15	4	2	124	25	72	0	3	10
low Na ⁺ /K ⁺	0	0	4	2	124	0	112	0	3	10
EGTA-SS	110	2	4	2	124	0	0	5	3	10

All solutions were adjusted to pH 7.25, and saturated with O₂

solution and 6 ml of 6.67 μ M SNARF-5F in standard saline solution. Two preparative steps were critical for sufficiently loading hair cells. First, the loading solutions were prepared immediately prior to use; while the sacculi were digesting in protease XXIV. Second, all the dye solutions were vortexed for 1 min and then sonicated in a bath sonicator for 1 min. To prepare the loading solutions, 100 μ l of the appropriate saline was added to the SNARF-5F stock solution then added to the final volume of saline solution to reach the desired concentrations of SNARF-5F.

To load hair cells, sacculi were incubated for 5 min with 3.33 μ M dye supplemented with DNase I (50 mg/ml) and allowed to recover for 5 min in fresh 3.33 μ M dye. Hair cells were isolated as described above. The low- Ca^{2+} dye solution was exchanged for standard saline solution containing 6.67 μ M SNARF-5F. After 20 min, the dye solution was replaced with standard saline solution. The solution was again changed with fresh standard saline solution 20-30 min later. For some experiments we used seminaphthorfluorescein-calcein (SNAFL-calcein), which was used in the same manner as SNARF-5F.

Confocal microscopy

Hair bundles from isolated hair cells were viewed with a Plan Apo 60x (numerical aperture, 1.40) oil lens on a Nikon TE 300 inverted microscope with a Bio-Rad MRC1024 confocal imaging system (Hercules, CA). SNARF-5F can be excited at 488 nm or 514 nm and has dual emission maxima at 580 nm (protonated) and 640 nm (unprotonated). Cells loaded with SNARF-5F were illuminated with 488 nm; emission was monitored at 570 nm (40 nm bandwidth) and 640 nm (40 nm bandwidth).

Ratio pixel values from hair bundles were converted to pH using:

$$\text{(Equation 1) } \text{pH} = \text{pK}_a - \log [(R - R_{\min}) / (R_{\max} - R)]$$

pK_a , R_{\min} , and R_{\max} were determined from an *in situ* pH calibration curve generated with solutions of pH 6-9 consisting of: (in mM) 130 KCl, 10 NaCl, 1 CaCl₂, 1 MgCl₂, 5 MES (2-[N-morpholino]ethanesulfonic acid), and 10 μM nigericin (Molecular Probes), a K^+/H^+ ionophore, which allows equilibration of intracellular and extracellular pH (Ikeda et al., 1992). Solutions were applied from acidic to basic, allowing at least one minute for equilibration. The standard curve was fit with the following equation:

$$\text{(Equation 2) } y = m3 + (m2 - m3) * 10^{M0} / (10^{m1} + 10^{M0});$$

$$M0 = \text{pH of calibration solution, } m1 = \text{pK}_a, m2 = R_{\max}, m3 = R_{\min}.$$

The fit is initially made with estimations of the R_{\max} , R_{\min} based on data collected from each experiment. A stock solution of 10 mM nigericin was made in DMSO, aliquoted, and stored in single use aliquots at -20°C.

Image analysis

Regions of interest (ROI) were drawn around the entire bundle, small areas of the soma, and outside the cell for a background reference. Images were acquired at 5-10 s intervals with TimeCourse, software available with the MRC1024 confocal imaging system. Data analysis was performed in Excel (version 11.1, Microsoft) and Kaleidagraph (version 3.6, Synergy Software). Data from the confocal imaging system were downloaded as spreadsheets consisting of the raw pixel data for each ROI. The background was subtracted from each channel and a running average was made from the

resulting ratio data; the middle value was averaged with the timepoint just preceding and just following. The pH was calculated from Equation 1 and all the values were normalized to the average resting pH. Time constants (τ) for pH change were calculated by exponential fits in Kaleidagraph. Equation 3 was used to calculate τ after the NH_4Cl is removed and Equation 4 was used to calculate τ of pH recovery.

$$\text{(Equation 3)} \quad y = \Delta\text{pH} * [\exp(-(M0-t_1)/m1)] + \text{pH}_a;$$

ΔpH = maximal drop in pH; $M0$ = calculated pH (Equation 1); t_1 = time the NH_4Cl is removed; $m1 = \tau$, left as a variable; pH_a = pH nadir

$$\text{(Equation 4)} \quad y = m2 * [1 - \exp(-(M0-t_2)/m1)] + \text{pH}_a;$$

$m2$ = final pH, left as a variable; $M0$ = calculated pH (Equation 1); t_2 = time the recovery starts; pH_a = pH nadir

The rates of recovery were calculated by dividing the concentration of the H^+ load by τ of recovery. The H^+ load is assumed to be 25 mM since we are loading with 25 mM NH_4Cl .

Pharmacological manipulation

All saline solution changes were done using bath exchange (Table 2 and Table 5). Saline solutions were prepared as 10x stocks, aliquoted, and stored at -20°C . All saline solutions were diluted in 18 Mohm water. Compounds listed in Table 5 (conditions 8-12) were obtained from Sigma (St. Louis, MO). DIDS (4,4'-diisothiocyanatostilbene-2,2'-disulfonic acid) was prepared in 0.1 M potassium bicarbonate at 100 mM; benzamil was made as a 28 mM stock in DMSO; bafilomycin A_1 was prepared as a 1.6 μM stock

solution in DMSO; ouabain was prepared in hot water as a stock solution of 85.5 mM. All compound stock solutions were diluted in NMDG⁺ saline for working concentrations.

cDNA synthesis from the mouse inner ear

The inner ears from postnatal day 14 Black-Swiss mice were dissected and frozen in liquid nitrogen. Approximately 1 g of tissue was ground with a frozen mortar and pestle in liquid nitrogen and transferred to a dounce for homogenization with 13 ml Tri-Reagent (Sigma). Crude homogenates were aliquoted and centrifuged at 16,000x g, supernatants were transferred to a fresh tube with 100 µl isopropanol per 1 ml aliquot, and re-centrifuged. Total RNA was precipitated with 0.5 ml isopropanol and washed with cold 70% ethanol. Mouse brain and kidney were collected at the same time; however, total RNA was isolated with a Qiagen RNeasy kit (Valencia, CA) following the standard protocol. First strand cDNA was synthesized from 100 µg total RNA primed with random hexamers using Superscript III reverse transcriptase (Invitrogen). The reaction was incubated at 25°C for 10 min, 50°C for 50 min, and terminated with a 5 min incubation at 85°C.

Amplifying NHEs from the mouse inner ear

Amino acid sequences of the four organellar NHEs (NHE6-9) and NHE1 were aligned, and non-conserved regions spanning introns were selected to design primers for amplification by polymerase chain reaction (PCR). Primers are listed in Table 3. The cycling conditions comprised 95°C for 90 s, 40 cycles of 94°C for 45 s, 60°C for 45 s,

72°C for 30 s, and final 5 min extension at 72°C. The annealing temperature to amplify mNHE9 was 64°C. All products were amplified using Taq DNA polymerase (Promega, Madison, WI.), cloned (TA cloning; Invitrogen), and sequenced.

Cloning mNHE6 and mNHE9

A full-length NHE9 cDNA was cloned by PCR from mouse inner-ear cDNA using primers listed in Table 3. EcoRI and HindIII sites were added to the 5' and 3' ends, respectively, to facilitate subsequent cloning into the pJPA5 vector. Mouse NHE9 was cloned into the EcoRI and HindIII sites downstream from the CMV promoter with a C8 epitope tag and EGFP. A mouse NHE6 cDNA clone was amplified in two parts. Taking advantage of a unique SfcI site near the middle of the cDNA (T1212 from ATG), EcoRI to SfcI and SfcI to HindIII fragments were amplified. The full-length cDNA was achieved by a three-part ligation into the EcoRI and HindIII sites of pJPA5 (no epitope tags). Phusion DNA polymerase (MJ Research) was used for each PCR. Mouse NHE9 was amplified with the following cycling conditions: 1 min 98°C, 35 cycles of 98°C for 15 s, 68°C for 30 s, 72°C for 60 s, and a final 5 min at 72°C. The 3' end of mNHE6 was amplified with similar conditions although the annealing temperature was 64°C. The 5' end of mNHE6 required the addition of 3% DMSO and annealing temperature of 66°C. All products were sequenced and confirmed by alignment to the mouse genome sequence.

TABLE 3. Primers for amplifying Na⁺/H⁺ exchangers

Name	Primer Sequence (5'-3')	Product
NHE1F(2067) NHE1R(2227)	TGGAGATGAAGCAGGCCATTGA TTTGCGGATCTCTTCCTCCTTGTC	160
NHE6F(845) NHE6R(948)	TCTCTTCGGGGAAAGTGTCTCAAT TAACGTCAAAGGTGTGGCTGTTGTC	103
NHE7F(1330) NHE7R(1435)	GCCCCATTTTCATCATCGGAG CCAATCTTATGCCTTCTGCCCA	105
NHE8F(595) NHE8R(752)	GCCACTATTGCGATTTTCAACGC TTGCCACCCACTGACATCTGACATA	158
NHE9F(1072) NHE9R(1437)	TGAGTTCCCGATGCTGGAGAC GGAATCTTCTGCTTTCTGCCCAG	365
<u>Full-length clones</u> mNHE6-Eco5'add mNHE6-SfcI3'	<u>GAATTCAAGACATGGCTGGGGCTC</u> GTTCTATGCTGAGACTCTGTAGACAAA	1222
mNHE6-SfcI5' mNHE6-Hnd3'add	GTCTACAGAGTCTCAGCATAGAAC <u>AAGCTTGCTTAGGCCGGACTGT</u>	898
mNHE9-Eco5'add mNHE9-Hnd3'add	<u>GAATTCATGGCTGGGCAGCTTCGGTTTAC</u> CAGA <u>AAGCTT</u> ATTAGTCCATCTGGGGTTGACC	1951

*Added restriction sites are underlined.

Generating a polyclonal NHE9 antibody

A synthetic peptide was designed from the mouse NHE9 sequence, including an added C-terminal cysteine residue (SPSPSSPTTKLALDQKSSGC), and was used for the production of antisera (Genemed Synthesis, Inc. South San Francisco, CA). Antibodies were affinity purified by coupling the antigenic peptide to SulfoLink resin (Pierce Biotechnology) via their terminal cysteine residues (1 mg peptide/ml resin).

Antisera were diluted with 10 vol of 25 mM Tris-HCl pH 8.0 and incubated with 0.5-1.0 ml peptide-resin overnight at 4°C. The resin was poured into a column and washed with 20 vol of 25 mM Tris-HCl, pH 8.0 and 10 vol of 500 mM NaCl/25 mM Tris-HCl, pH 8.0. Antibodies were eluted with 100 mM glycine, pH 2.5, followed by 100 mM CAPS, pH 10.5. Eluates were neutralized, pooled, and dialyzed against PBS containing 0.02% sodium azide.

Immunofluorescence

COS-7 cells were grown to ~90% confluence on a coverslip in 24-well plates in DMEM supplemented with 10% FBS and penicillin/streptomycin. Cells were transfected with 0.5 µg pJPA5.C8-mNHE9 or pJPA5-mNHE6 using 0.75 µl Fugene 6. After 48 hr, the cells were washed with PBS and fixed in 3% formaldehyde in PBS for 20 min. Following another wash in PBS, the cells were permeabilized for 15 min with 0.2 % saponin in blocking solution (3% NDS and 10 mg/ml BSA in PBS), and blocked for 40 min in blocking solution without detergent. The cells were incubated for 2 hr with

primary antibody diluted in blocking solution (5 $\mu\text{g/ml}$ anti-NHE9, anti-NHE6, or anti-C8), washed in PBS, and then incubated with a secondary antibody, 7.5 $\mu\text{g/ml}$ Cy3-conjugated donkey anti-rabbit IgG or 7.5 $\mu\text{g/ml}$ Alexa 488-conjugated donkey anti-mouse IgG (Molecular Probes) in blocking solution for 2 hr. Cells were washed, mounted, and viewed as described for immunofluorescence METHODS I.

Bullfrog sacculi were dissected in standard saline (Table 2). Hair cells were isolated as described above (see **Hair-cell isolation**). Tissue and dissociated cells were fixed, permeabilized, and blocked as described for COS cells. Tissues and cells were incubated overnight at room temperature with primary antibody (10 $\mu\text{g/ml}$ anti-NHE6 or anti-NHE9, 1:500 5F10 (ascites)) in the blocking solution, washed in PBS, and incubated with a secondary antibody (7.5 $\mu\text{g/ml}$ Cy5-conjugated donkey anti-rabbit IgG, Alexa 488-conjugated goat anti-rabbit IgG, or Rhodamine RedX-conjugated goat anti-mouse IgG; Molecular Probes) and 0.25 μM FITC-phalloidin (Sigma) or Alexa 660-conjugated phalloidin (Molecular Probes) in blocking solution for 2 hours. In some experiments, sacculi were co-labeled with an antibody against the calcium-binding protein calretinin (1:250, Chemicon, Temecula, CA). Cells and tissues were washed in PBS, mounted with Vectashield (Vector), and viewed with a Plan Apo 60x (numerical aperture, 1.40) oil lens on a Nikon TE 300 inverted microscope with a Bio-Rad 1024 confocal imaging system (Hercules, CA). Acquired images were processed with ImageJ (version 1.32j) and Photoshop (version 7.0; Adobe Systems, San Jose, CA).

Auditory and vestibular organs from postnatal day 21 rats were dissected in MEM supplemented with 25 mM HEPES, pH 7.5. Tissues were fixed, permeabilized, and blocked as described for COS cells, except in some experiments normal goat serum was

substituted for normal donkey serum. Tissues were incubated overnight with primary antibody (10 $\mu\text{g/ml}$ anti-NHE6 or anti-NHE9, 1:500 5F10) diluted in the blocking solution, washed in PBS, and incubated with a secondary antibody (7.5 $\mu\text{g/ml}$ Cy5-conjugated goat anti-rabbit IgG, Alexa 488-conjugated goat anti-rabbit IgG, Rhodamine RedX-conjugated goat anti-mouse IgG or Alexa 488-conjugated goat-anti-mouse IgG; Molecular Probes) and 0.25 μM FITC-phalloidin, TRITC-phalloidin (tetramethylrhodamine B isothiocyanate; Sigma), or Alexa 660-conjugated phalloidin (Molecular Probes) in blocking solution for 2 hours. Tissues were washed in PBS, mounted with Vectashield (Vector), viewed and processed as described for PMCA2w.

Antigenic peptide competition

Primary antibody was incubated for 1 h at room temperature in the presence of 5 μg antigen peptide per 1 μg antibody prior to applying complex to the tissue.

Immunoprecipitation

Frog hair-bundle isolation

Bullfrog sacculi were isolated in standard saline in the presence of 0.2 mM PMSF. The otoconia and otolithic membrane were removed and tissues were incubated for 30 min at room temperature in 0.5 mg/ml NHS-PEO₄-Biotin (Pierce Biotechnology) prepared in standard saline at pH 8.0 with 0.2 mM PMSF. Following several washes in 50 mM Tris-HCl pH 8.0 to stop the biotinylation reaction, hair bundles were purified by using the twist-off technique (Gillespie and Hudspeth, 1991). Briefly, a coverslip with a

teflon ring was dotted with 1 μ l aliquots of Cell-Tak (BD Biosciences, Bedford, MA); the Cell-Tak was allowed to air-dry and the process repeated. Within 5 min of drying, the Cell-Tak was thoroughly rinsed with deionized water and sacculi were affixed to the Cell-Tak under standard saline. The saline-filled chamber was transferred to a bath of standard saline at 34°C and equilibrated for 3-4 min. The warm saline filled chamber was then transferred to a Petri dish and 3% molten agarose (34°C) was poured over the sacculi. After a minute, the Petri dish was transferred to 4°C for 10 min. The agarose was quickly twisted within the ring, causing the bundles to shear from the residual macula. The agarose-embedded bundles were perfused with standard saline containing protease inhibitors (0.2 mM PMSF, 0.5 μ g/ml leupeptin, 0.5 μ g/ml pepstatin A) while any remaining macula and the surrounding agarose were cleaned away. For each experiment, we estimated the number of saccular equivalents, also called ear equivalents, of bundles that were isolated; one saccular equivalent is 100% recovery. Agarose-embedded bundles and maculae were sonicated in separate tubes for 20 s in 5 μ l/ear equivalent of extraction buffer (in mM: 60 HEPES pH 7.4, 150 NaCl, 3 KCl, 5 EDTA, 3 EGTA, 0.2 PMSF, 1% Triton X-100, 0.1 mg/mL hemoglobin, 0.1 mg/mL BSA) and incubated at 4°C for 30 min, gently flicking the tube at 15 min. Detergent-soluble proteins were isolated by centrifuging samples for 30 min at 12,000x g. Extracts were incubated overnight with 2 μ g of affinity-purified anti-NHE6, 2 μ g of anti-HRP (Jackson ImmunoResearch Laboratories), or 1:500 dilution of 5F10. For peptide competition, 10 μ g of NHE6 peptide was incubated with 2 μ g anti-NHE6 at room temperature for 1 h prior to adding to the extracts. The volume for the overnight incubation was approximately 20-40 μ l. Immune complexes were precipitated by adding 15 μ l of Protein-G Plus agarose (Santa

Cruz Biotechnology, Inc, Santa Cruz, CA) and incubating for 2 h at room temperature with gentle agitation. The volume was increased to 500 μ l with extraction buffer and the complexes were incubated 1 h at room temperature with rotation. The precipitant was washed with four 1 ml aliquots of extraction buffer and one time with extraction buffer without Triton X-100. The immune complexes were recovered by incubating at room temperature for 5 min in an SDS-PAGE sample buffer that included 2% SDS and 100 mM DTT; this step was repeated and the two eluates combined.

COS-7 cell lysates

COS-7 cells were grown to ~90% confluence in 35-mm plates (Fisher Scientific) using DMEM (Invitrogen) supplemented with 10% FBS and penicillin/streptomycin. Cells were transfected with 1 μ g pJPA5-C8-EGFP-mNHE9, pJPA5-mNHE6, or 0.5 μ g of each plasmid using 6 μ l Fugene 6. After 48 hr, the cells were washed three times in cold PBS and incubated for 10 min with rocking at 4°C with 0.5 ml per plate of 1% n-dodecyl- β -D-maltoside (DM, Dojindo Molecular Technologies, Gaithersburg, MD) in PBS with protease inhibitors (0.2 mM PMSF, 4 μ g/ml aprotinin, 1 μ g/ml leupeptin). The cells were harvested into a 1.7 ml microfuge tube and agitated for 30 min at 4°C. The lysates were centrifuged at 12,000x g for 10 min at 4°C to pellet the nuclei. The supernatants were transferred to clean tubes and quantitated by a bicinchoninic acid (BCA) assay. Equal amounts of protein were aliquoted into fresh tubes, brought to equal volumes (500 μ l) with the lysis solution and incubated overnight at 4°C with 2 μ g of anti-NHE6, anti-NHE9, or anti-C8. Immune complexes were precipitated by adding 15 μ l of Protein-G Plus agarose (Santa Cruz Biotechnology, Inc, Santa Cruz, CA), incubating for

2 h at room temperature with gentle agitation. The beads were pre-washed three times with 0.1% DM in PBS. The precipitant was washed with four 1 ml aliquots of 0.1% DM in PBS and one time with PBS alone. The immune complexes were recovered by incubating at room temperature for 5 min in an SDS-PAGE sample buffer that included 2% SDS and 100 mM DTT. This step was repeated and the two eluates were combined.

Rat hair-bundle isolation

There were only minor modifications of the frog bundle isolation protocol made for rat tissue. Sacculi and utriculi from postnatal day 5 Sprague Dawley rats were dissected in MEM supplemented with 25 mM HEPES. The otoconia and otolithic membrane were removed and hair bundles were purified by using the twist-off technique, although for rat we used 4% low-melting agarose at 37°C. The bundles were cleaned during HEPES/MEM perfusion. The agarose-embedded bundles were incubated at room temperature in sample buffer with 100 mM DTT and loaded onto a 15% acrylamide gel with forceps. The macular proteins were extracted as described for frog. Electrophoresis and blotting protocols are described below.

Preparing microsomes expressing NHEs

COS-7 cells were grown to ~90% confluence in 10-cm plates using DMEM supplemented with 10% FBS and penicillin/streptomycin. Cells were transfected with 17.5 µg pJPA5-HA-hNHE6 plasmid, using 35 µl Fugene 6. The cells were washed and harvested as described. There were a few modifications to the NHE microsome

procedure. The cells were pelleted and resuspended in an ice-cold hypotonic solution (in mM: 20 HEPES, pH 7.2; 1 MgCl₂; 1 EGTA; 2 DTT; 0.2 PMSF; 4 µg/ml aprotinin; 1 µg/ml leupeptin), incubated on ice for 15 min, and diluted with an equal volume in a sucrose solution (in mM: 500 sucrose, 280 KCl, 20 HEPES, pH 7.2; 1 MgCl₂; 3 EGTA; 2 DTT, 4 CaCl₂, 4 ATP). The cells were gently homogenized (30 strokes) and centrifuged at 3,000x g for 15 min. The microsomes were pelleted at 150,000x g for 30 min. The final pellets were resuspended in 0.25 M sucrose, 0.14 M KCl, 20 mM HEPES, pH 7.2, 2 mM CaCl₂, 2 mM ATP, 2 mM DTT, assayed for protein concentration by a standard Bradford assay, aliquoted, and stored at -80°C.

SDS-PAGE and immunoblotting

Proteins were separated by SDS-PAGE on 10%-15% acrylamide gels with a 150:1 acrylamide-to-bisacrylamide ratio and were transferred to PVDF blotting membranes as described previously. Membranes were blocked for 1 h in 5% Liquid Block prepared in PBS. Biotinylated proteins were detected with alkaline phosphatase coupled to avidin (AVIDx-AP; Tropix, Bedford, MA) at a dilution of 1:5000 in 5% Liquid Block. Alkaline phosphatase activity was detected by a 5 min incubation in 0.1 mM of the chemiluminescent reagent CSPD (disodium 2-chloro-5-(4-methoxyspiro(1,2-dioxetane-3,2'-(5'-chloro)-tricyclo[3.3.1.3⁰.7]decan)-4-yl)-1-phenyl phosphate; Tropix), prepared in assay buffer (in mM: 50 2-amino-2-methyl-1-propanol, 1 MgCl₂, PBS) and 10% Sapphire (Tropix), an enhancing reagent.

If proteins were to be directly detected with antibody, 1 mL of blocking solution was removed from the membranes as primary antibody diluent. The diluted antibody was

added to the remaining solution on the membrane and incubated for 2 h at room temperature with gentle rocking. Primary polyclonal antibodies were used at a concentration of 2 µg/ml and monoclonal antibodies were used at 0.2 µg/ml (anti-C8 and anti-HA). Following 3 x 5 min washes in PBS/0.3% Tween, the membranes were incubated for 2 h with peroxidase-conjugated donkey anti-rabbit IgG or peroxidase-conjugated donkey anti-mouse IgG (Jackson ImmunoResearch Laboratories) diluted 1:20,000 in blocking solution. Membranes were washed 5 x 5 min in PBS/0.3% Tween and peroxidase activity was detected by a 5 min incubation with SuperSignal West Pico chemiluminescent substrate (Pierce Biotechnology). Immunoblots were exposed to film (X-Omat Blue, Kodak).

Molecular weight markers

Perfect Protein Markers (10-225kDa, Novagen, Madison, WI) and Benchmark Prestained Protein Ladder (Invitrogen) markers were used in all gels. Perfect Protein Markers were detected with S-protein conjugated to alkaline phosphatase, diluted 1:10,000 or S-protein conjugated to peroxidase, diluted 1:20,000.

Membrane fractionation from mouse brain

Mouse brain including cerebellum, but without any brain stem, was dissected and immediately transferred to ice cold HEPES/sucrose (HS) solution (in mM: 320 sucrose, 10 HEPES pH 7.4, 0.2 PMSF, 4 µg/ml aprotinin, 1 µg/ml leupeptin, 1 µg/ml pepstatin A, 1 mM EGTA). Two brains per 10 ml HS were homogenized with 30 strokes using a

rotating pestle on a glass/Teflon homogenizer. The homogenate was centrifuged for 10 min at 900x g and the supernatant carefully removed to a 70Ti tube. To extract more membranes, the pellet was resuspended in HS and spun again for 10 min at 900x g; both supernatants were pooled. The crude membrane supernatant was centrifuged for 15 min at 10,000x g. The supernatant contained “light membranes” or LM. The LM supernatant was pelleted in 70Ti tubes at 45,200 rpm (150,000x g) for 30 min. The LM pellet was resuspended thoroughly in HS (0.2-0.4 ml/brain). Ten micrograms of protein was run on a SDS gel and immunoblotted as described above.

Amino-acid alignments

Amino-acid alignments were created with MegAlign software using the ClustalV algorithm (DNASTAR, Inc., Madison, WI). Amino-acid sequence similarities (Table 4) were generated from Vector NTI Suite 7 software using the AlignX module with the ClustalW algorithm (Invitrogen).

Antibodies

Primary antibodies used for this dissertation were obtained from the following: C8, gift of Dr. T. Strassmaier; NHE6, gift of Dr. M. Sakaguchi; NHE8, gift of Dr. P. Aronson; NR2 and PMCA2w antisera, gift of Dr. E. Strehler; NHE6 and NHE7, Alpha Diagnostics (San Antonio, TX); 5F10, Affinity Bioreagents (Golden, CO); horseradish peroxidase (HRP), Jackson ImmunoResearch Technologies (West Grove, PA); calretinin,

Chemicon (Temecula, CA); hemagglutinin (HA), Roche Applied Science (Indianapolis, IN).

Animals

Bullfrogs (*Rana catesbeiana*) were obtained from Rana Ranch (Twin Falls, ID) or Niles Biological (Sacramento, CA). All mice were from The Jackson Laboratory (Bar Harbor, ME) and rats were supplied by Charles River Laboratories, Inc (Wilmington, MA). All animals were maintained in OHSU facilities by personnel in the Department of Comparative Medicine. Procedures involving animals were evaluated and approved by the Institutional Animal Care and use Committee in keeping with the guidelines established by the National Institutes of Health.

Acknowledgements for methods

Thank you to Dr. Meredith LeMasurier for constructing the pJPA5-C8 vector, correcting the nucleotide deletion, and sub-cloning PMCA2z/a. Dr. LeMasurier also made the heroic effort of isolating hundreds of ear equivalents of rat hair bundles and maculae and painstakingly loaded the gel; she generously provided the blot for NHE localization. I also thank Dr. Timothy Strassmaier for preparing the mouse brain membranes used for the NHE immunoblots. I am grateful to Dr. Diane Ronan for the inner-ear epithelia cultures, gene-gun transfections, and gene gun images reported here. And finally, thank you to Bethany Johnson for assistance with constructing PMCA2w/a and PMCA2x/a expression vectors.

RESULTS I

Generation of antibodies specific to PMCA2a splice A variants

To localize splice A variants of PMCA2a, we generated polyclonal antibodies to use for immunocytochemistry. Since the peptides used for PMCA2x and PMCA2z are found within PMCA2w, we attempted to generate selective antibodies by performing sequential negative and positive affinity selection with short peptides corresponding to the regions that span the splicing site in PMCA2x/a or PMCA2w/a (Figure 15). This protocol did not yield any functional “x”- or “z”-specific antibodies (data not shown). Using a peptide specific for the “w” variant, however, we successfully purified antibodies specific to PMCA2w.

COS-7 cell lysates expressing PMCA2w/a, PMCA2x/a, or PMCA2z/a were immunoblotted with an antibody against PMCA2w or a pan-PMCA2 antibody, NR2 (Figure 16). NR2 detects a band of apparent molecular weight of 150 kDa (PMCA) in lysates expressing PMCA2w/a and PMCA2z/a; the low molecular weight bands detected in the PMCA2x/a lane suggests this variant is not stable in COS-7 cells. In contrast, the PMCA2w antibody recognizes the 150 kDa band only from PMCA2w/a COS cell lysates. The specificity of the PMCA2 antibody was also demonstrated by immunocytochemistry. Again, anti-PMCA2w only detects the “w”-variant of PMCA2a when expressed in COS-7 cells (Figure 16).

Figure 15. Splice site A variants of PMCA2. Bullfrog splicing region A variant PMCA2v (fPMCA2v) aligned with rat PMCA2 splice region A variants “w”, “x”, and “z” (rPMCA2w, rPMCA2x, rPMCA2z, respectively). The peptides used for affinity purification of variant-specific antibodies are underlined. The 12 aa of the “v” sequence that interrupts the sequence of the “w” variant is indicated with a grey highlight. The human PMCA2 (hPMCA2) peptide sequences used for immunizing rabbits are shown in grey above each rat variant sequence for comparison.

fPMCA2v EDE-KKDKKGKKNQDGASLPVGSTHPPSHPPAATDGAAGANVTDNANANLVNGKMQDGNVGTIQNKAKQQDGAAA

hPMCA2w

GDGLQLP-----AADGAAASNAADS

rPMCA2w EEEEEKKDKKGVKKGDGLQLP-----AADGAAPANAAGSANA SLVNGKMQDGSADSSQSKAKQQDGAAA

hPMCA2x

DDKKG-----KMQDGNVDA

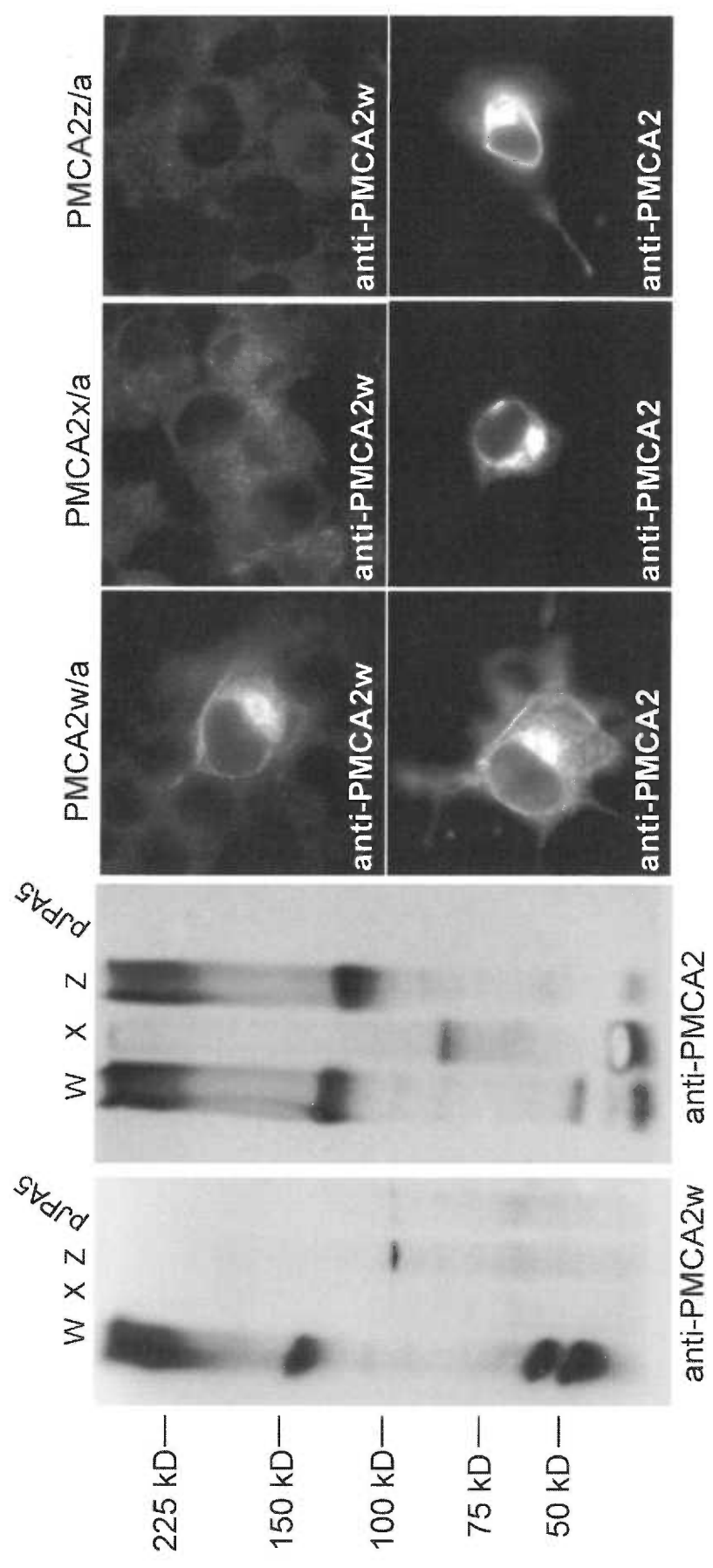
rPMCA2x EEEEEKKDKKGVKKG-----KMQDGSADSSQSKAKQQDGAAA

hPMCA2z

DDKK-----AKQQDGAAA

rPMCA2z EEEEEKKDKK-----AKQQDGAAA

Figure 16. Immunodetection with PMCA2w-specific antibody. Immunoblot of microsomes expressing the “w”, “x”, or “z” variant of PMCA2a. Anti-PMCA2w only detects the predicted 150-kDa band of PMCA2w/a. NR2, a polyclonal antibody against the N-terminus of PMCA2 verifies that PMCA2w/a and PMCA2z/a are expressed, however PMCA2x/a is likely an unstable variant. Blank microsomes transfected with the pJPA5 vector alone were run as a negative control. The PMCA2w antibody also works by immunocytochemistry in COS-7 cells, recognizing PMCA2w/a but not the other two variants.



Localization of PMCA2w in the rat inner ear

The PMCA2w-specific antibody was used to detect this variant in rat auditory and vestibular organs (Figures 17 and 18). Hair bundles of outer hair cells were labeled intensely by the “w”-specific antibody (Figure 17). The tissues were co-labeled with the pan-PMCA antibody, 5F10, which labels the outer hair cell bundles as well as the somata of the inner hair cells. The soma labeling was previously shown to be PMCA1x/b (Dumont et al., 2001). Also consistent with Dumont et al. is the paucity of PMCA labeling in the cell bodies of outer hair cells as well as the bundles of inner hair cells. There is some PMCA2w labeling in a ring at the apical surface, the pericuticular necklace, of the inner-hair cells (bottom row).

As in the auditory system, hair bundles of the vestibular organs intensely labeled with anti-PMCA2w (Figure 18). Because the morphology of the ampulla lends itself to clear lateral presentations of hair cells (top row), one can easily see the intense labeling of the hair bundles by anti-PMCA2w and 5F10. In addition, we observed “w”-specific labeling in the region of the cuticular plate (asterisk, upper right panel), which was consistent with the intense labeling seen in the pericuticular necklace of utricular hair cells (arrowheads, middle row). For each of these features, labeling was specific; no labeling was observed with an irrelevant primary antibody.

Figure 17. Localization of PMCA2w in rat organ of Corti by immunofluorescence.

Confocal cross sections through the adult rat organ of Corti (P21). *Left column*, PMCA2w; *middle left column*, PMCA (5F10); *middle right column*, actin (phalloidin); *right column*, combined PMCA2w (green), PMCA (blue), actin (red). Hair bundles of outer hair cells were intensely labeled with anti-PMCA2w (top row); however, there is little or no labeling in the somata (middle row, same tissue optical plane is 12 μm lower). PMCA2w immunoreactivity in inner hair cells is restricted to the pericuticular necklace (arrow); there is little to no labeling in the bundles or somata (bottom row, different tissue). The cell bodies of the inner hair cells, however, label intensely with the pan-PMCA antibody 5F10 (arrowheads, top and bottom rows); this immunoreactivity is PMCA1x/b (Dumont et al., 2001). Scale bars are each 10 μm for each row.

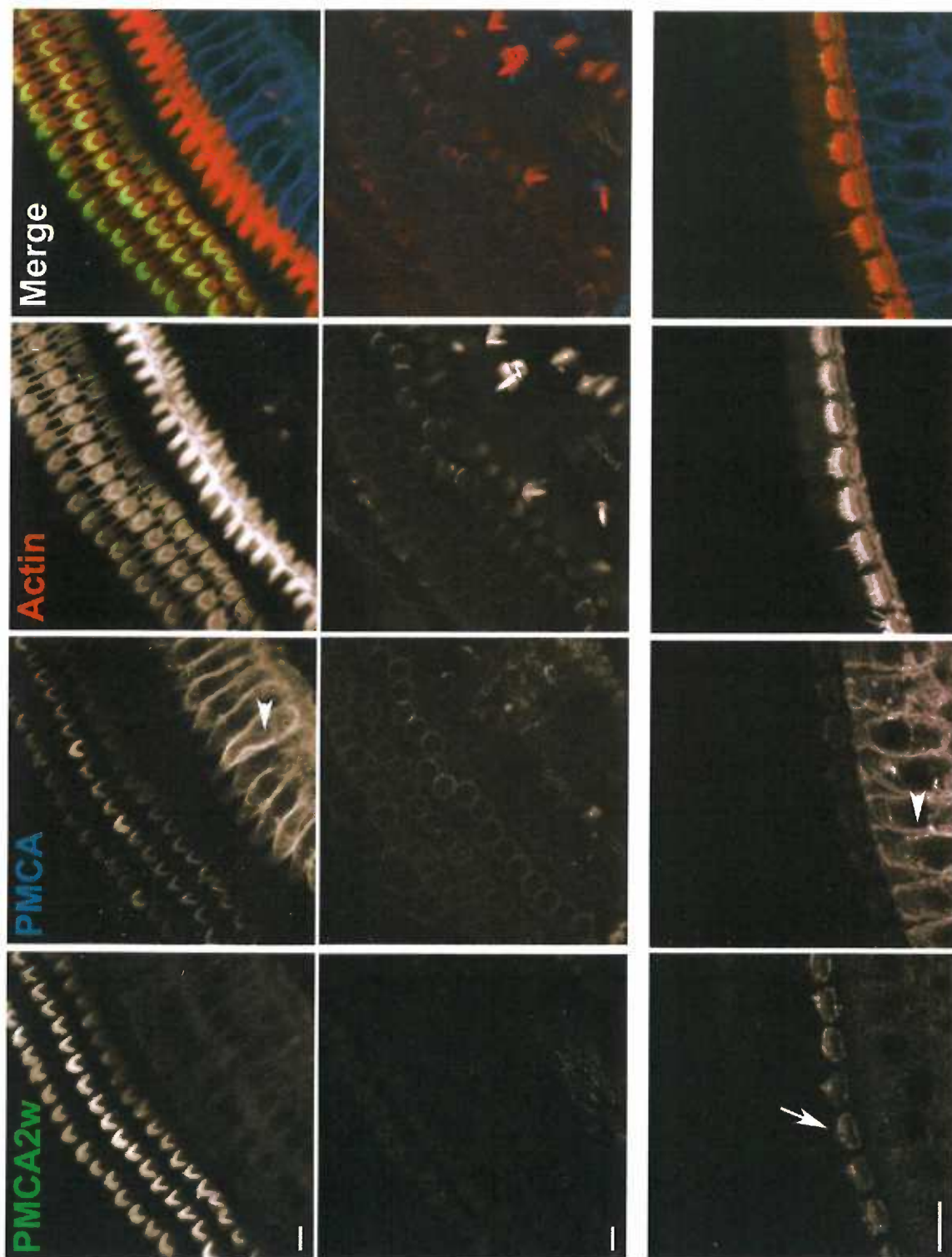
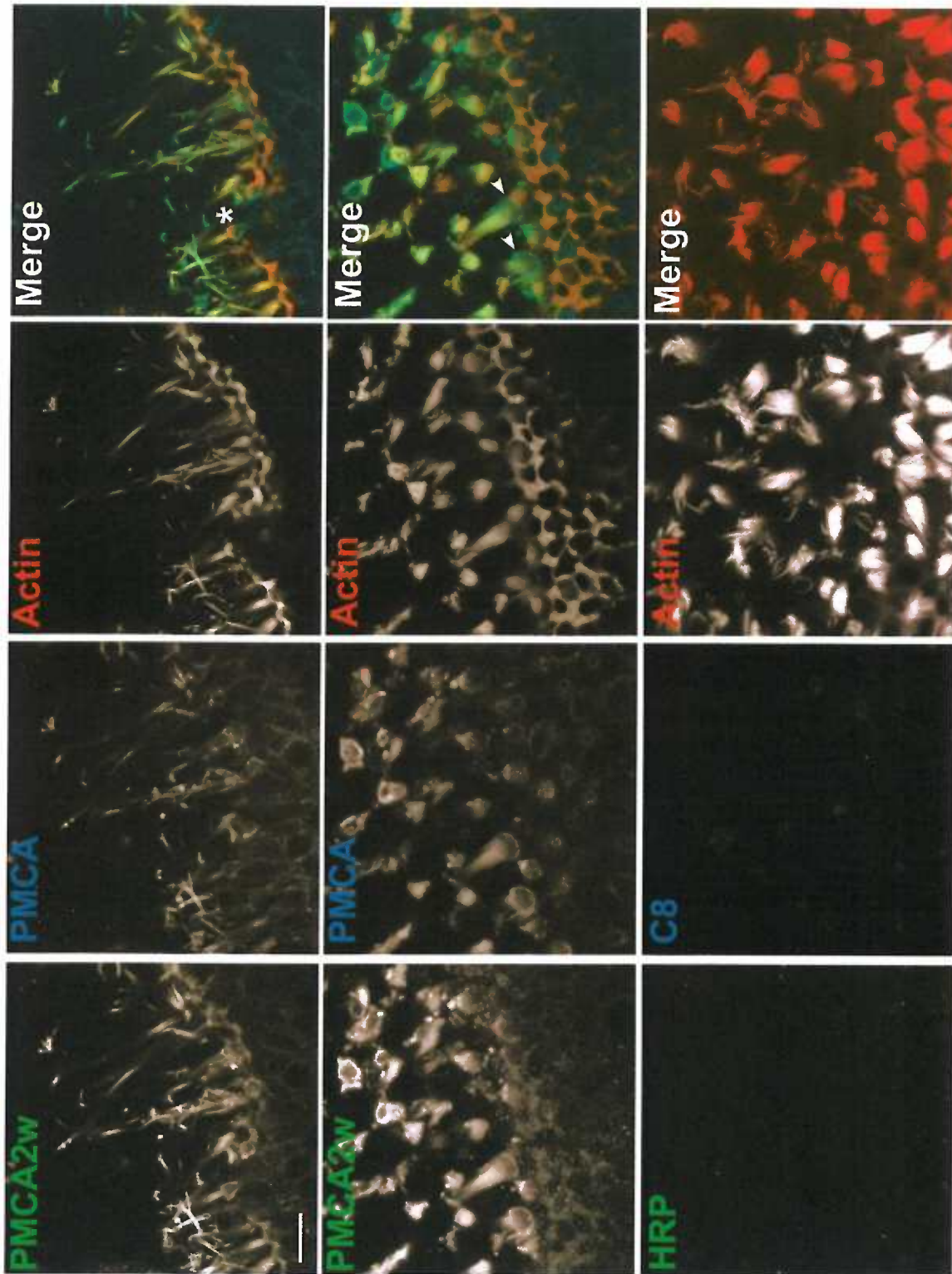


Figure 18. Localization of PMCA2w in rat vestibular organs by immunofluorescence. Cross sections through the rat ampulla (top row) and utricle (middle and bottom rows). For the top two rows, *Left column*, PMCA2w; *middle left column*, PMCA (5F10); *middle right column*, actin (phalloidin); *right column*, combined PMCA2w (green), PMCA (blue), actin (red). Hair bundles of both vestibular organs were intensely labeled with anti-PMCA2w; however, there is no labeling in the somata. There is PMCA2w labeling in the pericuticular necklace of utricular hair cells (middle row, arrowheads) as well as in the apical region of a few hair cells of the ampullae (top row, asterisk). The bottom row shows background labeling with two irrelevant antibodies, anti-horseradish peroxidase (HRP), a polyclonal antibody control for PMCA2w and anti-C8, a monoclonal antibody control for 5F10. Scale bar is 10 μm for the entire figure.



Expression of PMCA splice A variants in rat inner ear

Further experiments were undertaken to investigate the expression of PMCA2w/a, as well as PMCA2x/a and PMCA2z/a in rat hair cells. We previously determined that hair cells primarily express PMCA1x/b in their basolateral membranes and since we were not able to detect PMCA2x by RT-PCR, we believe that the 2x/a variant is not a major component of hair cells. To determine whether the A splice region would have an effect on targeting, we generated the “w”, “x”, and “z” splice A variants in the context of the splice site C variant “a”. We used gene-gun transfection to introduce the C8 epitope-tagged PMCA splice forms into hair cells. To facilitate locating the transfected cells, we co-transfected with EGFP-actin, previously shown to incorporate into stereocilia actin cores (Schneider et al., 2002).

Consistent with the immunocytochemistry results, PMCA2w/a was transported exclusively to hair bundles of rat auditory and vestibular organs (Figure 19). In one example (Figure 19, top row), EGFP-actin, which targets to the basolateral membrane as well as the stereocilia, clearly demarks the soma of a transfected outer hair cell; there is no expression of PMCA2w/a-C8 in the soma. By contrast, PMCA2x/a-C8 labeling was diffuse throughout the soma, indicating expression in intracellular membranes (Figure 20). EGFP-actin expression was distinctly annular, demarking the plasma membrane. Although PMCA2z/a is transported to the plasma membrane, it is excluded from the hair bundle and targeted strictly to the basolateral membrane (Figure 21). Unlike the diffuse labeling of PMCA2x/a-C8, PMCA2z/a-C8 expression colocalized with EGFP-actin in the

soma. In a few cells we could detect faint expression of PMCA2z/a or PMCA2x/a in the bundle, but only in the presence of PMCA2-C8 expression in the soma; in contrast, even in the presence of high bundle expression, PMCA2w/a was never observed in the basolateral membrane.

Figure 19. Expression of PMCA2w/a-C8 in rat hair bundles following gene gun transfection. Two outer hair cells (top and middle rows) and one utricular hair cell (bottom row) show bundle-specific PMCA2w/a-C8 expression when detected by C8 immunoreactivity 24 h after gene gun transfection. *Left column*, epithelia were labeled with anti-C8 to detect the epitope tagged PMCA2w/a. *Middle left column*, hair cells were co-transfected with EGFP-actin; *middle right column*, phalloidin labeled actin; *right column*, combined PMCA2w/a-C8 (green), EGFP-actin (blue), phalloidin-actin (red). PMCA2w/a is exclusively transported to the hair bundle. The punctate anti-C8 labeling in the top row is likely PMCA2w/a in vesicles caused by over expression, whereas the puncta in the middle row are background from the secondary antibody used to detect the C8 epitope tag. Scale bars are 5 μ m for each row.

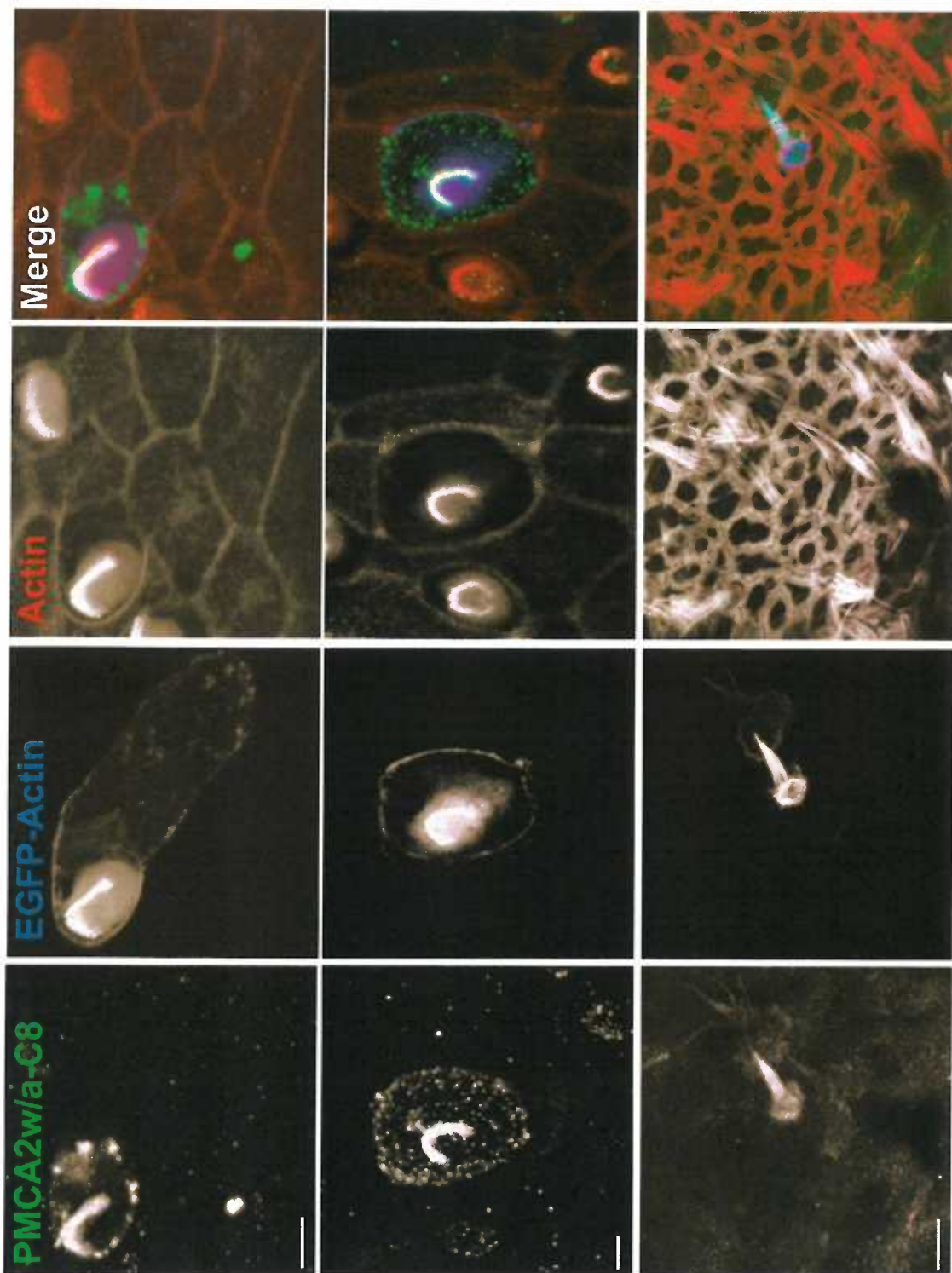


Figure 20. Expression of PMCA2x/a-C8 in rat vestibular hair cells following gene gun transfection. PMCA2x/a-C8 is expressed in intracellular membranes of a utricular hair cell. The diffuse intracellular labeling does not colocalize with the plasma membrane expression of EGFP-actin. *Left column*, epithelia were labeled with anti-C8 to detect the epitope tagged PMCA2x/a. *Middle left column*, hair cells were co-transfected with EGFP-actin; *middle right column*, phalloidin labeled actin; *right column*, combined PMCA2x/a-C8 (green), EGFP-actin (blue), phalloidin-actin (red). *Top row*, bundle with cuticular plate. *Middle row*, 8 μm lower, upper-soma. *Bottom row*, 6 μm lower, mid nucleus. Scale bar is 5 μm for the entire figure.

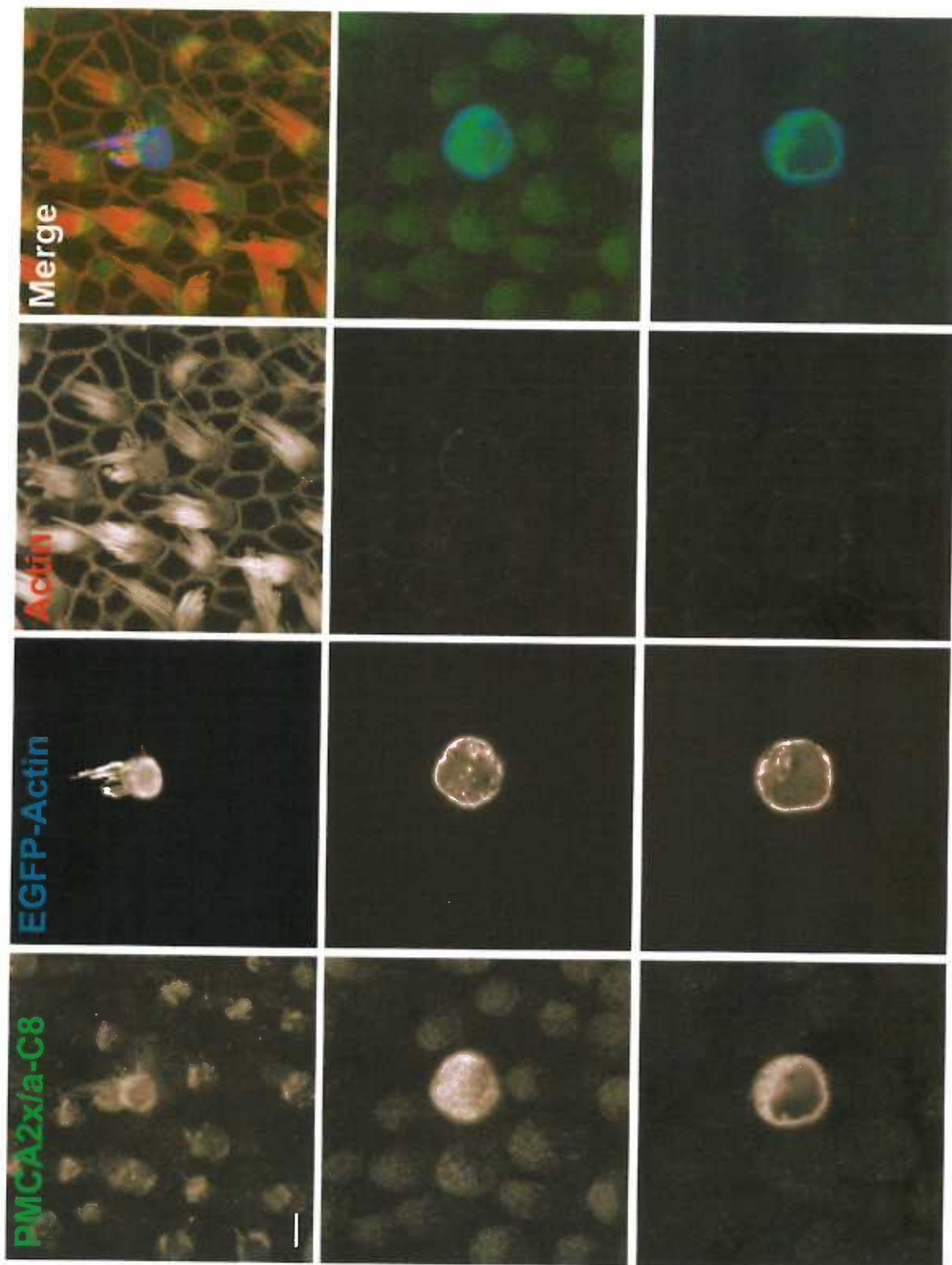
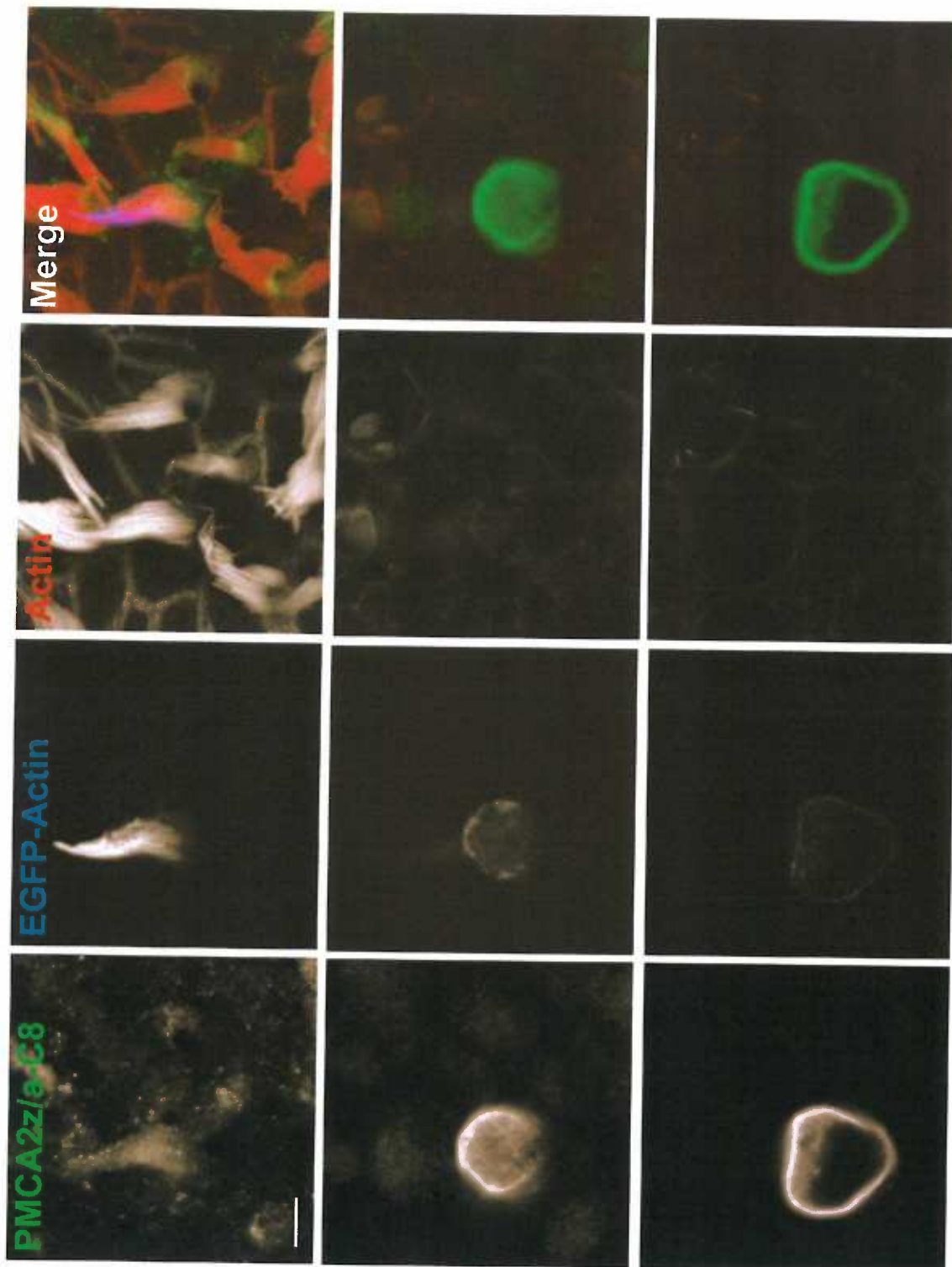


Figure 21. Expression of PMCA2z/a-C8 in basolateral membranes of rat vestibular hair cells following gene gun transfection. PMCA2z/a-C8 is transported to the basolateral membrane of a utricular hair cell; colocalizing with the plasma-membrane associated EGFP-actin. The EGFP-actin is not very strong in the soma of this cell; in the merge panel the EGFP signal is occluded by the intense C8 labeling. *Left column*, epithelia were labeled with anti-C8 to detect the epitope tagged PMCA2z/a. *Middle left column*, hair cells were co-transfected with EGFP-actin; *middle right column*, phalloidin-labeled actin; *right column*, combined PMCA2z/a-C8 (green), EGFP-actin (blue), phalloidin-actin (red). *Top row*, bundle. *Middle row*, 6 μm lower, upper-soma. *Bottom row*, 12 μm from bundle, mid-nucleus. Scale bar is 5 μm for the entire figure.



DISCUSSION I

PMCA isozymes are differentially localized in rodent auditory and vestibular epithelia; the predominant forms are PMCA1 in the soma and PMCA2 and in the bundle (Dumont et al., 2001). We initially characterized splice site C variants of PMCA2 in rat bundles, identifying PMCA2a as the bundle isoform (Dumont et al., 2001). We have now further defined a targeting sequence in PMCA2 necessary for dictating hair bundle localization: the “w” sequence, which is created by alternative splicing at region A. These results establish that the rodent hair-bundle calcium pump is PMCA2w/a.

Role of splice site C in regulation and targeting of PMCA

Splicing at the C-terminus modifies the affinity of PMCA for calmodulin, a potent activator of PMCA activity. PMCA2b has a 10-fold higher affinity for calmodulin than PMCA2a (Enyedi et al., 1991), although this difference is presumably irrelevant in the hair bundle, given the bundle's calmodulin concentration of 70 μ M (Walker et al., 1993). Moreover, because the “b” variants are known to interact with PDZ domains (DeMarco et al., 2002; Kim et al., 1998), conjecture held that this region would also be responsible for targeting. PDZ domains are known to be involved in targeting and retention of several membrane proteins (Fanning and Anderson, 1999; Hung and Sheng, 2002).

Splice site A is necessary for apical targeting

Despite cogent evidence suggesting that splice site C codes for targeting and regulation of PMCA, this study establishes the necessity of splice region A for PMCA

targeting in hair cells. These data are consistent with the following recent isoform detection and cellular localization studies. The apical surface of lactating mammary epithelia is enriched for PMCA2, where PMCA2 is posited to play an essential role in Ca^{2+} transport into the milk. RT-PCR analysis demonstrates that the predominant form of PMCA2 in this polarized epithelium is PMCA2w/b (Reinhardt et al., 2000; Reinhardt and Horst, 1999; Reinhardt et al., 2004). Furthermore, we demonstrated frog hair bundles are enriched for the PMCA2v/a isoform (Dumont et al., 2001). The novel “v” variant has only been identified in frogs and encodes a 57 amino acid insert that is nearly identical to the “w” sequence, differing only by a 12 amino acid insertion (Figures 14 & 15). Additionally, PMCA2a and PMCA2b splice site A variants expressed in MDCK cells show that only “w”-containing constructs are transported to the apical membrane (Chicka and Strehler, 2003). The splice site C context seems to be of lesser importance since the “a” or “b” variant can be expressed at the apical surface *in vitro* (MDCK cells) and *in vivo* (mammary epithelial).

Is splice site A sufficient for apical targeting?

In this study, we established that the “w” splicing is necessary for apical targeting of PMCA2a in mammalian hair cells. It is not, however, evident that this splice site A variant is sufficient for dictating apical targeting. In all cases demonstrated here, the “w” (or “v” in frog) sequence was used exclusively for PMCA2; would any of the other PMCA isoforms such as PMCA1, PMCA3, or PMCA4 be targeted apically if the 45 amino acid corresponding to “w” were inserted at splice site A? Furthermore, the

minimal targeting sequence has yet to be identified; “w” and “x” share 13 amino acids, which is not sufficient for coding for apical translocation (Figures 14 & 20).

Role of splice site A in regulation of PMCA activity

In contrast to the demonstrated regulation of calmodulin binding by splice region C, a role for splice site A in regulation of PMCA activity has not been established. Splice site A is located in the first intracellular loop near a phospholipid-sensitive domain (Zvaritch et al., 1990; Figure 14). A peptide corresponding to the phospholipid-responsive domain inhibited PMCA activation by acidic phospholipids and, surprisingly, completely blocked enzyme activity when the calmodulin-binding domain was proteolytically cleaved. These data suggest that stimulation of PMCA activity by acidic phospholipids could be an alternate to, or additive to calmodulin, as an important stimulatory mechanism (Brodin et al., 1992).

Among the acidic phospholipids that stimulate PMCA activity, of particular relevance to hair bundle function is phosphatidylinositol-4,5-bisphosphate (PIP₂) (Choquette et al., 1984). The Gillespie lab has recently shown that PIP₂ is required for mechanoelectrical transduction and adaptation in hair cells (Hirono et al., 2004). Moreover, strict regulation of Ca²⁺ is also required for these two events (Crawford et al., 1991; Eatock et al., 1987; Zhao et al., 1996). It is reasonable then to predict that the additional 45 amino acids of the “w” splice form, which includes many hydrophobic residues, confers an alternate conformation upon the protein that would enable a higher affinity interaction of the phospholipid-sensitive domain with phospholipids like PIP₂. Phospholipid activation of PMCA4b in human erythrocytes has been studied; however,

future experiments will be necessary to test the effects of PIP_2 and other acid phospholipids on “w”, “x”, and “z” variants of PMCA2a.

This study is the first to define a targeting sequence that directs a protein to the hair bundle. This work is a springboard for examining how and why PMCA2w/a is targeted to the hair bundle.

RESULTS II

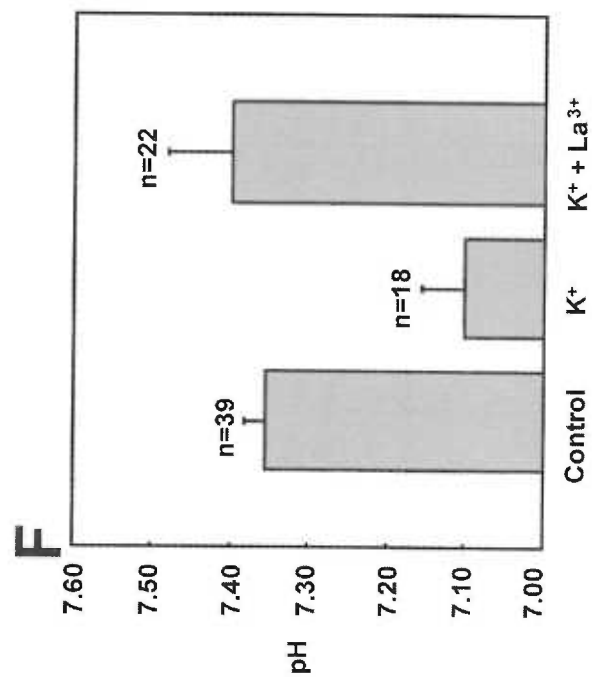
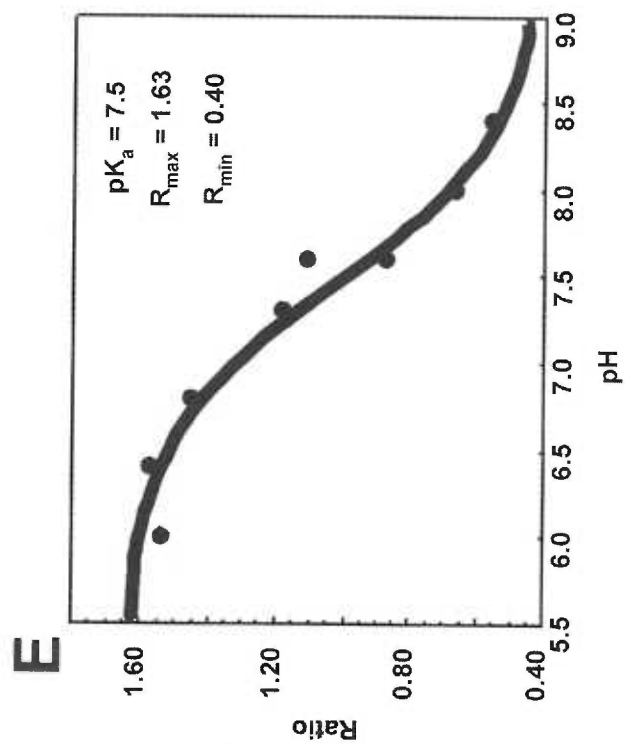
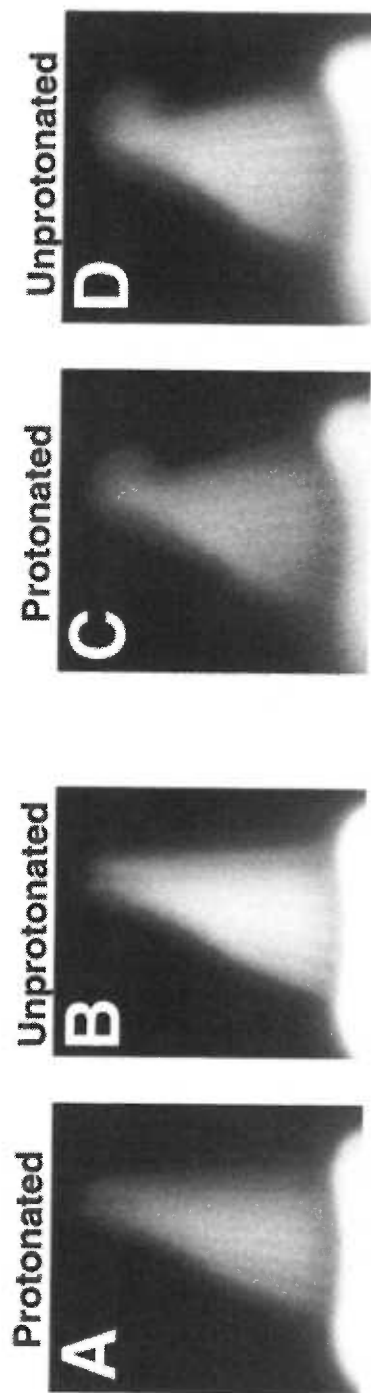
PMCA activation increases hair bundle H^+ -load

To test whether PMCA activity affects hair bundle pH, we loaded hair cells with a ratiometric pH-sensitive dye, SNAFL-calcein, and measured bundle pH signals (Figure 22A-D). An *in situ* calibration of the pH-dependence of the SNAFL-calcein signal showed a pK_a of 7.5 (Figure 22E). Using this calibration curve we measured the resting hair-bundle pH to be 7.35 ± 0.03 (mean \pm SEM; $n=39$ bundles). Depolarization should open voltage-dependent Ca^{2+} channels, permitting Ca^{2+} entry into the soma. Some Ca^{2+} may then diffuse to the hair bundle, where PMCA should pump it out in exchange for a H^+ , resulting in a reduction of pH. Depolarizing the cells with 20 mM K^+ (Figure 22F, Table 2) reduced bundle pH by >0.2 pH units (7.10 ± 0.05 ; $n=18$). In order to test the role of PMCA, we applied the PMCA inhibitor La^{3+} (Figure 22F) following the initial K^+ depolarization. The K^+ -induced pH decrease was completely reversed by the presence of La^{3+} (7.40 ± 0.08 ; $n=22$). By taking static measurements, we determined that we could measure H^+ dynamics in hair bundles and hair bundle pH recovered after a PMCA-induced acid load.

Hair bundles and somata have independent H^+ transporters

To more accurately extract the individual behaviors of bundles and somata in response to H^+ loading, we used a time course protocol to follow single cells over several minutes of pharmacological manipulations. Unfortunately, we found that SNAFL-calcein

Figure 22. Detection of pH changes in hair cells with SNAFL-calcein. Isolated bullfrog saccular hair cells were loaded with the AM ester of SNAFL-calcein and viewed by confocal microscopy. *A-D*, SNAFL-calcein signals from two hair bundles. *A*, *C*, protonated form of dye at 522 nm. *B*, *D*, unprotonated form of dye at 605 nm. *E*, calibration of hair-bundle pH signal (ratio = 522 nm/ 605 nm). *F*, increase in H^+_i upon depolarization with 20 mM K^+ ; La^{3+} (100 μ M), a PMCA inhibitor, prevents the decrease in pH. *E*, *F*, Means \pm SEM presented, circles obscure error bars in *E*.



rapidly photobleaches when the bundle is scanned every 10 seconds (data not shown). We therefore switched to a more photostable pH-sensitive dye, seminaphthorhodamine-5F (SNARF-5F). We were required to increase the laser power (i.e. enhance the signal) for SNARF-5F detection, though its photostability eliminated any risk of fast photobleaching.

Isolated cells loaded with SNARF-5F were scanned every 5 sec for 5 min; we compared bundle and soma responses to acid-loading, using the classic method of pulsing hair cells with a weak acid (25 mM NH_4Cl). pH in both the soma and hair bundle recovered rapidly ($k_{\text{recover}} = 1.5$ and 1.9 mM s^{-1} , respectively) when the NH_4Cl pulse was followed with standard Na^+ -containing saline (Figure 23A, B, Table 2). In contrast, when we allowed hair cells exposed to NH_4Cl to recover in Na^+ -free saline (Table 2), we observed different behaviors for H^+ extrusion in the soma and bundle (Figure 23C, D). Although the pH of the hair bundle quickly returned to the resting value, albeit slightly less rapidly than in standard saline ($k_{\text{recover}} = 1.0 \text{ mM s}^{-1}$), the soma pH recovered much more slowly ($k_{\text{recover}} < 0.025 \text{ mM s}^{-1}$). These data are summarized in Figure 24; on average there is no difference between the soma and bundle recovery rates when extracellular sodium is present ($k_{\text{recover}} = 1.48 \pm 0.65 \text{ mM s}^{-1}$; $1.52 \pm 0.18 \text{ mM s}^{-1}$, respectively). By contrast, removing extracellular sodium has a much greater effect on the soma's ability to remove H^+ . The soma pH recovered at less than 5% the rate of the bundle ($k_{\text{recover}} = 0.04 \pm 0.01 \text{ mM s}^{-1}$; $k_{\text{recover}} = 0.90 \pm 0.04 \text{ mM s}^{-1}$, respectively).

We replaced sodium with *N*-methyl-D-glucamine (NMDG^+), a bulky cation generally not cell-permeant. Evidence suggests, however, that goldfish hair cells are

Figure 23. Detection of pH changes in hair cells with SNARF-5F. *A*, Acid loading of a hair-cell soma with NH_4Cl . During superfusion with standard saline, the addition of 25 mM NH_4Cl alkalinized the soma. Removal of NH_4Cl caused a precipitous drop in pH, followed by rapid a recovery to resting pH. *B*, Acid loading of a hair-cell bundle with NH_4Cl . During superfusion with standard saline, the addition of 25 mM NH_4Cl transiently increased bundle pH. Removal of NH_4Cl caused a rapid acidification of the bundle, and as with the soma, the pH rapidly recovered to resting value. *C*, Soma pH does not recover in the absence of Na^+ . During superfusion with standard saline, 25 mM NH_4Cl in a NMDG^+ (Na^+ -free) solution alkalinized the soma. Removal of NH_4Cl caused a rapid acidification with no recovery. This suggests that the primary mechanism for H^+ extrusion in the hair-cell soma is Na^+ -dependent. *D*, Bundle pH recovers in the absence of Na^+ . During superfusion with standard saline, 25 mM NH_4Cl in the NMDG^+ solution alkalinized the bundle. Removal of NH_4Cl caused a rapid acidification with a fast recovery to resting pH. Unlike the soma, hair bundles appear to express a Na^+ -independent H^+ exchanger.

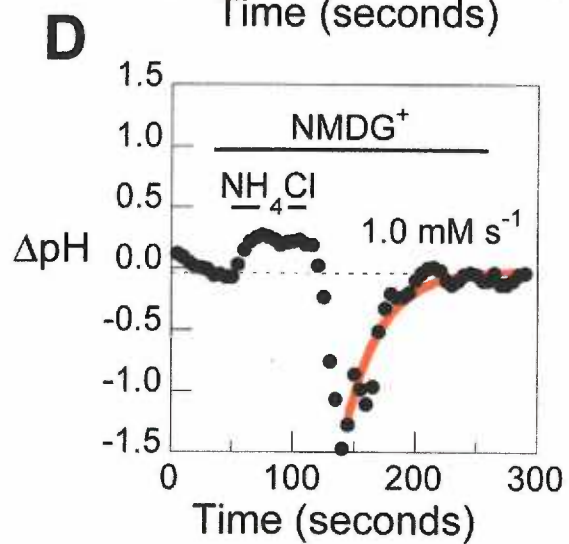
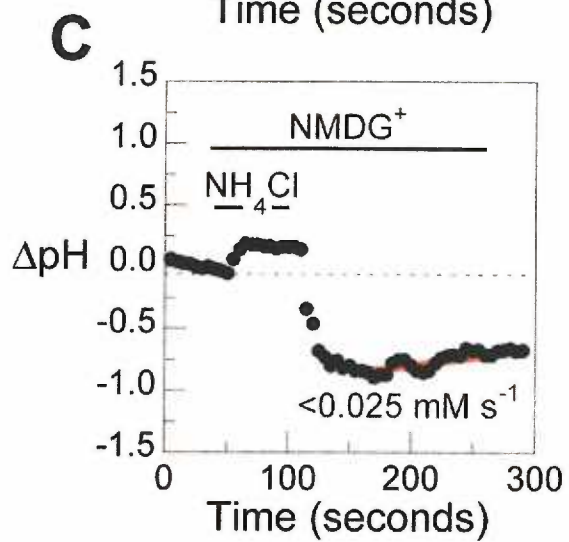
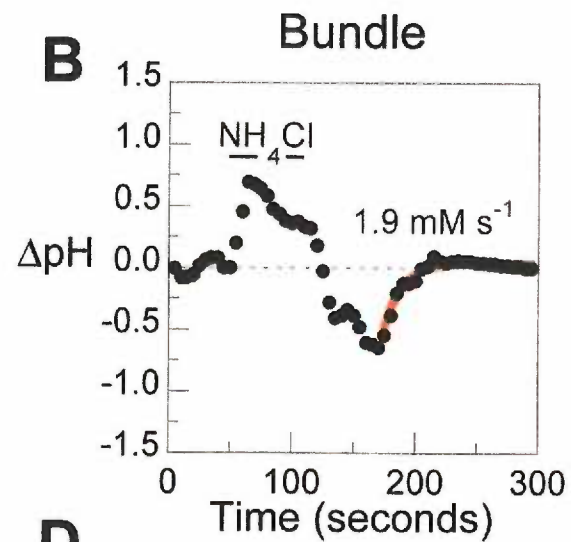
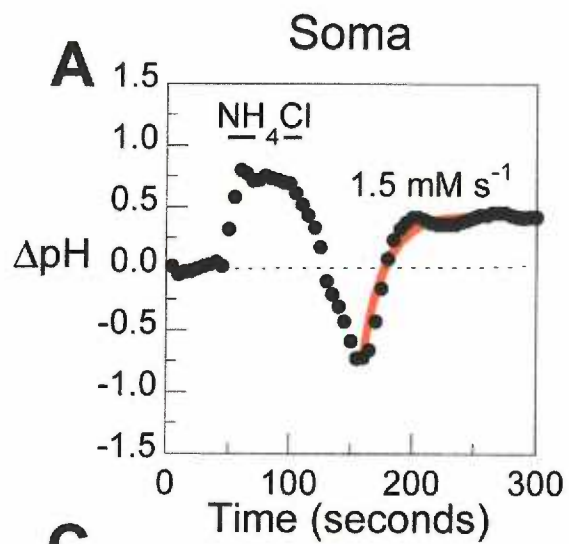
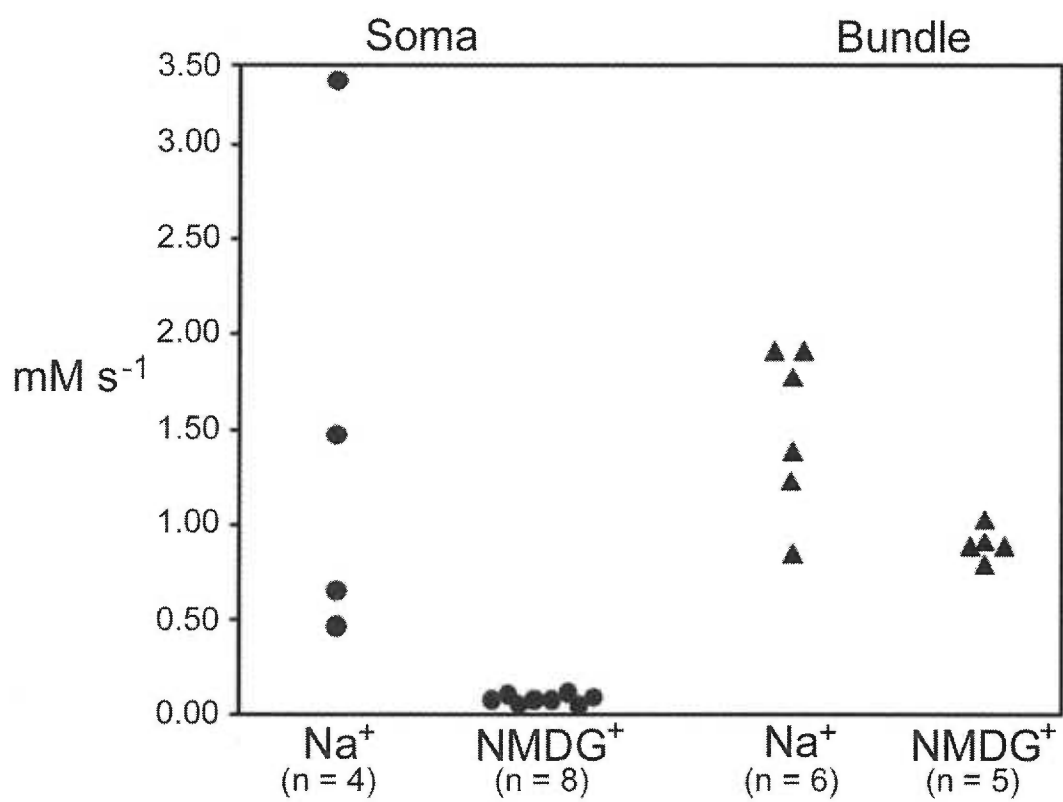


Figure 24. Summary of pH recovery rates in bundles and somata. In the presence of Na^+ , hair cell somata and bundles recover rapidly from an acid load ($k_{\text{recover}} = 1.48 \pm 0.75 \text{ mM s}^{-1}$; $1.52 \pm 0.19 \text{ mM s}^{-1}$, respectively). In comparison, when Na^+ is replaced with NMDG^+ the bundle is still able to recover, albeit slower ($k_{\text{recover}} = 0.90 \pm 0.04 \text{ mM s}^{-1}$); however, the soma's ability to recover to resting pH is nearly abrogated by the lack of Na^+ ($k_{\text{recover}} = 0.04 \pm 0.01 \text{ mM s}^{-1}$). (Mean \pm SEM)



permeable to NMDG⁺; application of NMDG⁺ caused a decrease in soma pH (Mroz and Lechene, 1993). We applied NMDG⁺ for approximately 2 min prior to the NH₄⁺ pulse and observed no change in resting bundle pH (data not shown).

The intrinsic buffering capacity (β_{int}) is an estimate of the ability of a cell to buffer the influx of H⁺ created by the 25 mM NH₄⁺ pulse. β_{int} was determined during the superfusion of NMDG⁺ and was estimated by dividing the H⁺ load (25 mM) by the decline in pH_i induced by NH₄⁺ removal. The β_{int} of the hair cell soma and hair bundle were not significantly different at $47 \pm 7 \text{ mM} \cdot \text{pH unit}^{-1}$ and $33 \pm 13 \text{ mM} \cdot \text{pH unit}^{-1}$, respectively (Student's *t*-test). These data suggest that there is not a remarkable difference in the ability for the bundle and soma to buffer entering H⁺, despite the large volume differences.

These results suggest Na⁺/H⁺ exchangers play a primary role in pH homeostasis of the hair-cell soma. Furthermore, consistent with the lack of a Na⁺-transmembrane gradient at the hair bundle, a Na⁺-independent mechanism for H⁺ extrusion maintains bundle pH, regardless of a low soma pH (Figure 23). It is important to note that no extracellular HCO₃⁻ was added for these experiments, which suggests that the HCO₃⁻/Cl⁻ antiporter contributes little to the pH recovery observed in Figure 23.

To test the role of K⁺ in hair bundle H⁺ transport we made a washout solution containing nominal levels of Na⁺ and K⁺ (Table 2, low Na⁺/K⁺). Although the rate of recovery was slowed compared to NMDG⁺ solution (0.56 mM s^{-1} , compare to 0.90 mM s^{-1}), we could get data from only a single cell; therefore, the significance of this decrease is unclear (data not shown).

Na⁺/H⁺ exchangers are expressed in the mouse inner ear

Although most members of the Na⁺/H⁺ exchanger family (NHE) are selective for Na⁺/H⁺ exchange, new members of the family have recently been described (NHE6-9). Moreover, several of these new family members can demonstrably use K⁺ to drive H⁺ extrusion (NHE6-8) (Brett et al., 2005b; Goyal et al., 2005; Numata and Orlowski, 2001). Amino acid sequence alignments of NHE6-9 with NHE1, the canonical plasma membrane NHE, show that these newest members of the family have the characteristic predicted 12 membrane-spanning domains and a large C-terminal domain (Figure 25). Sequence similarity is very low (<20%) between these organellar NHEs and NHE1 (Table 4). The overall similarity of NHE8 to the other isoforms is also low, 34%-45%, while NHE6 and NHE7 share 70% similarity. NHE9 also showed high similarity to NHE6 (62 % identity) and NHE7 (60% identity). The areas of highest divergence among NHE6, NHE7, and NHE9 are the N-terminus (aa 1-23 in NHE9), the second loop (aa 71-128), and two regions in the C-terminus (aa 495-517 and aa 570-644).

Primers for amplifying NHE6-9 as well as NHE1 were designed by analyzing the divergent regions (Table 3). As expected, all five NHEs were detected in mouse brain and kidney by RT-PCR; in addition, all NHEs examined were detected in mouse inner ear (Figure 26). Previous *in situ* hybridization studies for NHE1-4, observed the predominant message in hair cells was for NHE1 (Bond et al., 1998), this was later supported by immunodetection of NHE1 in the basolateral membrane of hair cells (Goto et al., 1999). These data suggest that NHE1 is likely the Na⁺/H⁺ exchanger in the hair cell soma. NHE6-9, however, have singular characteristics that make one or more of them great candidates for a H⁺ exchanger in hair bundles.

Figure 25. Alignment of amino-acid sequence of mouse NHE isoforms. Amino-acid residues conserved over two or more isoforms are inverted and shaded in black. The twelve predicted transmembrane domains, based on NHE6-9 alignment, are shaded in dark grey. The immunizing peptide for the NHE6 antibody we obtained, and the immunizing peptide sequence for NHE9 antibody production are highlighted in light grey. The sequences used are NHE1 (mouse, AAA92976), NHE7 (mouse, Q8BLV3), and NHE8 (mouse, AAL89753). The NHE6 and NHE9 are sequences cloned from mouse inner ear cDNA.

mNHE1 MMLRWSGVWGFHFPFRIEPLLVVVALVGLLPVLRSHGLQHSPTAS 45
 mNHE6 MAGARRG-WRLAPVVRGVCGPRARPLMRPLWL LFAVSFFGWTGAL 44
 mNHE7 MEPSDAA--RPGPGRAFPRGLSPRLLLLPPLLPVLLGRGLRAGAAAS 43
 mNHE8 MAEEEFSS-NTTHETFNFTLHTTLGVTTKLV L- - - - - 31
 mNHE9 MAGQLR- - - - - 7

mNHE1 TIRGSEPPRERSIGDVTTAPSEPLHRPDDHNLTNLIIEHGGKPSR 90
 mNHE6 DGSGGTTRAMDEEIVSEKQAEESHRRQDSANLLIFILLLTTLTILTI 89
 mNHE7 SGAAAEDSSAMEELATEKEAEESHRRQDSVSLLTIFILLLTTLTILTI 88
 mNHE8 - - - - PTPAKPILPVQTGEQAQQEEQSSGMTIFFSLLVLAICITILV 71
 mNHE9 - - - - - FTSGKDEDHFQHQGAVELLAFNFIILLLTTLTILTI 38

mNHE1 KAFBVLDDIDYPHVRTPFETISLWILLACLMKIGFHVVIPTISSIVPE 135
 mNHE6 WLFKRRRARFLHETGLAMIYGLLVGLVLRVYGI-HVPSDVNNVTLS 133
 mNHE7 WLFKRRRVRFHETGLAMIYGLLVGLVLRVYGT-PATSGHDKSLSLSC 132
 mNHE8 HLLIRYRLHFLPESVAVVSLGILMGAVIKV- - - - - 102
 mNHE9 WLFKNHRRFRFLHETGGAMVYGLIMGLILRYATAPTDIDSGTVYNC 83

mNHE1 SCLLIVVGLLVGGLIKGVGE- - - - - T PPF 159
 mNHE6 CEVQSSPTTLLVNVSGKFFYEYTLKGEISSHELNNVQDNEMLRKVT 178
 mNHE7 TQEDRAFTLLVNVSGKFFYEYTLKGEISPGKINNVEQNDMLRKVT 177
 mNHE8 - - - - - IEFKKLANWKEEM 115
 mNHE9 GNLFSPSTLLVNI TDQVYEVKYQREINQHNI SPHQGNALIEKMT 128

mNHE1 LQSDVFFLFLLPPIILDAGYFLPLRQFTENLGTILIFAVVGT LWN 204
 mNHE6 FDPEVFFNILLPPIIFHAGYSLKRRHFFRNLSILAYAFGLTAIS 223
 mNHE7 FDPEVFFNILLPPIIFHAGYSLKRRHFFRNLSILAYAFGLTAIS 222
 mNHE8 FRPNMFFLLLLPPIIFESGYSLHKGNFFQNLIGSITLFAVFGTAIS 160
 mNHE9 FDPEIFFFNVLPPPIIFHAGYSLKRRHFFQNLGSILTYAFGLTAIS 173

mNHE1 AFFLGGLLYAVC- - - - LVGGEQINNIGLLDTLLFGSIIISAVDPVA 245
 mNHE6 CFVIGSIMYGCVTLMKVTGQL-AGDFYFTDCLLFGAIVSATDPVT 267
 mNHE7 CFIIIGNLMYGVVKLMKIVGQL-SDKFYFTDCLFFGAIIISATDPVT 266
 mNHE8 AFVVGGGIYFLGQADVVIS- - - - - KLNMTDSFAFGSLISAVDPVA 199
 mNHE9 CVVIGLIMYGFVKAMVHAGQLKSGDFHFTDCLFFGSLMSATDPVT 218

mNHE1 VLAVFBEIHIHINELHLILVFGESILNDAVTVVLYHLFEEFASYD- - 289
 mNHE6 VLAIFHELQVDVELYALLFGESVLNDAVAIVLSSSIVAYQAPAGDN 312
 mNHE7 VLAIFNELHADVDLYALLFGESVLNDAVAIVLSSSIVAYQAPAGLN 311
 mNHE8 TLAIFNALHVDPVLMNLVFGESI LNDAVSIVLTNTAEGLTRKHM- 244
 mNHE9 VLAIFHELHVDPDLYTLLFGESVLNDAVAIVLTYISISIYSPKE-N 262

mNHE1 - - SVGISDIFLGLFLSFFVVALGGVFVG VVYGVIAAFTSRFTS- - H 329
 mNHE6 SHTFDVTAMFNSIGIFLGIFSGSFAMGAATGVVTALVTKFTKLRE 357
 mNHE7 THAFDAAAFEKSVGIFLGIFSGSFTMGAVTGVTALVTKFTKLHC 356
 mNHE8 SDVSGWQTFSSQALGYFLKMFFGSAAAGTLTG LISA LVLKHIDLRK 288
 mNHE9 PNAFDTA AAFQSVGNFLGIFAGSFAMGSAYAVVTALLTKFTKLRE 307

mNHE1 IRVIEPLFVFLYSYMA YLSAE L FHL SGI MALIASGVVMRPYVEAN 374
 mNHE6 FQILETGLFFLMSWSTFLLAEACGFTGVVAVLFCGITQAHYTYNN 402
 mNHE7 FPLLETALFFLMSWSTFLLAEACGFTGVVAVLFCGITQAHYTYNN 401
 mNHE8 TPSLEFGMMIIFAYLPYGLAEGISLSGI MALIFSGI VMSHYTHHN 333
 mNHE9 FPMLETGLFFLLSWSAFLSAEAAGLTGIVAVLFCGVVTQAHYTYNN 352

mNHE1 ISHKSHHTTIKYFLKMWSSVSETLIFIFLGVSTVA-GSHOWNWTFV 418
 mNHE6 LSTESQHRTKQLFELLNFLAENFI FSYMGLTLETFQNHVFNPTFV 447
 mNHE7 LSVESRSRSKQLFEVLHFLAENFI FSYMGLALETFQKHVFSPIFI 446
 mNHE8 LSPVTQILMQQTLRTVAFLCETCVFAFLGLSIFSP-HKFEISFV 377
 mNHE9 LSSDSKLR TKQLFEFMNFLAENVIFCYMGLALFTFQNHIFNALFI 397

mNHE1 I S T L L F C L I A R V L G V L V L T W F I N K F R I V K L T P K D Q F I I A Y G G L R G 493
 mNHE6 V G A F I A I F L G R A A N I Y P L S L L L N L G R R S K I G S N F Q H M M M F A G L R G 492
 mNHE7 I G A F V A I F L G R A A H I Y P L S F F L N L G R R H K I G W N F Q H M M M F S G L R G 491
 mNHE8 I W C I V L V L F G R A V N I F P L S Y L L N F F R D H K I T P K M M F I M W F S G L R G 422
 mNHE9 L G A F L A I F V A R A C N I Y P L S F L L N L G R K Q K I P W N F Q H M M M F S G L R G 442

mNHE1 A I A F S L G Y L L D K K H F F M C D L F L T A I I T V I F F T V F V Q G M T I R P L V D 508
 mNHE6 A M A F A L A I R D T - - A T Y A R Q M M F S T L L I V F F T V W V F G G G T T A M L S 535
 mNHE7 A M A F A L A I R D T - - A S Y A R Q M M F T T L L I V F F T V W V I G G G T T P M L S 534
 mNHE8 A I P Y A L S L H L G L E P M E K R Q L I G T T T I V I V L F T I L L L G G S T M P L I R 467
 mNHE9 A I A F A L A I R N T - - E S Q P K Q M M F T T L L L V F F T V W V F G G G T T P M L T 485

mNHE1 L L A V K K K Q E T K R S I N E E I H T Q F L D H L L T G I E D I C G H Y G H H W K D K 553
 mNHE6 C L H I R V G V D S D Q E H L - - - - - - - - - - - - - - - - - - - - - - - - - - - 551
 mNHE7 W L N I R V G V E E L S E E D Q N E N R - - W Q Y F R V G V D P D Q D P P P N N D S F Q V 577
 mNHE8 L V D I E D A R A R R R S K K D V N L S - - - - - - - - - - - - - - - - - - - - - 488
 mNHE9 W L Q I R V G V D L D E S L K E E P S S - - - - - - - - - - - - - - - - - - - - - 506

mNHE1 L N R F N K K Y V K K C L I A G E R S K E P Q L I A F Y H K M E M K Q A I E L V E S G G M 598
 mNHE6 - - - G V P D N E R R T T K A E S A W L F R M W Y N F D H N Y L K P L L T H S G P P L T 591
 mNHE7 L Q G D G M D S V G G S R T K Q E S A W I F R L W Y I F D H N Y L K P I L T H S G P P L T 622
 mNHE8 - - - Q Q E A N K L D K N M T K T E S A Q L F R M W Y G F D H K Y L K P I L T H S G P P L T 488
 mNHE9 - - - Q Q E A N K L D K N M T K T E S A Q L F R M W Y G F D H K Y L K P I L T H S G P P L T 548

mNHE1 G K I P S A V S T V S M Q N I H P K A V T S D R I L P A L S K D K E E E I R K I L R S N L 643
 mNHE6 T T L P A C C G E I A R C L T S P Q A Y E N Q E Q L - - - - - - - - - - - - - - - 618
 mNHE7 T T L P A W C G L L A R C L T S P Q V Y D N Q E P L - - - - - - - - - - - - - - - 649
 mNHE8 - - - - - - - - - - - - - - - - - - - - - - - - - - - - - - - - - - - - - - - 488
 mNHE9 T T L P A W C G P V S R I L T S P Q A Y G - - E Q L - - - - - - - - - - - - - - - 573

mNHE1 Q K T R Q R L R S Y N R H T L V A D P Y E E A W N Q M L L R R Q K A R Q L E Q K I T N Y L 688
 mNHE6 - - - - - - - - - - - - - - - - - - - - - - - - - - - - - - - - - - - - - - 618
 mNHE7 - - - - - - - - - - - - - - - - - - - - - - - - - - - - - - - - - - - - - - 649
 mNHE8 - - - - - - - - - - - - - - - - - - - - - - - - - - - - - - - - - - - - - - 488
 mNHE9 - - - - - - - - - - - - - - - - - - - - - - - - - - - - - - - - - - - - - - 573

mNHE1 T V P A H K L D S P T L S R A R I G S D P L A Y E P K A D L P V I T I D P A S P Q S P E S 733
 mNHE6 - - - - - - - - - - - - - - - - - - - - - - - - - - - - - - - - - - - - - - 622
 mNHE7 - - - - - - - - - - - - - - - - - - - - - - - - - - - - - - - - - - - - - - 653
 mNHE8 - - - - - - - - - - - - - - - - - - - - - - - - - - - - - - - - - - - - - - 492
 mNHE9 - - - - - - - - - - - - - - - - - - - - - - - - - - - - - - - - - - - - - - 577

mNHE1 V D L V N E E L K G K V L G L N R G P R V T P E E E E E D E D G I I M I R S K E P S S P G 778
 mNHE6 D L I L N D G D I S L T Y G D S T V N T E S A T A S A P R - - - - - R F M G N S S E D 660
 mNHE7 D F I L T E G D L T L T Y G D S T V T A N G S S S S Y T A S T S L E C G R R T K S S S E E 698
 mNHE8 G N A I E S E H L S E L T E E E Y E A H Y I R Q Q D L K G F M W L D A K Y L N P F F T R R 537
 mNHE9 E C I V N Q D E L A M N Y Q E Q S P S P S S P T K L A L D Q K - - - S S G Q T P G K E N 619

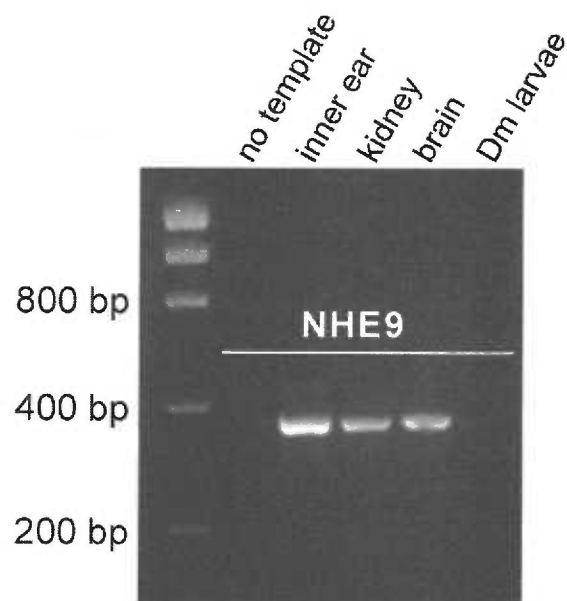
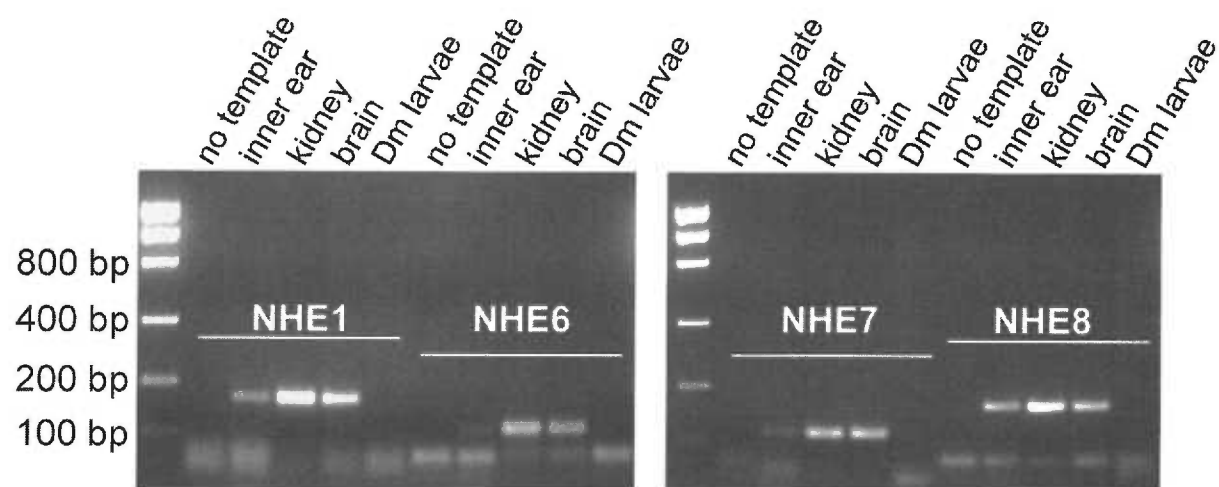
mNHE1 T D D V F T P G S S D S P S S Q R I Q R C L S D P G P H P E P G E G E P F F I P K G Q 820
 mNHE6 A L D R E L T F G D H E L V I R G T R L V L P M D D S E P A L N S L G D T R H S P A 702
 mNHE7 V L E R D L G M G D Q K V S S R G T P L V F P L Q E N - - - - - - - - - - - - - - - - A 726
 mNHE8 L T Q E D L H H G R I Q M K S L T N K W - - - Y E E V R Q G P S G S E D D E Q E L F 576
 mNHE9 I Y E G D L G L G G Y D L K L E Q T R G Q P Q M D - - - - - - - - - - - - - - - - 644

Table 4. Percent similarity of mouse NHE isoforms. Amino-acid sequences from five mouse NHEs were aligned by the ClustalW algorithm (Vector NTI, AlignX; Invitrogen). Although NHE6-9 are classified as intracellular, NHE8 is less than 50% similar to the other members of this subgroup. NHE6, NHE7, and NHE9 show greater than 60% similarity to each other. NHE1, a plasma membrane NHE has very little similarity ($\leq 20\%$) to the four intracellular NHE isoforms.

TABLE 4. Percent similarity of mouse NHE isoforms

	NHE1	NHE6	NHE7	NHE8	NHE9
NHE1	100	17	19	20	17
NHE6		100	70	37	62
NHE7			100	34	60
NHE8				100	45
NHE9					100

Figure 26. Expression of NHE isoforms in the mouse inner ear. Total RNA was isolated from mouse inner ear, kidney, and brain; cDNA was prepared by reverse transcription. Isoform specific primers were used to amplify cDNA fragments corresponding to each Na⁺/H⁺ exchanger isoform. Water was substituted for cDNA in the no template control. cDNA from *Drosophila melanogaster* larvae (gift of Dr. T. Strassmaier) was used as a negative control.



Because NHE6-9 are classified as organellar, their environment would consist of the K^+ -rich cytoplasm, a fluid very similar to the endolymph bathing the hair bundle. In fact, NHE7 and NHE8 were recently shown to be non-selective cation/ H^+ exchangers; using K^+ as well as Na^+ as a counterion (Numata and Orłowski, 2001; Nakamura et al., 2005). Additionally, the yeast ortholog of NHE6, Nhx1, was also shown to be a $Na^+(K^+)/H^+$ exchanger (Brett et al., 2005b). Phylogenetic analysis predicts NHE9 to be a non-selective cation/ H^+ exchanger as well (Brett et al., 2005a). Furthermore, despite their classification as organellar, NHE6, NHE8, and NHE9 appear, at least transiently, at the plasma membrane (Brett et al., 2002; Goyal et al., 2005); Figures 27 & 28), where they could be used for H^+ export.

Protein-immunoblot and immunoprecipitation analyses of hNHE6 and mNHE9

To determine whether one of the intracellular NHE isoforms plays a role in H^+ regulation in bullfrog hair cells, we obtained or generated antibodies to NHE6-9 (Figure 25). Initially we characterized a polyclonal antibody against hNHE6 we received as a gift from Dr. M. Sakaguchi and a polyclonal antibody against mNHE9, which we generated. Several control experiments established that immunocytochemistry, protein-immunoblotting, and immunoprecipitation analyses with these antibodies specifically detected NHE6 or NHE9. We received a full-length hemagglutinin-tagged human NHE6 (HA-hNHE6) clone from J. Orłowski, which was subsequently cloned into the pJPA5 expression vector. There are three human NHE6 splice variants, NHE6 (Numata et al., 1998), NHE6.1 (Miyazaki et al., 2001), and NHE6.2 (Orłowski and Grinstein, 2004);

however, to date, only one mouse NHE6 gene generating one isoform has been identified, which codes for a protein similar to the human NHE6.1 variant. Human NHE6.1 contains a 32 amino acid insert as compared to hNHE6; this insert is predicted to reside in the second exofacial loop. Since the anti-NHE6 is made against a C-terminal peptide that is 100% identical to the mouse sequence, we amplified full-length NHE6 from mouse inner ear cDNA to use in experiments in addition to the hNHE6. Mouse NHE6 was cloned into the pJPA5 expression vector without any epitope tags. In addition, full-length NHE9 was amplified from mouse inner ear cDNA and cloned into the pJPA5 expression vector containing a C-terminal C8 epitope tag and EGFP.

COS-7 cells expressing either HA-hNHE6 or C8-EGFP-mNHE9 were fluorescently immunolabeled with their cognate antibodies. Anti-NHE6 and anti-NHE9 intensely labeled intracellular membranes in transfected cells, but not in mock-transfected cells (Figure 27A, C; Figure 28A, C). Antibodies to the respective epitope tags recapitulated the NHE antibody labeling (Figure 27B, D; Figure 28B, D). There was no obvious plasma membrane expression of either NHE6 or NHE9; co-expressing NHE6 and NHE9 did not result in membrane localization (data not shown).

Immunoblots of microsomes expressing HA-hNHE6 reveal that the majority of hNHE6 has a mobility of ~120 kDa (Figure 27E). Incubating the microsomes overnight in sample buffer (containing 100 mM DTT) shifts the mobility to nearly 150 kDa. Some of NHE6 migrates at ~60 kDa, which suggests that the majority may be running as a dimer. Similar expression was seen when the blot was probed with antibody to the N-terminal HA epitope tag (Figure 27E). Detergent-resistant aggregation is not uncommon

Figure 27. Characterization of NHE6 antibody. *A-D*, Detection of HA-NHE6 in transfected COS-1 cells by immunofluorescence. *A*, *B*, Anti-NHE6 and anti-HA immunolabeling were identical in cells transfected with hNHE6-HA expression vector. *C*, *D*, There is no detectable labeling in cells transfected with empty vector. *E*, Immunoblots of 500 ng total protein from microsomes prepared from COS-1 cells transfected with HA-hNHE6. Microsomes were mixed with 1x sample buffer with 100 mM DTT and incubated at room temperature for the indicated times. Blank microsomes from vector-only transfections were incubated 60 min. Blots were probed with anti-NHE6, against the C-terminus or anti-HA, at the N-terminus. Both antibodies detected the majority of NHE6 at above 100 kDa with a fraction of the protein having a faster mobility around 50 kDa. Incubating overnight caused NHE6 to aggregate, shifting the mobility to nearly 150 kDa. *F*, Mouse NHE6 is expressed on the plasma membrane of COS-1 cells. Surface biotinylation was performed on COS-1 cells transiently expressing mNHE6 or vector alone, total cell lysates were immunoprecipitated (IP) with anti-NHE6. The blot was probed with alkaline phosphatase conjugated to streptavidin. A prominent NHE6 band was detected just above 50 kDa. *G*, NHE6 is expressed in mouse brain membranes and rat hair cells. Immunoblot of purified mouse brain membranes, rat residual maculae, and rat hair bundles with anti-NHE6. Ten μ g total brain membrane protein, 5 ear equivalents of maculae, and 128 ear equivalents of bundles were loaded per well. An equivalent amount of agarose from the bundle isolations was loaded as a control. A single band at 120 kDa appears in the maculae and hair bundles; this is also the predominant band in mouse brain membranes.

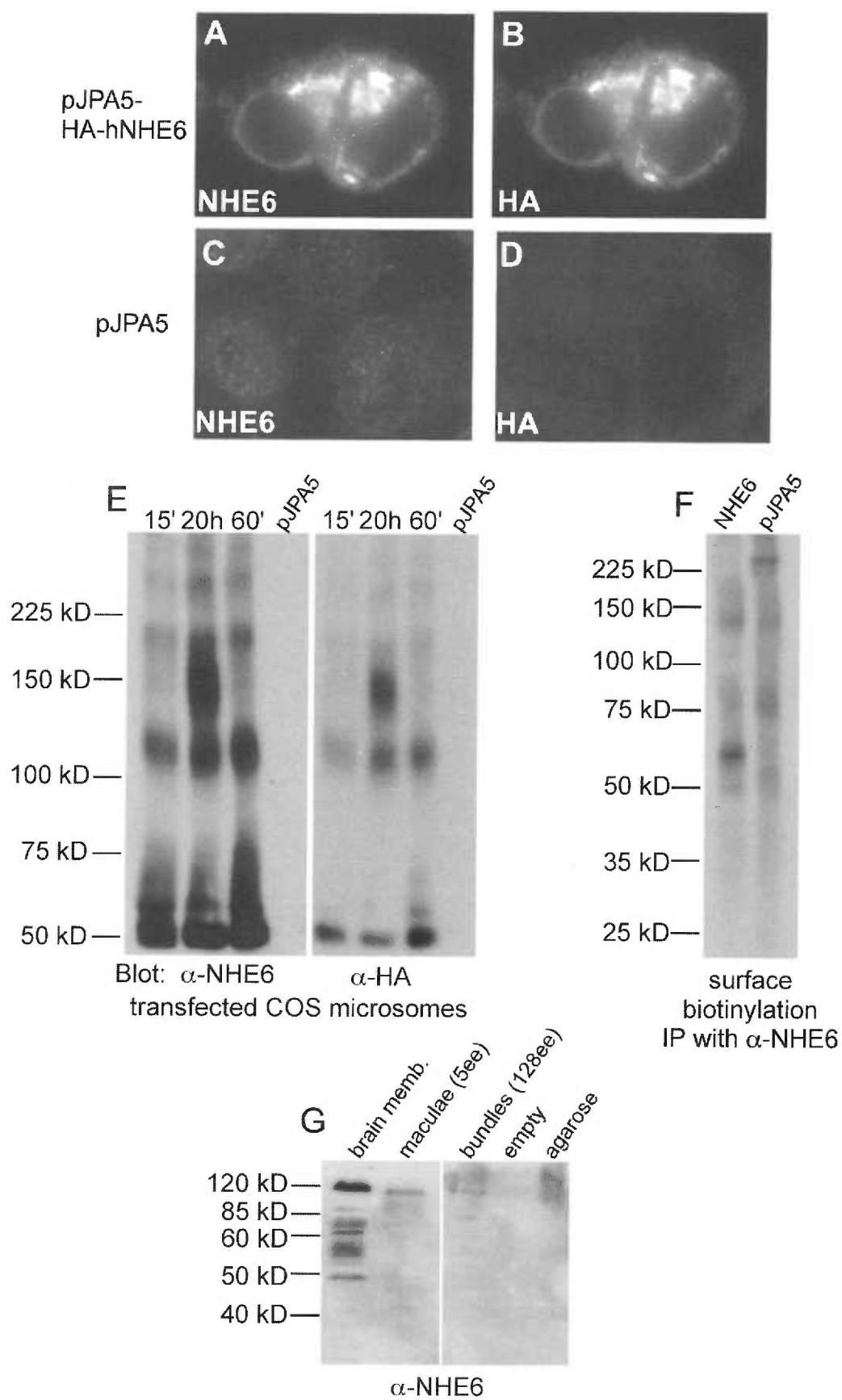
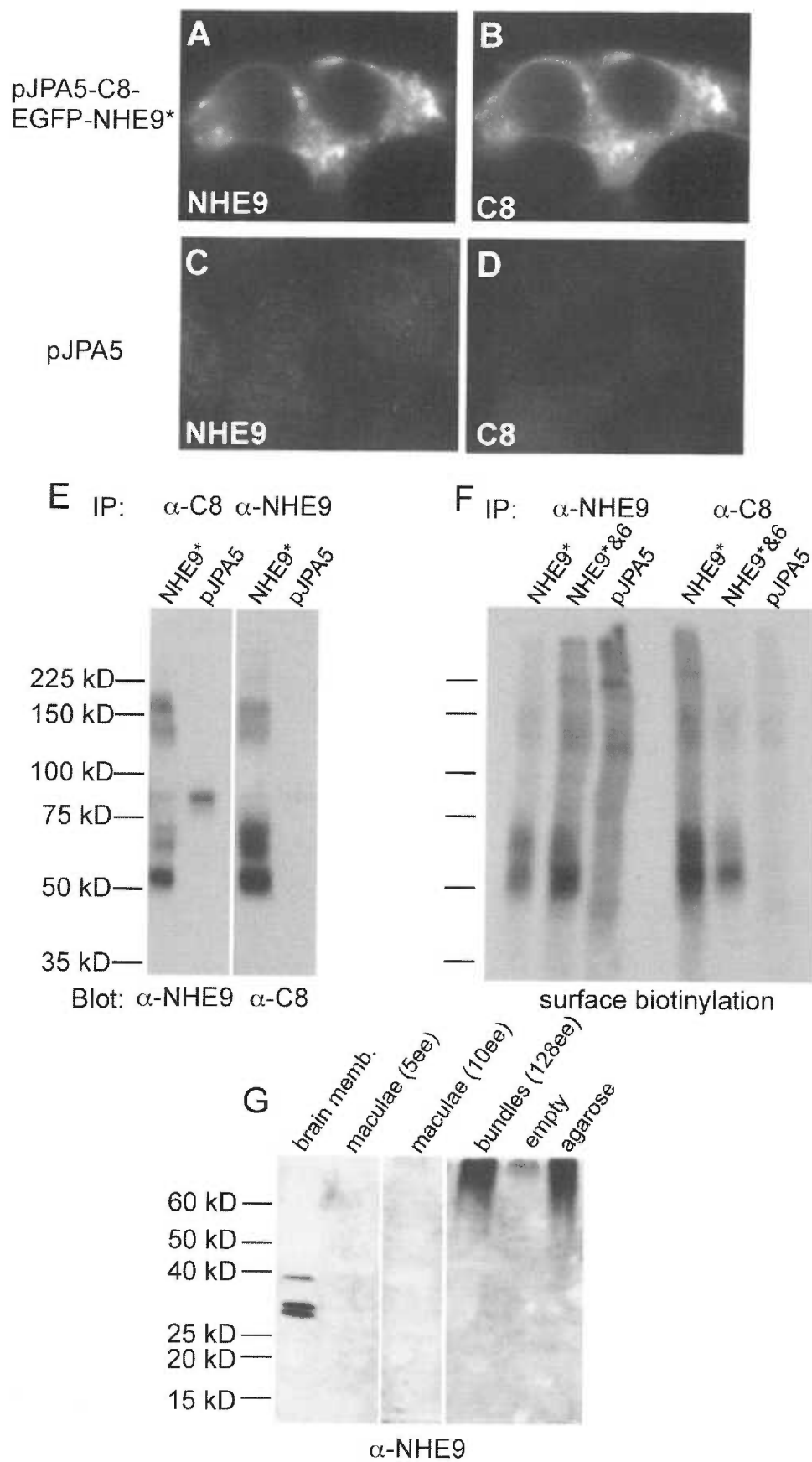


Figure 28. Characterization of NHE9 antibody. Anti-NHE9 detects mouse NHE9 in COS-1 cells. *A-D*, Detection of C8-mNHE9 in transfected COS-1 cells by immunofluorescence. Anti-NHE9 and anti-C8 immunolabeling were identical in cells transfected with a C8-EGFP-mNHE9 expression vector. *C*, *D*, There is no detectable labeling in cells transfected with empty vector. Asterisk indicates that transfections for panels *E* and *F* were with this vector. *E*, Total cell lysates from COS-1 cells transfected with pJPA5-C8-EGFP-mNHE9 (NHE9*) or empty vector (pJPA5-C8) were immunoprecipitated (IP) with anti-NHE9 (C-terminus), or the monoclonal anti-C8 (N-terminus), and detected with the reciprocal antibody. Anti-C8 immunoprecipitated a protein that migrated above 75 kDa in the NHE9 transfected cells as well as the vector alone; however, this band does not show up in the reciprocal immunoprecipitation. *F*, Mouse NHE9 is expressed on the plasma membrane of COS-1 cells. Surface biotinylation was performed on COS-1 cells transiently expressing mNHE9-EGFP-C8, mNHE6 plus mNHE9-EGFP-C8, or vector alone, total cell lysates were immunoprecipitated with anti-NHE9 or anti-C8. The blot was probed with alkaline phosphatase conjugated to streptavidin. As in *E*, prominent NHE9 bands were detected between 50 kDa-75 kDa. There was no affect on mobility with the addition of mNHE6. *G*, NHE9 is expressed in mouse brain membranes but not rat utriculi. Immunoblot of purified mouse brain membranes, rat residual maculae, and isolated hair bundles with anti-NHE6. Ten μ g total brain membrane protein, 5 or 10 ear equivalents of maculae, and 128 ear equivalents of bundles were used. The detected bands are approximately 25 kDa smaller than those in *E* and *F*, which are EGFP fusion proteins. NHE9 was not detected in rat residual maculae or bundles.



for membrane proteins, including other members of the NHE family (Bullis et al., 2002; Sagne et al., 1996). Although the predicted molecular weight of hNHE6 is 72 kDa, it has been previously shown to have a mobility near 60 kDa (Miyazaki et al., 2001). Since the anti-NHE6 is made against a C-terminal peptide and the HA is located at the N-terminus, this would rule out the low molecular weight products being a result of proteolysis.

Total cell lysates from COS-7 cells expressing C8-EGFP-mNHE9 were immunoprecipitated with anti-C8 or anti-NHE9, separated by SDS-PAGE, and subsequent blots were probed with the reciprocal antibodies (Figure 28E). Not unlike NHE6, mNHE9 runs faster than its predicted 70 kDa molecular weight; C8-EGFP-mNHE9 was detected as a prominent band at 50 kDa and a doublet near 60 kDa in blots probed against the N-terminus, anti-C8, and against the C-terminus, anti-NHE9 (Figure 28E).

mNHE6 and mNHE9 are expressed on the plasma membrane of COS-7 cells

Cell surface expression is a requisite for a bundle H^+ transporter and since NHE6 was previously reported to be transiently expressed on the plasma membrane of CHO cells (Brett et al., 2002), we addressed this issue in COS-7 cells with mNHE6 and mNHE9. Surface biotinylation was performed on COS-7 cells expressing mNHE6, C8-EGFP-mNHE9, or co-expressing both proteins. Following immunoprecipitation of cell lysates with anti-NHE6, anti-NHE9, or anti-C8, proteins were separated by SDS-PAGE and electroblotted; surface-labeled proteins were detected with streptavidin-AP. Detection of the 60 kDa and 120 kDa bands from the mNHE6 expressing COS cells demonstrates that like hNHE6, mNHE6 traffics to the plasma membrane (Figure 27F).

Similarly, detection of the 50 kDa and 60 kDa bands verified surface expression of C8-EGFP-mNHE9 in transfected COS cells (Figure 28F).

NHE6 is expressed in rat hair cells

Since we detected message for NHE6 in mouse brain and inner ear, we examined mouse brain membranes and rat utricular hair cells for NHE6 expression. To define the location of NHE6 more precisely, we isolated hair bundles from the macula by imbedding the utriculi in agarose and twisting them off; the residual macula is the tissue remaining after the bundles are isolated. As predicted by the RT-PCR, immunoblots with anti-NHE6 detected a prominent 120 kDa, with a second band at 60 kDa in mouse brain membranes. In addition, NHE6 was expressed in the residual maculae, as well as in isolated hair bundles (Figure 27G). Likewise, immunoblotting mouse brain membranes with anti-NHE9 detected three bands 30 kDa-40 kDa, which is consistent with the predicted mobility of mNHE9 *sans* EGFP. In contrast to NHE6 expression, however, there was no detectable NHE9 in residual rat maculae or isolated bundles (Figure 28G).

NHE6 is expressed on the plasma membrane of bullfrog hair cells

In order to propose a role for NHE6 in bundle H^+ homeostasis, we needed to correlate the physiology observed in bullfrog with NHE6 expression. Since it is not feasible to collect tens or hundreds of ear equivalents of bundle protein for every experiment, we used surface biotinylation followed by immunoprecipitation to increase our sensitivity of detection; only 2.5 ear equivalents are required per

immunoprecipitation. We obtained a second NHE6 antibody (Alpha Diagnostics) also made against human NHE6, which we used in addition to our original NHE6 antibody, but it did not precipitate any bands of the predicted size of NHE6 in hair bundles or residual maculae (Figure 29A, B). By contrast, following immunoprecipitation with the NHE6 antibody from M. Sakaguchi and blotting with streptavidin-AP, a 60 kDa band (*) and faint 120 kDa band (**) were detected in isolated hair bundles (Figure 29A). These same two bands were detected in the residual maculae (Figure 29B). When the NHE6 antibody is incubated with the antigenic peptide prior to immunoprecipitating the antibody fails to precipitate those proteins (Figure 29C).

Three intense bands at 225 kDa (***) that were not apparent in the COS cell immunoblots were detected in hair bundles and residual maculae. Since the intensity of these bands was reduced with peptide competition, similarly to the lower molecular weight bands, we believe that these high molecular weight bands are NHE6 aggregates. Miyazaki et al. (2001) refer to some high molecular weight aggregation of hNHE6 but it is not shown. Also, hNHE7 shows similar aggregation when expressed in CHO cells (Numata and Orłowski, 2001).

NHE6 is expressed in a subset of bullfrog hair bundles

Immunocytochemistry on bullfrog sacculi showed that NHE6 intensely labeled only a subset of hair bundles (Figure 30A, B); these bundles had small diameters and belonged to small skinny hair cells. Consistent with the immunoprecipitation data, all hair cells show labeling in the soma; however, the small hair cells with bundle labeling showed strong apical labeling, whereas the larger cells only had pericuticular necklace

Figure 29. Immunoprecipitation of NHE6 from bullfrog sacculi. Surface proteins of bullfrog sacculi were biotinylated, hair bundles were isolated from the residual macula, and total protein was immunoprecipitated with anti-NHE6, anti-HRP, 5F10, or anti-NHE6 pre-absorbed with the antigenic peptide. For all lanes 2 ear equivalents were used. Two NHE6 antibodies were used in *A* and *B*; each lane 1 was anti-NHE6 a gift of M. Sakaguchi and each lane 2 was an anti-NHE6 from Alpha Diagnostics. Only the antibody from M. Sakaguchi was used in *C*. All blots were detected with streptavidin-alkaline phosphatase. *A*, Surface expression of NHE6 in isolated hair bundles. The 120 kDa band is indicated (**) along with two other bands that may be an NHE6 monomer (~60 kDa,*) and a tetramer (~225 kDa,***). *B*, NHE6 is expressed in a residual macula extract (hair bundles removed). The same bands in *A* are marked. *C*, NHE6 immunoreactivity is reduced by the antigenic peptide. The bands indicated, the same as in *A* and *B*, show a reduction in intensity when the NHE6 antibody is incubated with the antigenic peptide prior to the immunoprecipitation.

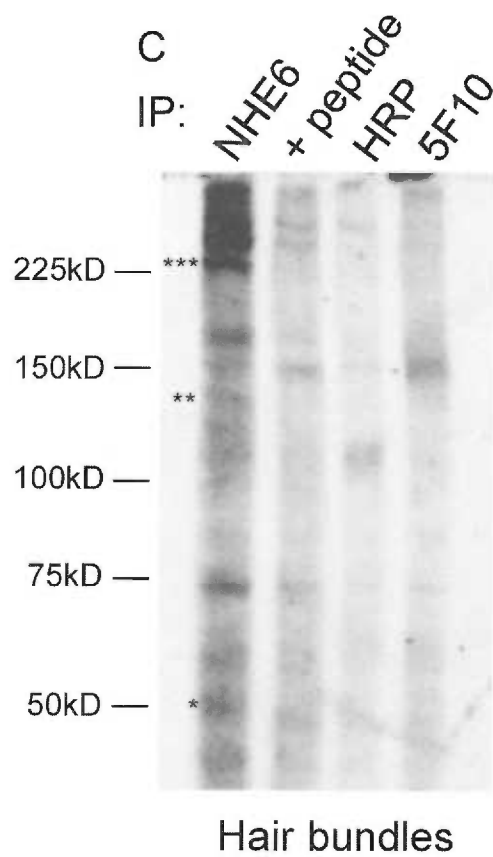
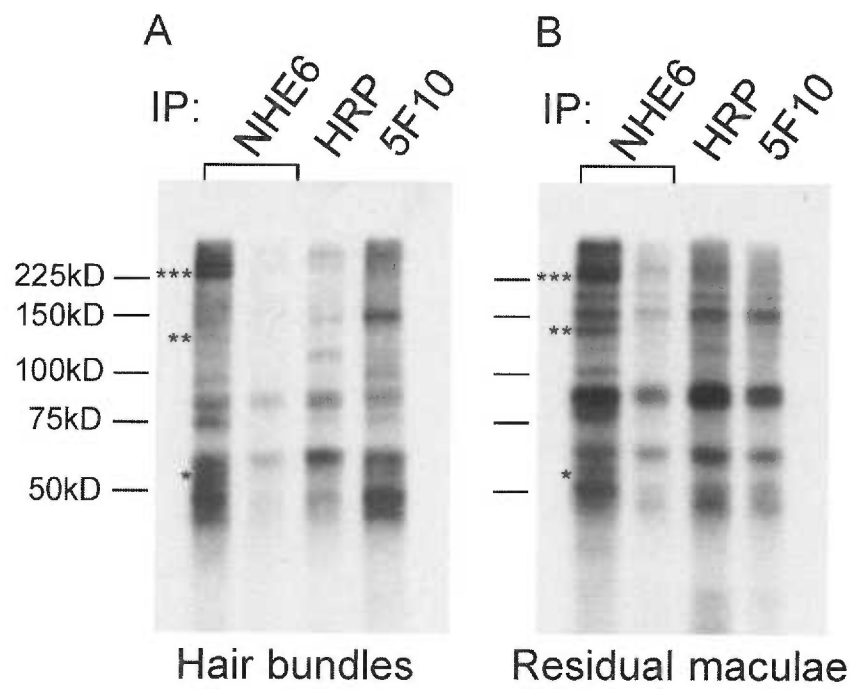
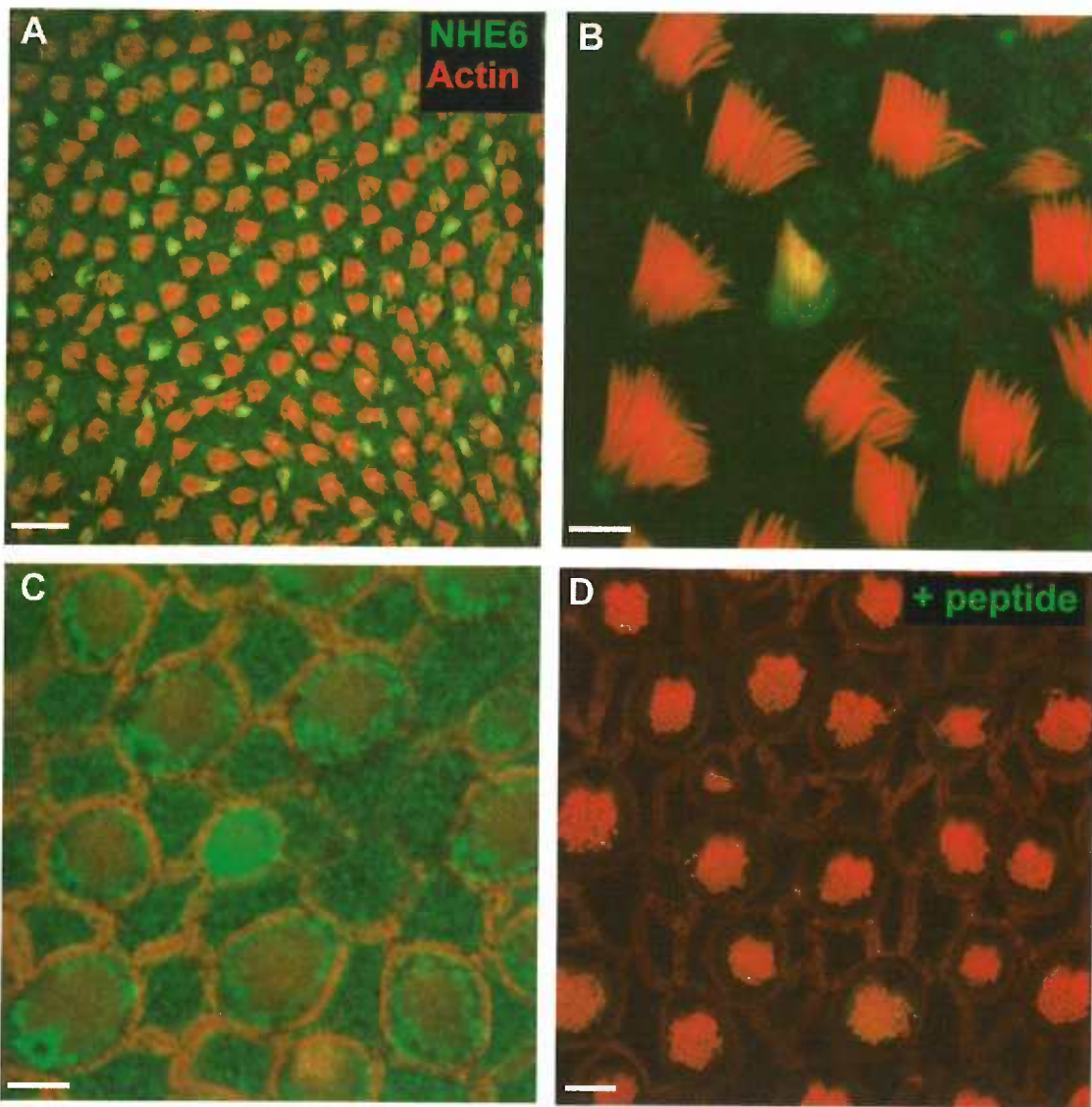


Figure 30. Localization of NHE6 in bullfrog sacculus by immunofluorescence. NHE6 labeling is very strong in a subset of hair bundles. *A, B*, Hair cells with small diameter bundles show strong bundle labeling. *C*, NHE6 labels the apical surface and pericuticular necklace of all hair cells. (Same tissue as *B*, 1.5 μm lower.) *D*, Labeling was abolished by the antigenic peptide. Scale bars *A*, 20 μm ; *B-D*, 5 μm .



labeling (Figure 30C). Competition with the antigenic peptide abolished soma and bundle labeling (Figure 30D).

Preparations of isolated saccular hair cells showed a similar dichotomy in immunofluorescent labeling with anti-NHE6. The skinny cells with small diameter bundles show hair-bundle NHE6 immunoreactivity as well as strong labeling in the apical one-third of the soma. By contrast the NHE6 in the hair cell with a large diameter bundle is detectable in the apical region of the soma, not in the bundle. As with the wholemount tissues, the NHE6 peptide completely blocked specific labeling (Figure 31).

In mammalian vestibular organs long, skinny hair cells with small diameter hair bundles are considered immature type II hair cells and are characterized by immunoreactivity for the calcium-binding protein calretinin (Dechesne et al., 1994; Dechesne et al., 1991). Recently, a subset of bullfrog saccular hair cells were also characterized by their high levels of calretinin (Edmonds et al., 2000). In wholemount bullfrog saccular tissues NHE6 colocalized with calretinin immunoreactivity (Figure 32, top), suggesting these cells with small diameter hair bundles are immature.

Our hypothesis is that hair bundles require a local mechanism for expelling H^+ in response to the influx created by PMCA activity; therefore, if H^+ exchange in the stereocilia is carried out by NHE6, then it should be colocalized with the Ca^{2+} pump. In conjunction with the polyclonal anti-NHE6, we used the monoclonal antibody 5F10 to detect all PMCAs in bullfrog sacculi. Although in this preparation there was not intense NHE6 bundle labeling of any cell, faint NHE6 immunoreactivity could be seen in many cells and colocalized with bundle PMCA. A few cells had a strong NHE6 signal at the apical surface (Figure 32, bottom).

Figure 31. NHE6 expression in isolated bullfrog saccular hair cells. NHE6 localizes mainly to the apical region of the hair-cell soma. Cells with small diameter bundles additionally show stronger NHE6 bundle labeling (panels 1 and 2) than hair cells with large bundles (panel 3). Specificity of the NHE6 labeling is demonstrated by competition with the antigenic peptide (panels 4-6). Insets show bundle-actin labeled with FITC-phalloidin. The cells are pseudo-colored for fluorescence signal intensity, red is saturating. Scale bar is 5 μ m for all of the panels.

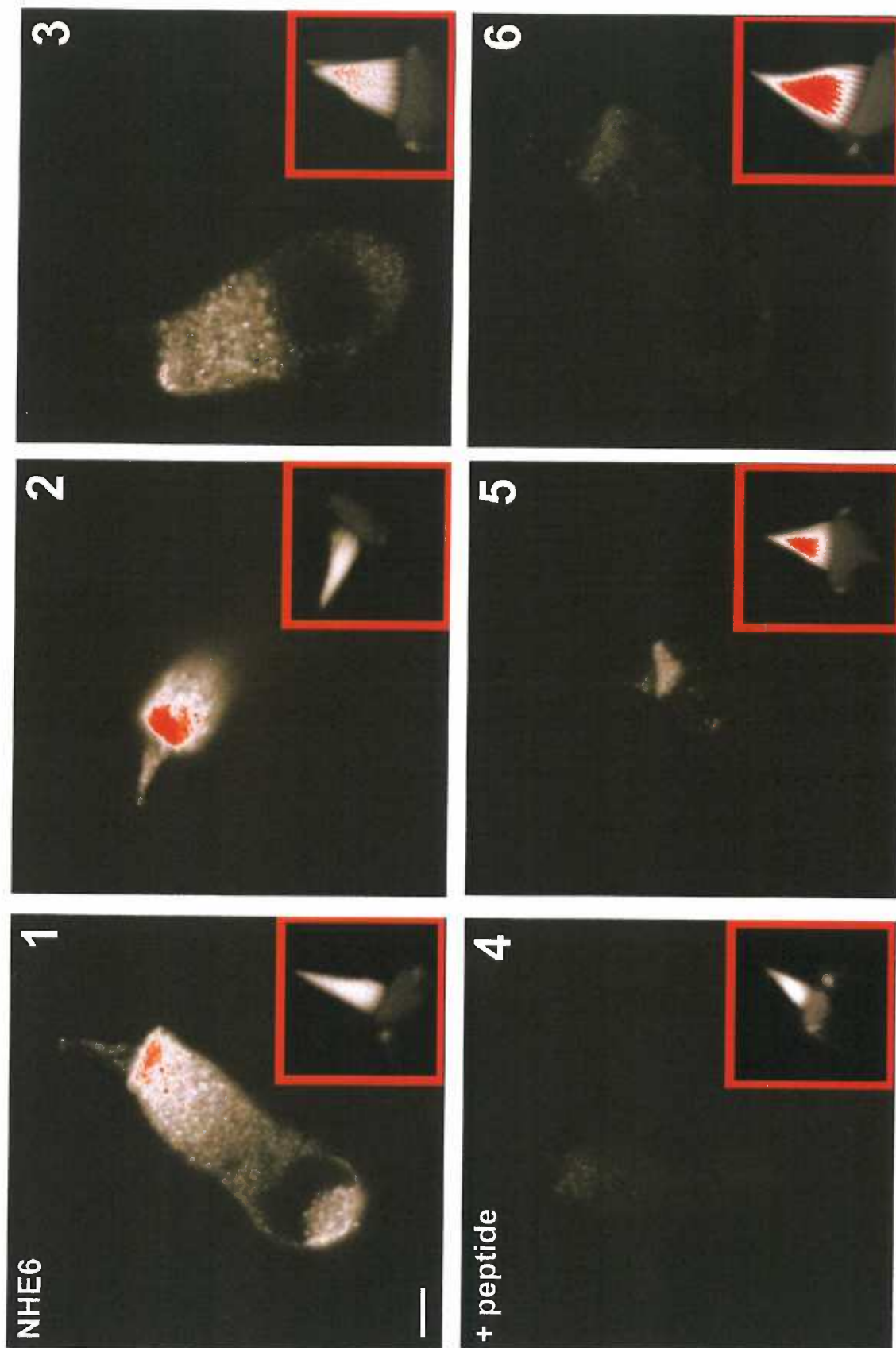
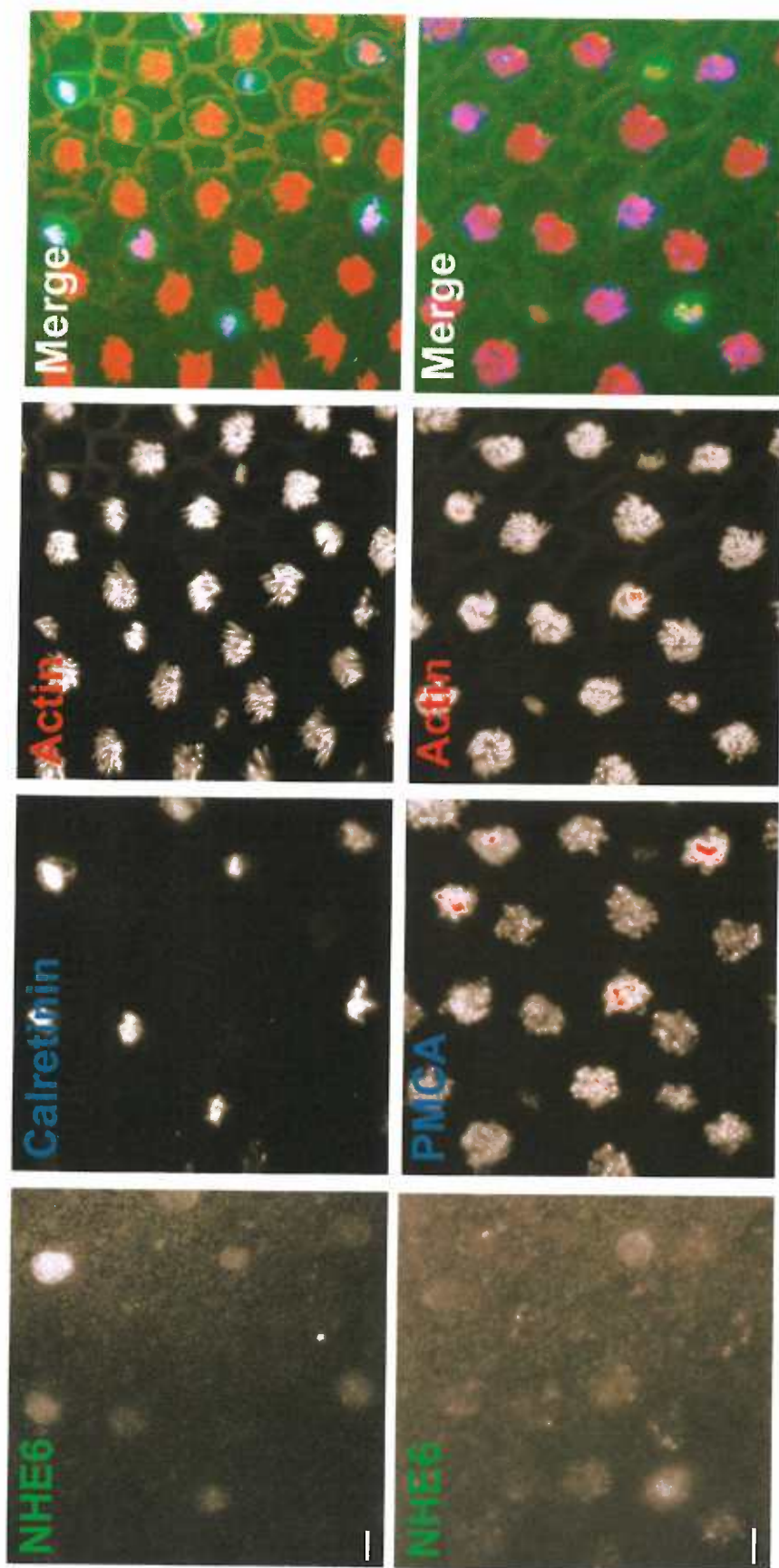


Figure 32. NHE6 colocalizes with PMCA2 and calretinin. Confocal cross sections of bullfrog sacculi. *Left column*, NHE6; *middle left column*, calretinin (top) or PMCA (5F10, bottom); *middle right column*, actin (phalloidin); *right column*, combined NHE6 (green), calretinin or PMCA (blue), actin (red). Calretinin and NHE6 are expressed in hair cells with small diameter bundles (top row). Although faint NHE6 labeling was observed in all bundles, expression was much lower than PMCA labeling and strongest in the apical region of the hair cell soma (bottom row). Scale bars are 5 μ m for each row.



NHE9 is expressed in bullfrog hair bundles

Because PMCA is expressed in all hair bundles and NHE6 only labels a subset of hair bundles, we sought to determine whether there were any other isoforms of NHE in hair bundles. To answer this question, we obtained antibodies against hNHE7 (Alpha Diagnostics) and mNHE8 (Dr. P. Aronson); immunofluorescence experiments showed no labeling with either antibody in bullfrog saccular hair cells (data not shown). Despite the result observed with the NHE9 immunoblot on rat tissue we examined bullfrog sacculi co-labeled with anti-NHE9 and 5F10; every bundle showed immunoreactivity for both antibodies (Figure 33A). NHE9 labeling was concentrated at the tips of stereocilia, where it colocalizes with PMCA (Figure 33A, B). The specificity of this labeling was demonstrated by pre-incubating the antibody with the antigenic peptide; abolishing all NHE9 immunoreactivity (Figure 33C, D). The distribution of NHE9 in isolated cells was remarkably similar to bundle PMCA; both were concentrated at the tips and in some cells in a band above the basal tapers (Figure 34). Neither antibody labeled the kinocilium. As with the wholemount tissues, NHE9 immunolocalization in the isolated cells was completely blocked by the antigenic peptide (Figure 35).

NHE9 is expressed in rat auditory and vestibular hair cells

Although we saw no NHE9 expression by immunoblots in neonatal rat vestibular organs (postnatal day 5), the bundle localization in adult bullfrogs raised the possibility that NHE9 may not be expressed or is not abundant in inner-ear tissue of young rats. We therefore examined the organ of Corti and utriculi from adult rats (postnatal day 21). In

Figure 33. Colocalization of NHE9 and PMCA in bullfrog sacculus by immunofluorescence. *A-D*, Green, NHE9; blue, PMCA (5F10); red, actin (phalloidin). *A, B*, NHE9 labels all hair bundles of saccular hair cells and is concentrated at the tips of the stereocilia. PMCA shows a similar labeling pattern. *C, D*, NHE9 immunolocalization was blocked completely in the presence of the antigenic peptide. Scale bar is 5 μm for all of the panels.

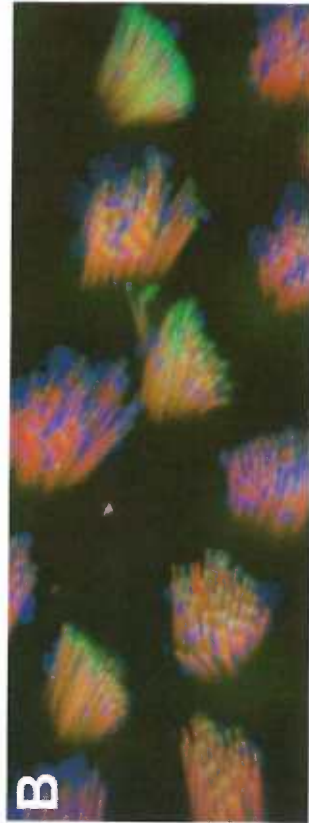
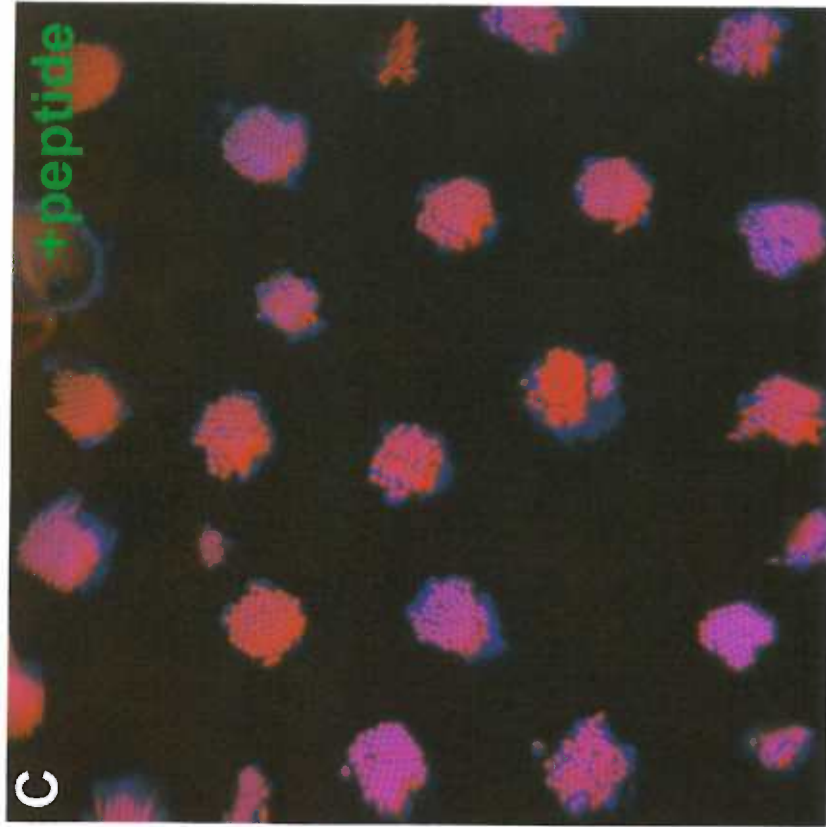


Figure 34. NHE9 expression in isolated bullfrog saccular hair cells. Three examples of NHE9 immunoreactivity in isolated hair cells. *Left column*, NHE9; *middle left column*, PMCA (5F10); *middle right column*, actin (phalloidin); *right column*, combined NHE9 (green), PMCA (blue), actin (red). NHE9 labeling is concentrated at the tips of the stereocilia and in bands above the tapers in some cells (arrow). This band is also prominent in the PMCA labeling. Scale bar is 2.5 μm for all of the panels.

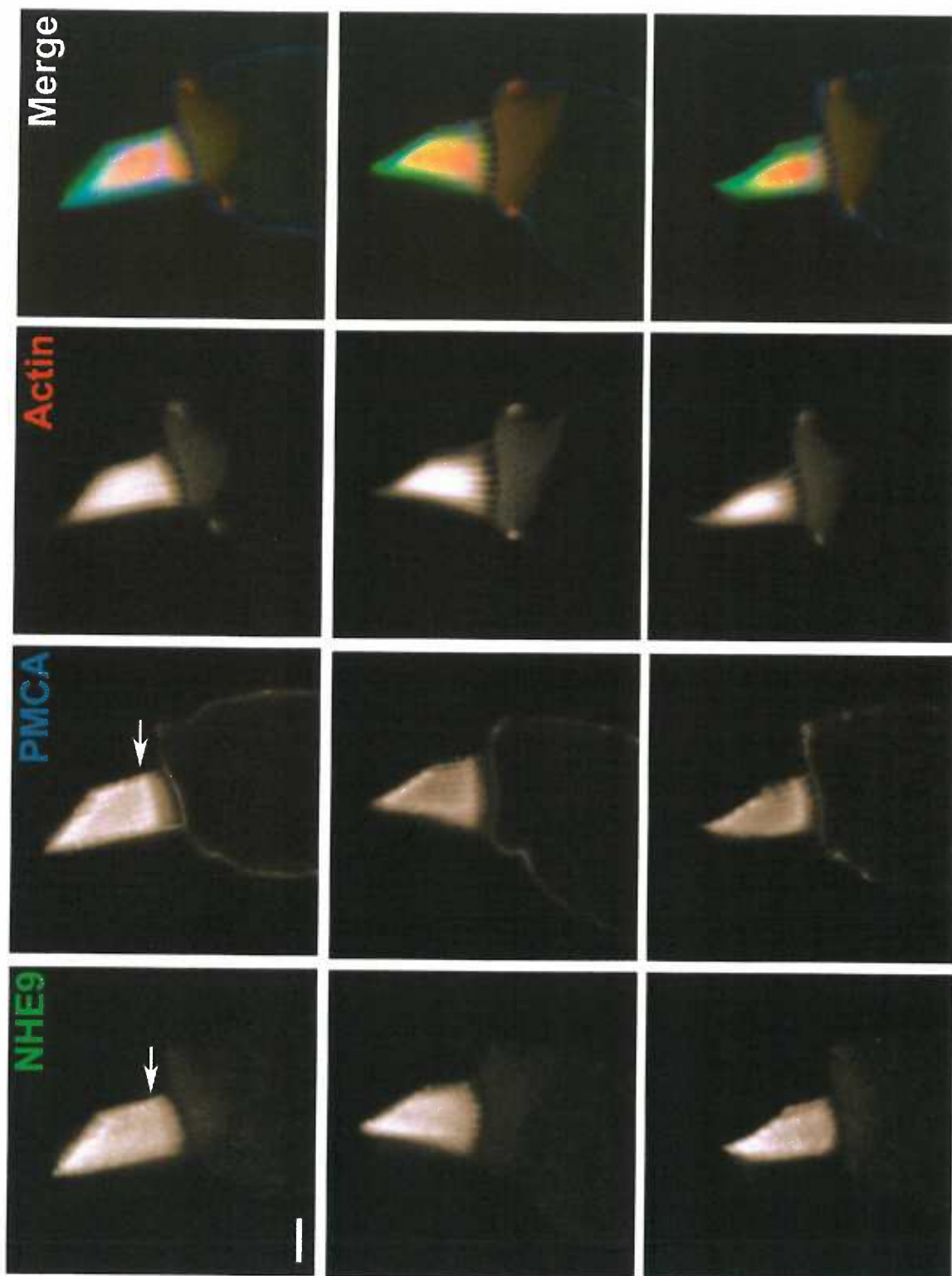
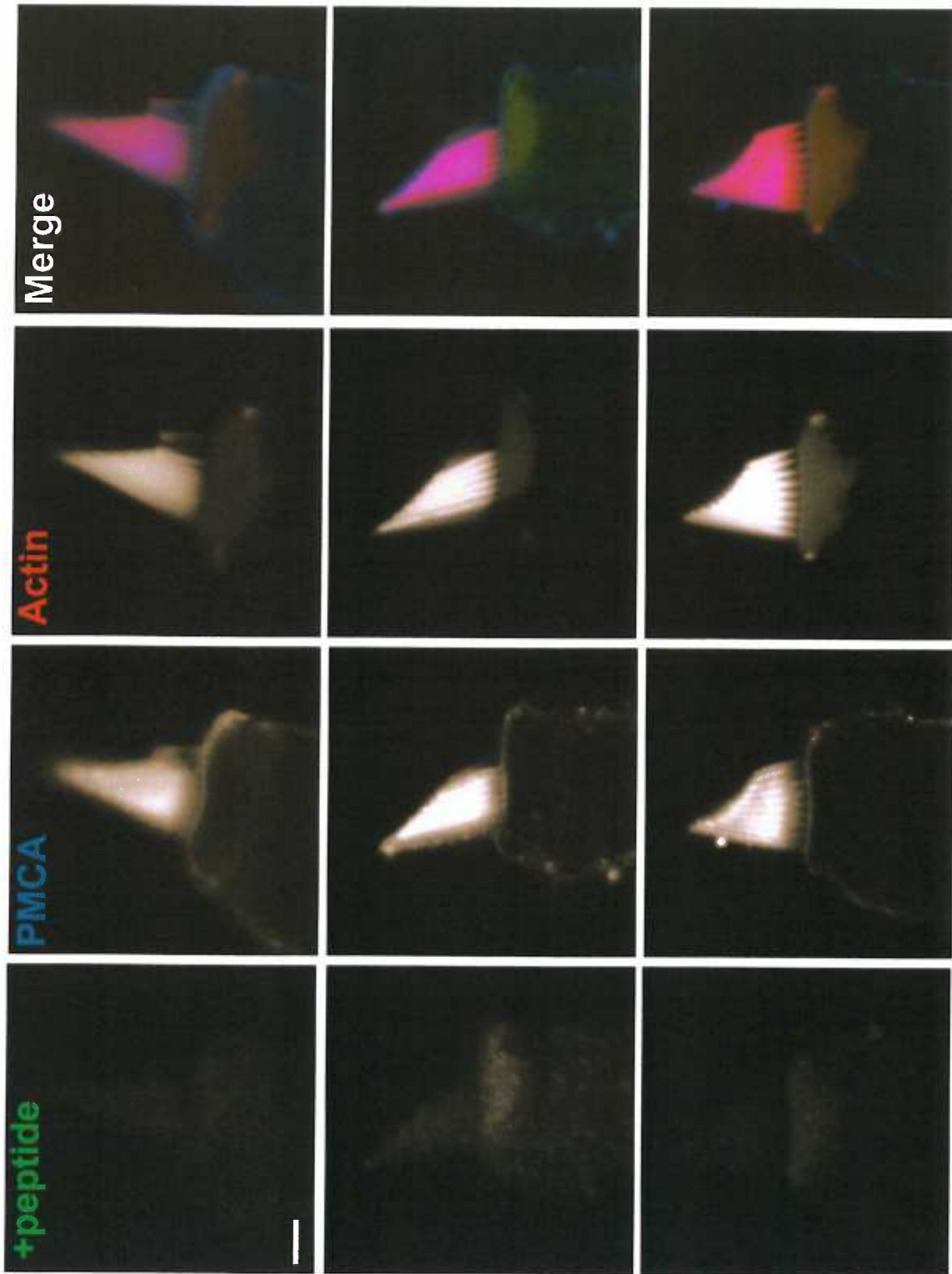


Figure 35. Antigen competition of NHE9 labeling in isolated bullfrog saccular hair cells. *Left column*, NHE9 with antigenic peptide; *middle left column*, PMCA (5F10); *middle right column*, actin (phalloidin); *right column*, combined NHE9 (green), PMCA (blue), actin (red). The NHE9 antibody was pre-incubated with the antigenic peptide for 1h prior to applying it to the cells; NHE9 immunoreactivity was blocked completely. Scale bar is 2.5 μm for all of the panels.



organ of Corti, NHE9 immunoreactivity in hair cells was observed in bundles of inner and outer hair cells (Figure 36). Sections at greater depths in the tissue revealed NHE9 labeling on intracellular membranes, which is best seen when compared to the plasma membrane localization of PMCA (Figure 36, compare left and middle left columns). NHE9 labeling was abolished in the presence of the antigenic peptide (Figure 37).

We saw similar labeling in the adult rat utricle. NHE9 immunoreactivity was detected in all hair bundles and on intracellular membranes. Again, co-labeling with 5F10 showed the plasma membrane localization of PMCA, whereas NHE9 labeling appears to be throughout the soma and does not overlap with the soma 5F10 signal (Figure 38, right column).

In addition, we observed membrane blebs labeled with the PMCA antibody 5F10 as well as with anti-NHE9, albeit sporadically with the latter (Figure 38, top row). Some of these membrane blebs are presumably from the stereocilia since they label with an antibody to PMCA2w, the bundle PMCA isoform (Figure 18). NHE9 immunoreactivity associated with the blebs and intracellular membranes was abolished and the bundle labeling was diminished considerably by pre-incubation with the antigenic peptide (Figure 39).

Figure 36. Localization of NHE9 in rat organ of Corti by immunofluorescence.

Confocal cross sections through the adult rat organ of Corti. Sections are from the same organ with 20 μm between top row and bottom row. *Left column*, NHE9; *middle left column*, PMCA (5F10); *middle right column*, actin (phalloidin); *right column*, combined NHE9 (green), PMCA (blue), actin (red). Hair bundles of outer (top row) and inner hair cells (second row, arrow) labeled with anti-NHE9. Anti-NHE9 labeled intracellular membranes of outer (arrowheads, third row) and inner hair cells (double arrows, bottom row); compare with the plasma membrane labeling of PMCA in the left middle column. Scale bar is 10 μm for the entire figure.

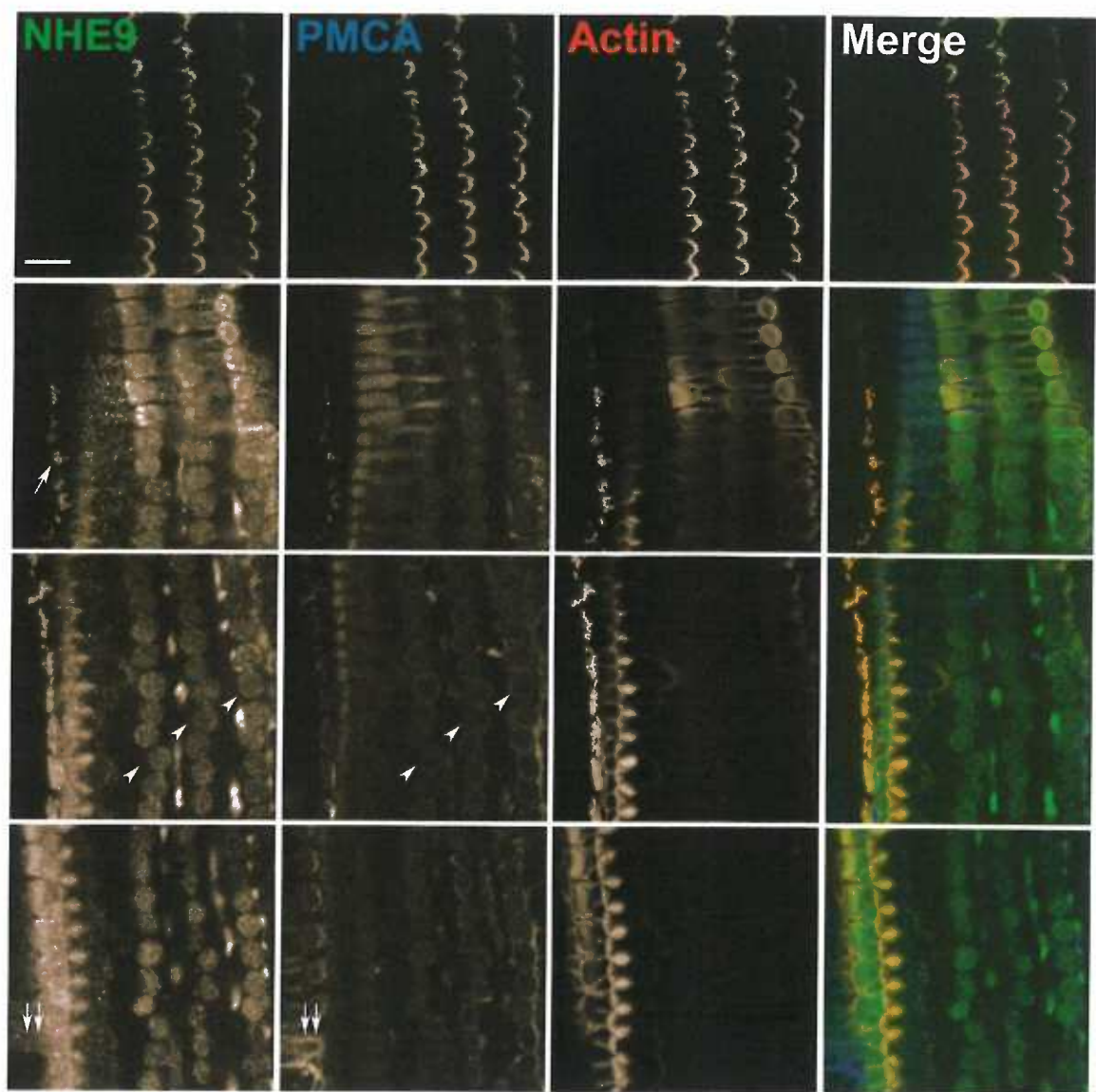


Figure 37. Antigen competition of NHE9 labeling in rat organ of Corti. Confocal cross sections through the adult rat organ of Corti. Sections are from the same organ with 20 μm between top row and bottom row. *Left column*, NHE9 + peptide; *middle left column*, PMCA (5F10); *middle right column*, actin (phalloidin); *right column*, combined NHE9 + peptide (green), PMCA (blue), actin (red). NHE9 immunoreactivity in hair bundles was reduced by the antigenic peptide. All intracellular membrane labeling was completely blocked. Scale bar is 10 μm for the entire figure.

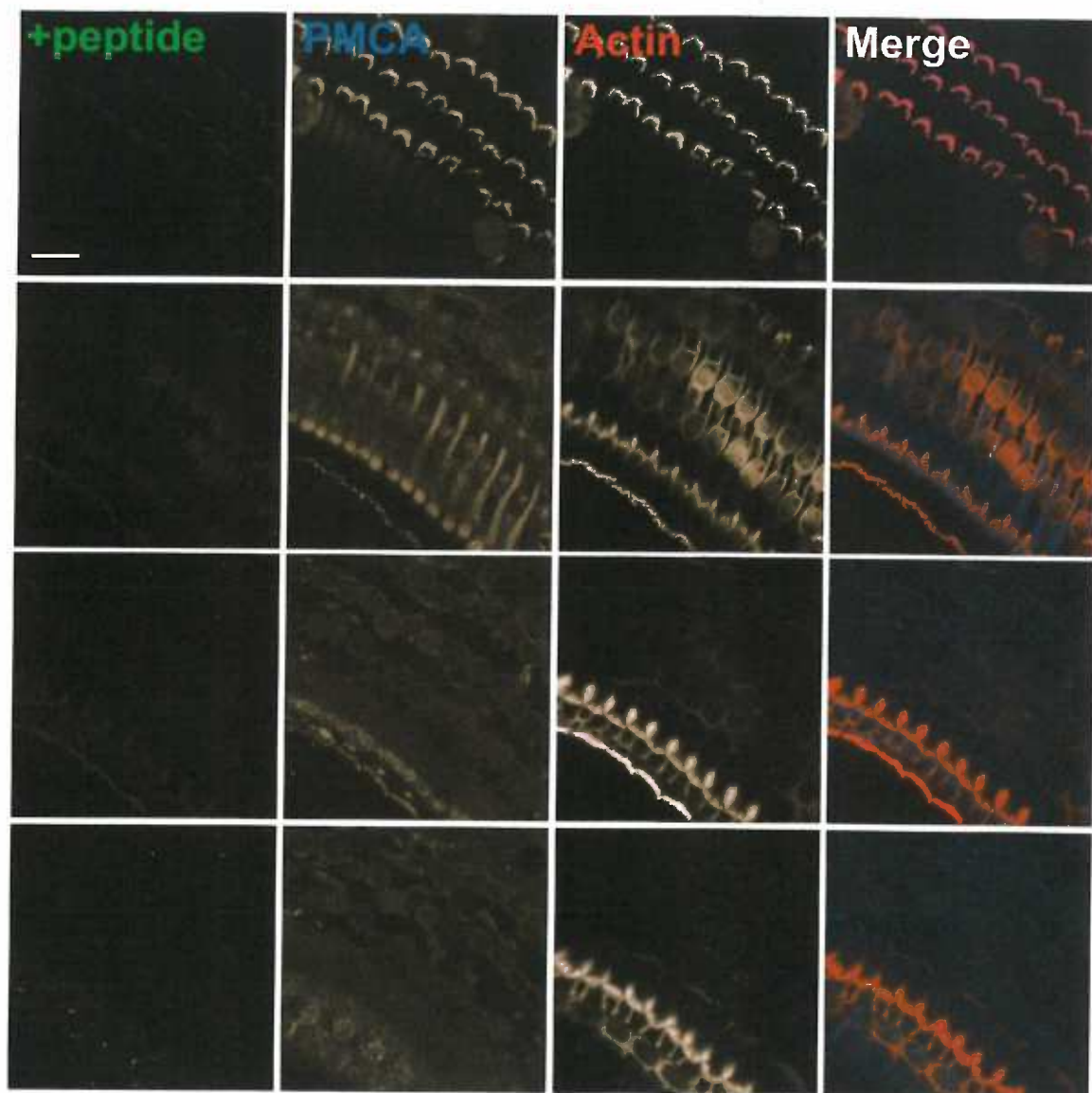


Figure 38. Localization of NHE9 in rat vestibular organs by immunofluorescence.

Confocal cross sections through the adult rat utricle. Sections are from the same organ with 15 μm between top row and bottom row. *Left column*, NHE9; *middle left column*, PMCA (5F10); *middle right column*, actin (phalloidin); *right column*, combined NHE9 (green), PMCA (blue), actin (red). NHE9 immunoreactivity was seen in all hair bundles and partially localized with PMCA. 5F10 immunoreactivity was seen in the basolateral membranes; however, anti-NHE9 labeled intracellular membranes of the soma (middle and bottom rows). Many cells showed some membrane blebbing that labeled brightly with 5F10 and sporadically with anti-NHE9 (arrow, top right). Scale bar is 10 μm for the entire figure.

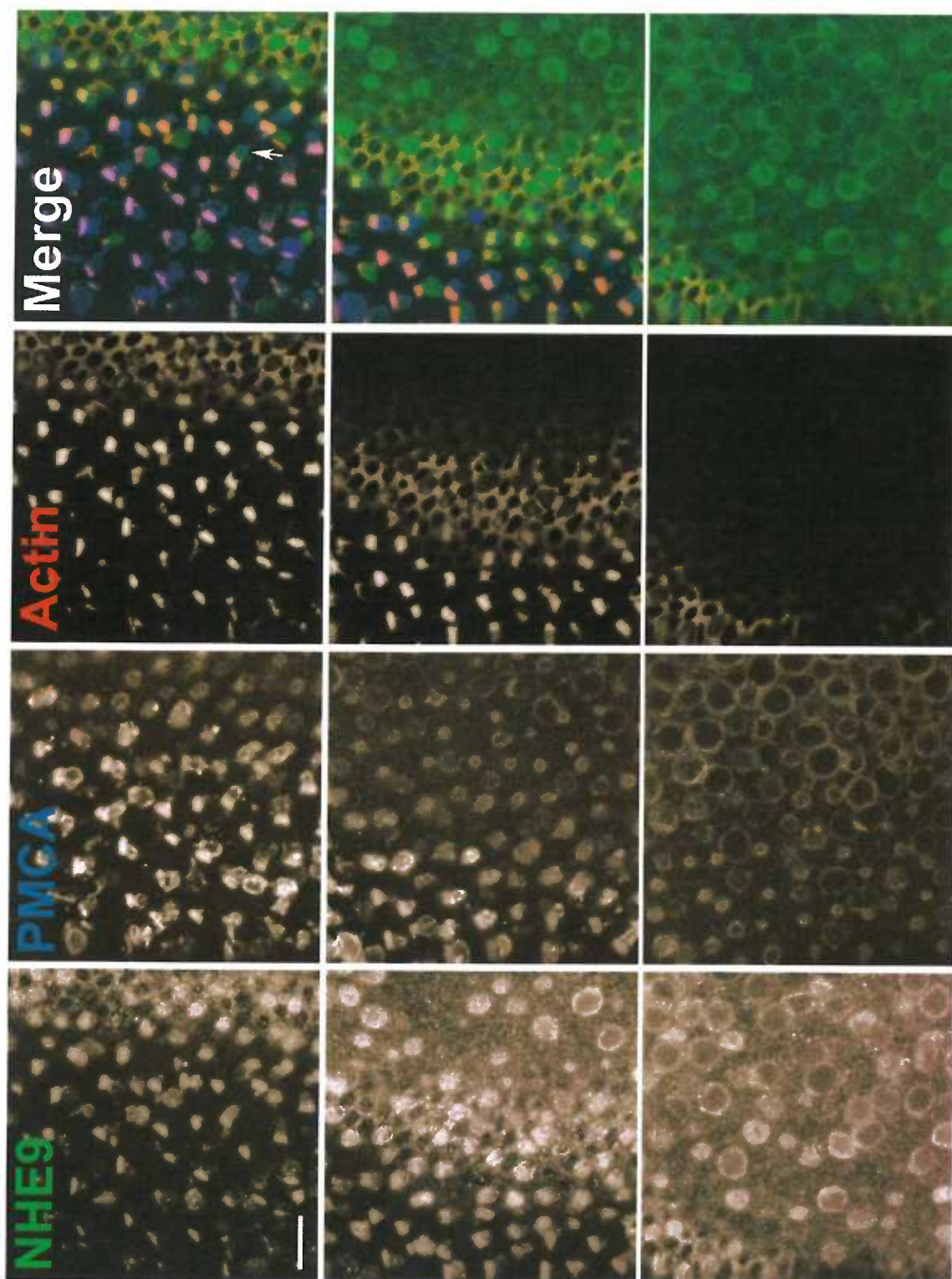
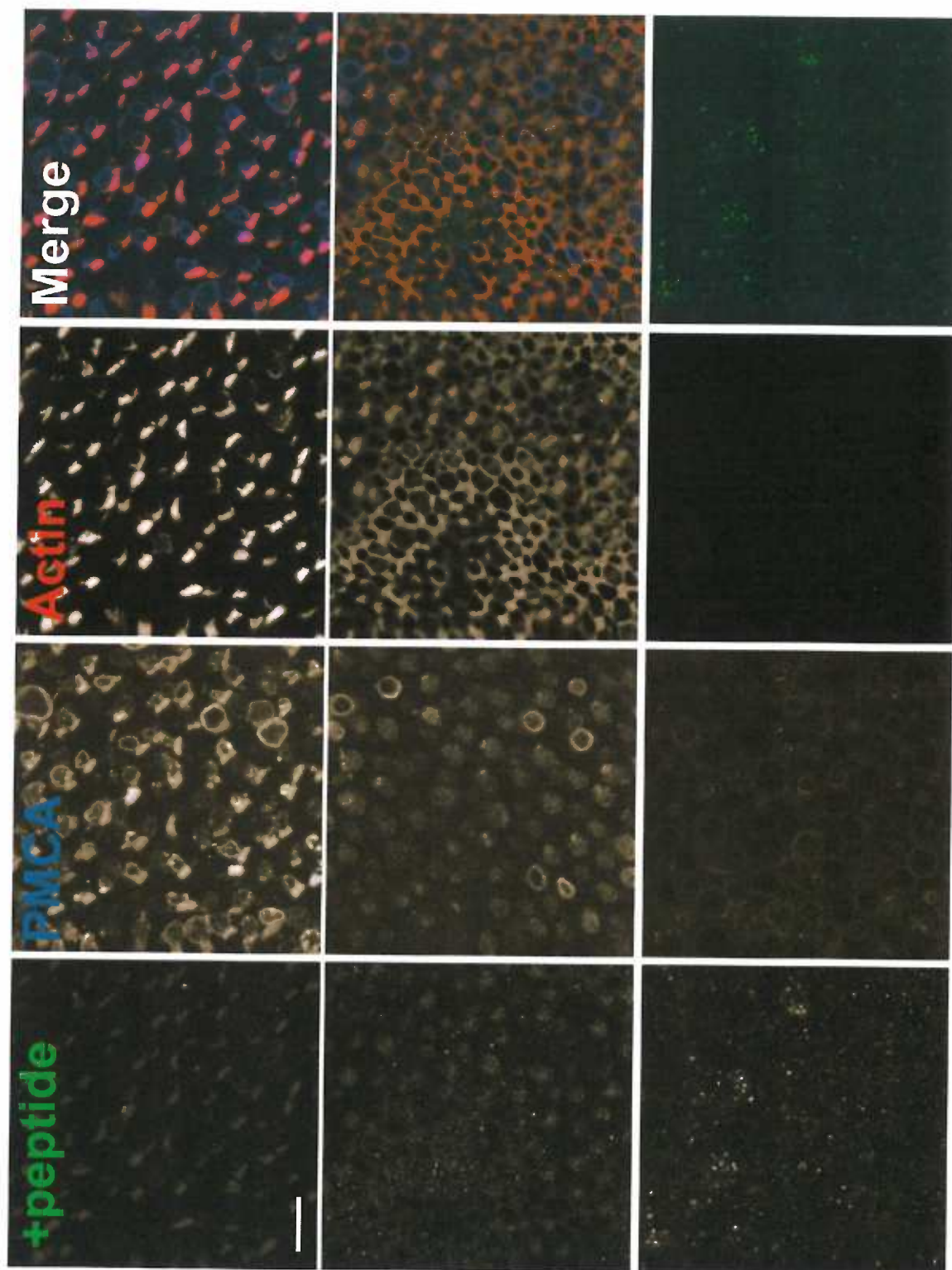


Figure 39. Antigen competition of NHE9 labeling in rat vestibular organs. Cross sections through the rat utricle. Sections are from the same organ with 15 μm between top row and bottom row. *Left column*, NHE9 + peptide; *middle left column*, PMCA (5F10); *middle right column*, actin (phalloidin); *right column*, combined NHE9 + peptide (green), PMCA (blue), actin (red). NHE9 immunoreactivity in hair bundles was reduced by the antigenic peptide. All labeling associated with the blebs and soma was completely blocked. Scale bar is 10 μm for the entire figure.



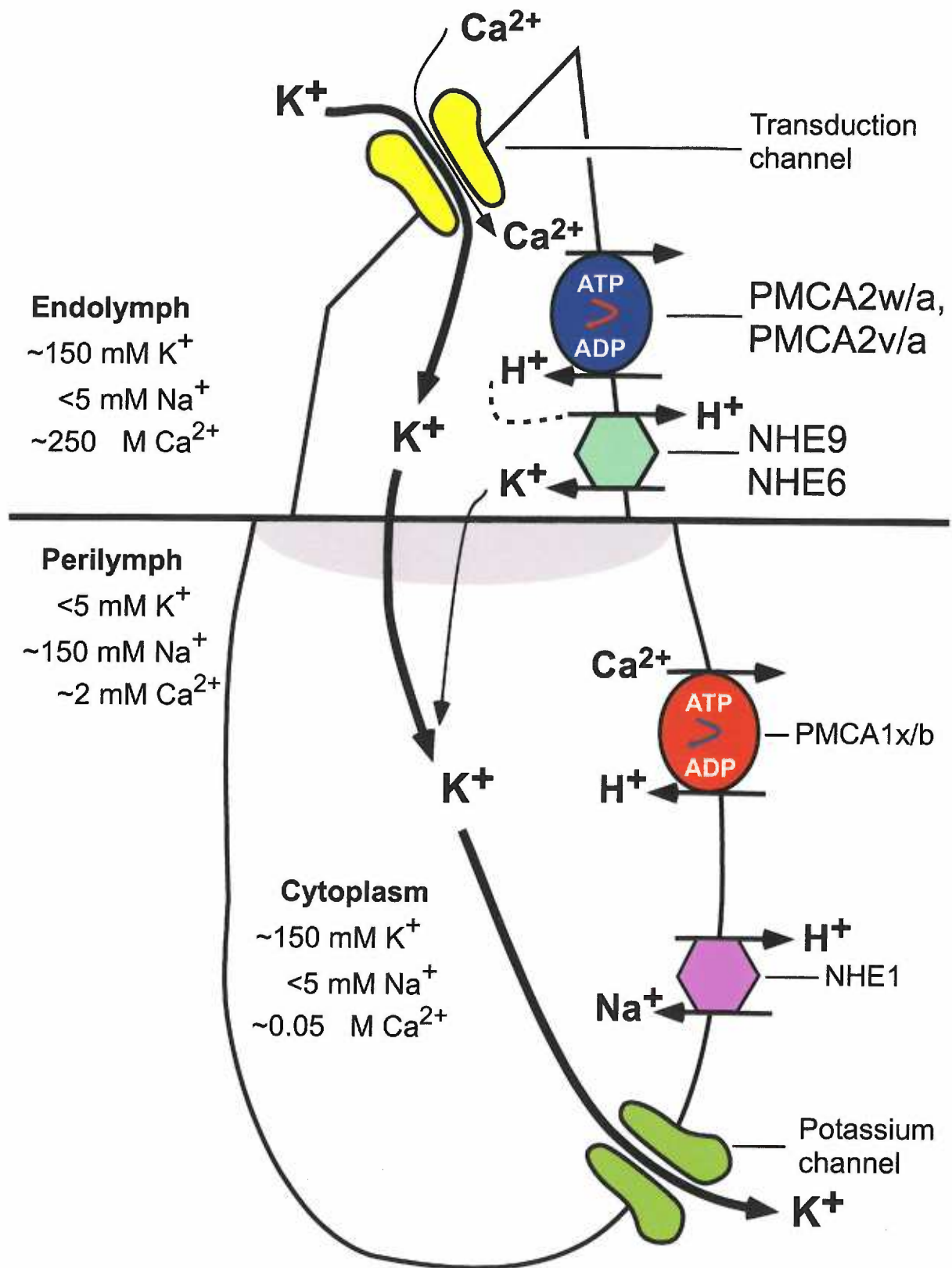
DISCUSSION II

These results demonstrate that hair bundles use a mechanism of H^+ extrusion that is distinct from that of the soma. The soma relies on the transmembrane Na^+ gradient to drive H^+ removal; we propose, however, that hair bundles use NHE9 and perhaps NHE6 for K^+ -dependent H^+ exchange. H^+ transport with members of the NHE family is a particularly elegant solution for the hair bundle. Since K^+ is at similar concentrations on either side of the plasma membrane of the hair bundle, the electroneutral transport of the NHEs would allow the bundle to respond only to an imbalance in the concentration of H^+ . In this model, there would be no net transport of H^+ into or out of the hair bundle; H^+ would be locally recycled. Since K^+ is the major charge carrier during transduction, the K^+ counterion used for H^+ transport would not pose a problem to the hair cell because there is already an established pathway for cycling K^+ back to the endolymph (reviewed in Wangemann, 2002b). Lastly, since the NHEs are not ATP dependent, there would not be an increased burden for the hair cell to supply ATP both to the pump bringing in H^+ (PMCA) and to the transporter removing H^+ (Figure 40).

PMCA activity acidifies hair bundles

Sustained K^+ depolarization results in a decrease in bundle pH, presumably due to Ca^{2+} entering through voltage dependent calcium channels (VDCC) in the soma, diffusing to the bundle, and being extruded by PMCA2v/a. Inhibition of PMCA with 100 μM La^{3+} blocks the pH decrease. VDCC also show a sensitivity to La^{3+} block that could

Figure 40. Model for the regulation of ion flux in hair cells. During transduction, the influx of Ca^{2+} activates PMCA2w/a (rat) or PMCA2v/a (frog). These obligatory $\text{Ca}^{2+}/\text{H}^{+}$ pumps use the energy from ATP hydrolysis to extrude Ca^{2+} from the hair bundle. We hypothesize that the influx of H^{+} ($\sim 1 \text{ mM s}^{-1}$) resulting from the Ca^{2+} extrusion is removed primarily by the non-ATP dependent NHE9 and NHE6 in exchange for K^{+} . The small influx of K^{+} from NHE-mediated exchange will be cycled out of the hair cell using the same recycling pathway for K^{+} entering through the transduction channel. K^{+} from the bundle will passively flow to the soma and across the basolateral membrane down its concentration gradient (K^{+} -leak channels); supporting cells transport the K^{+} back to the endolymph. $\text{Ca}^{2+}/\text{H}^{+}$ exchange in the soma is mediated by PMCA1x/b. NHE1 uses the high Na^{+} transmembrane gradient across the basolateral membrane to maintain soma pH.



contribute to the lack of pH change. Recent evidence, however, suggests that L-type calcium channels, such as are expressed in hair cells, require millimolar concentrations of La^{3+} for inhibition and would not be greatly affected by the 100 μM used in Figure 22 (Yeoman et al., 1999). Furthermore, since the hair cells are initially Ca^{2+} -loaded by K^+ -depolarization, the VDCC would not need to play a major role in Ca^{2+} flux during the subsequent application of K^+ plus La^{3+} . Therefore, we conclude that the reversal of pH seen in Figure 22F is from the La^{3+} inhibition of PMCA, and not a failure to Ca^{2+} load the hair cell.

The significant change in pH seen during a K^+ depolarization is presumably due to the prolonged (~ 5 min) stimulus. When PMCA is inhibited, we propose that NHE9 can then restore homeostatic pH. We postulate that during a physiological stimulus, the rate of the NHE transport can maintain a constant H^+ concentration in response to PMCA activity. In fact, in extreme cases of calcium loading, PMCA is predicted to exchange Ca^{2+} for H^+ at $\sim 1 \text{ mM s}^{-1}$ (Yamoah et al., 1998); this is identical to the rate of H^+ extrusion we measure during an extreme H^+ load in hair bundles ($\sim 1 \text{ mM s}^{-1}$; Figures 23 & 24).

NHE6 and NHE9 are candidates for the hair bundle H^+ transporter

Since we find NHE6 only in a subset of bullfrog saccular hair cells, perhaps this isoform plays a more significant role in development; by contrast, NHE9, which is expressed in all hair bundles, is likely responsible for pH maintenance in mature cells. There is very little known about the specific function of the hair cells with small diameter bundles where NHE6 is primarily localized. The strong immunolabeling with anti-

calretinin is reminiscent of developing type II cells of the mammalian vestibular system (Dechesne et al., 1994). Based on these results, we propose that NHE9 is the primary H^+ transporter in hair bundles and will focus this discussion largely on this isoform.

NHE9 is localized to bullfrog saccular hair bundles

Surface biotinylation of tissue culture cells demonstrates that NHE6, NHE8, and NHE9 can all traffic to the plasma membrane; although the function of transient surface expression is unclear, it is believed to be a necessary step in the targeting of NHEs to intracellular compartments (Brett et al., 2002; Goyal et al., 2005); Figures 27 & 28). Cell fractionation and fluorescence immunodetection experiments with NHE8 localized this isoform to the apical membranes of kidney proximal tubules and intestinal epithelia (Goyal et al., 2003; Xu et al., 2005). Our results from immunolabeling with antibodies revealed a striking distribution for NHE9 in bullfrog hair cells; NHE9 is located specifically in the hair bundle, concentrated at the tips of the stereocilia, and is excluded from the soma. This result suggests that the localization of NHE9 reflects specific targeting of a H^+ transporter to the stereocilia, rather than transient trafficking.

To characterize the role of NHE9 as the bundle H^+ transporter, we propose to examine the protein interaction of PMCA and NHE9. Initially, we will use co-immunoprecipitation analysis from surface biotinylated bundles. Close proximity of NHE9 to PMCA is not a requirement for counterbalancing PMCA activity; nevertheless, identifying interactions may give us insight into targeting and regulation of these two important bundle proteins.

NHE9 is expressed in rat auditory and vestibular organs

Localization of NHE9 in rodent auditory and vestibular tissue was more ambiguous than in bullfrog sacculus. Fluorescence immunolabeling localized NHE9 to hair bundles as well as to the soma of hair cells from adult rats, although NHE9 was not detected in neonatal rat utricular bundles or maculae by immunoblot. The circumstances for loading the gel, nevertheless, were not ideal and may explain these results. The bundles were originally isolated and run on a gel primarily for detecting a protein that would aggregate upon heating. Therefore, the agarose-embedded bundles (see METHODS) were incubated at room temperature in sample buffer, and the agarose blocks were loaded into a well of an acrylamide gel with forceps. It is possible that not all the proteins were extracted by the sample buffer, so that NHE9 might not have run into the gel. It is also possible that NHE9 is not expressed in the neonatal utricle, since the immunohistochemistry results clearly show NHE9 immunoreactivity in the utriculi of adult rats. Immunoprecipitating surface biotinylated bundle proteins is a much more practical method for localizing NHE9 to the surface of rat or frog hair-bundles. Only a few ear equivalents are needed for biotinylation assays, compared to the tens or hundreds of ear equivalents necessary for direct detection.

NHE9 also localized to membrane blebs that formed near the apical surface of rat utricular hair cells. A recent paper identified membrane blebs from guinea pig inner hair cells as part of an apical membrane recycling pathway (Shi et al., 2005). Interestingly, NHE9 does not colocalize with PMCA in every bleb. Because it appears that NHE9 is expressed in intracellular membranes of the soma, not colocalizing with PMCA, the distribution of NHE9 and PMCA in the blebs suggests that some membrane blebs are

forming from the stereocilia and others are budding from the soma apical surface. These data could also represent different recycling pathways for these two proteins. Biotinylation of surface proteins, immunoprecipitation with NHE9, and avidin detection will be a sensitive method for determining membrane localization of NHE9 in rat utricle. Additionally, we can examine membrane localization by fluorescence microscopy by co-labeling cells with anti-NHE9 and fluorescently labeled annexin V, which binds phosphatidylserine, the major anionic phospholipid in the intracellular leaflet of the plasma membrane. This question would also lend itself to gene-gun transfection, using a similar approach as described in the PMCA section.

SDS-PAGE analysis of NHE isoforms: glycosylation and aggregation

An interesting challenge that has arisen with working with NHE proteins is the inconsistency between predicted molecular weights and their observed mobilities on SDS gels. Recent studies with NHE8 suggest that because surface NHE8 is glycosylated, it often appears on SDS gels as two bands: a strong band at 80 kDa, the “mature” glycosylated form, and a weaker band at 55 kDa, the “immature” form (Goyal et al., 2005). Although sensitivity to endoglycosidase H suggests that NHE6 is also glycosylated (Miyazaki et al., 2001), glycosylation does not seem to be the complete answer to the size paradox. Using epitope-tagged protein expression in COS-7 cells, we found that NHE6 appears to aggregate, similarly to NHE7; bands of >200 kD corresponding to each have been detected in immunoblots (Figure 29; (Numata and Orłowski, 2001). Although NHE9 does not appear to aggregate to the extent of NHE6 and NHE7, surface biotinylation experiments show two prominent bands between 50 kDa

and 75 kDa; these could be “immature” and “mature” forms of the protein, comparable to those of NHE8. Immunoblots of mouse brain membrane preparations also show a multi-band pattern when probed with anti-NHE9, which could reflect splicing or posttranslationally modified variants of NHE9. Although this family does not have a reputation for multiple splice variants, there is precedent for alternate mRNA splicing with hNHE6 (Orlowski and Grinstein, 2004; Miyazaki et al., 2001).

Cation selectivity of NHE9

Replacing Na^+ with NMDG^+ did not cause a significant reduction in the rate of H^+ extrusion from hair bundles. These results suggest that NHE9 could be using NMDG^+ as a counterion for H^+ transport, which is very unusual given the size of this cation. The Na^+ -containing and Na^+ -free solutions each have 2 mM K^+ (Table 2); this concentration should not be high enough to drive the pH back to resting levels. It is likely that NHE9 is using the Na^+ in the standard saline and is using the NMDG^+ in the Na^+ -free solution to regain resting pH. In order to understand how NHE9 functions *in vivo*, where it is unlikely to use Na^+ , it will be important to demonstrate that NHE9 can use K^+ as a counterion for H^+ exchange and show that NMDG^+ , despite its size, can be used as an NHE substrate. Using microsomes from NHE9 transfected COS-7 cells, we will use *in vitro* $^{86}\text{Rb}^+$ assays to examine the ability of NHE9 to use K^+ and NMDG^+ . Rb^+ can act as a substrate for K^+ -dependent transporters and $^{86}\text{Rb}^+$ is often substituted for $^{42}\text{K}^+$ because it is a lower energy radionuclide and has a longer half-life. These assays are based on methods published for $^{45}\text{Ca}^{2+}$ flux assays for PMCA reconstituted in microsomes (Enyedi et al., 1993).

Using pharmacological manipulations to identify the bundle H^+ transporter

In our quest to find a hair bundle H^+ transporter, we tried several pharmacological treatments to elucidate the identity of the responsible molecules. Moreover, we ran into many technical challenges associated with reproducibly acid loading hair cells. Many of the inhibitors we tried yielded inconclusive results because we could not get a sufficiently large acid load to monitor recovery. An added frustration of working with NHE6-9 is the lack of specific inhibitors, unlike the Na^+ -selective NHE isoforms, which are highly sensitive to amiloride and its derivatives, NHE6-9 are generally insensitive to these reagents (reviewed in Orłowski et al., 1997); therefore, we were unable to directly examine the pharmacology of NHE9 in hair bundles. Table 5 summarizes the treatments used to manipulate hair cell pH. Conditions 1-3 were the standard conditions for data reported in this dissertation. We used inhibitors (conditions 8-12) to several common H^+ transporter families; however, the sample sizes were never large enough to gain any significance from the results. In a futile attempt to increase the acid load, we tried K^+ depolarization (15 mM) in conjunction with the NH_4^+ pulse. Although the exact mechanism by which NH_4^+ enters cells is poorly understood, we postulated that the ion could enter through the cation non-selective mechanotransduction channels. There is controversial evidence suggesting that when tip links are broken, the associated transduction channels remain open for a few minutes (Meyer et al., 1998). To facilitate channel opening and thus an increase in NH_4^+ permeability, we used EGTA to chelate calcium and break tip links. Application of 5 mM EGTA for 5 min did not cause a

subsequent increase in acidification from the NH_4^+ pulse. In addition to the *in vitro* assays discussed above, we are continuing to work on conditions that will give us consistent acid loads in hair cells, required in order to fully characterize NHE9 as the bundle H^+ transporter.

TABLE 5. Pharmacological manipulations for assaying
pH recovery in hair bundles

	Pre-Pulse	NH_4^+ pulse	Washout
1	Standard Saline	NH_4^+	Standard Saline
2	Standard Saline	NH_4^+	NMDG $^+$
3	Standard Saline	NH_4^+ /NMDG $^+$	NMDG $^+$
4	NMDG $^+$	NH_4^+ /NMDG $^+$	Standard Saline
5	NMDG $^+$	NH_4^+ /NMDG $^+$	NMDG $^+$
6	Standard Saline	NH_4^+ /NMDG $^+$	Low Na^+/K^+
7	EGTA/Standard Saline	NH_4^+ /15 mM K^+ /NMDG $^+$	NMDG $^+$
8	Standard Saline	NH_4^+ /15 mM K^+ /NMDG $^+$	NMDG $^+$ /DIDS (300 μM)
9	EGTA/Standard Saline	NH_4^+ /15 mM K^+ /NMDG $^+$	NMDG $^+$ /DIDS
10	Standard Saline	NH_4^+ /NMDG $^+$	NMDG $^+$ /ouabain (1 mM)
11	Standard Saline	NH_4^+ /NMDG $^+$	NMDG $^+$ /bafilomycin A_1 (50 nM)
12	Standard Saline	NH_4^+	NMDG $^+$ /benzamil (1 mM)

SUMMARY AND CONCLUSIONS

Nearly 30 million Americans suffer from hearing deficits; at an annual cost to society of over \$50 billion, it is incumbent upon us to understand the underlying causes of hearing impairment in order to reduce these significant personal and financial burdens. Whereas age-related hearing loss is the prevailing form of impairment, many other factors, including environmental and pharmacological insults and inherited genetic defects, cause hearing and balance dysfunction. Damage to the sensory cells of the inner ear is the most frequent underlying cause.

A properly functioning hair bundle is crucial for the overall function of the hair cell. Mutations in some hair-bundle proteins have already been identified as causative factors of hearing and vestibular defects. One such protein is the plasma membrane Ca^{2+} -ATPase (PMCA), responsible for removing over two-thirds of the Ca^{2+} that enters the hair bundle during transduction (Lumpkin and Hudspeth, 1998). Given the critical role of Ca^{2+} regulation in transduction, one goal of this dissertation was to contribute to the understanding of how Ca^{2+} is regulated. Although the Gillespie lab had previously identified the frog hair-bundle PMCA isozyme as PMCA2v/a (Dumont et al., 2001), we were not able to identify the specific PMCA2a splice site A variant expressed in rodent hair bundles. Using isoform specific antibodies and gene gun transfection we established that the rodent hair-bundle Ca^{2+} pump is PMCA2w/a. Furthermore, this is the first identification of a region within a protein that dictates bundle-specific targeting.

Given the critical role for PMCA in hearing and balance, we hypothesized that H^+ regulation would be equally important for proper hair-bundle function. Over a decade has

passed since Ikeda et al. (1992) reported a Na^+ -dependent H^+ transporter in the soma of guinea pig outer hair cells. A few years later, the same group used *in situ* hybridization to localize NHE1 mRNA in guinea pig outer hair cells (Goto et al., 1999). Since then, very little literature has appeared on the regulation of pH in hair cells; in particular, no studies specifically looking at regulation in the hair bundle have appeared.

There are two mechanisms by which hair bundles could remove H^+ as a counterbalance to PMCA activity: a) H^+ could be buffered, allowed to diffuse to the soma, and be extruded by Na^+/H^+ exchange, or b) there could be a local H^+ transporter. We demonstrated that hair bundles have a H^+ extrusion mechanism that is independent from that of the soma. Bundles have the ability to restore pH to the resting level despite the pH remaining low in the soma. Integrating cell biology, biochemistry, and molecular biology, we identified two candidate molecules as bundle H^+ transporters, NHE6 and NHE9, both of which are members of the Na^+/H^+ exchanger family. Although the more familiar family members NHE1-5 are Na^+ selective, the newer members, NHE6-9, can use (or are predicted to use) K^+ as a counterion for H^+ transport. We propose that NHE9, and perhaps NHE6, are targeted to stereociliary membranes and use the K^+ -rich endolymph to remove H^+ from hair bundles.

OPEN QUESTIONS

This section summarizes open questions related to PMCA2w/a targeting and H⁺ regulation in hair bundles. Although future experiments were mentioned within their relevant discussions, specific experiments are highlighted here to illustrate our approach to answering these questions.

Characterization of hair bundle PMCA2w/a in rodent hair bundles

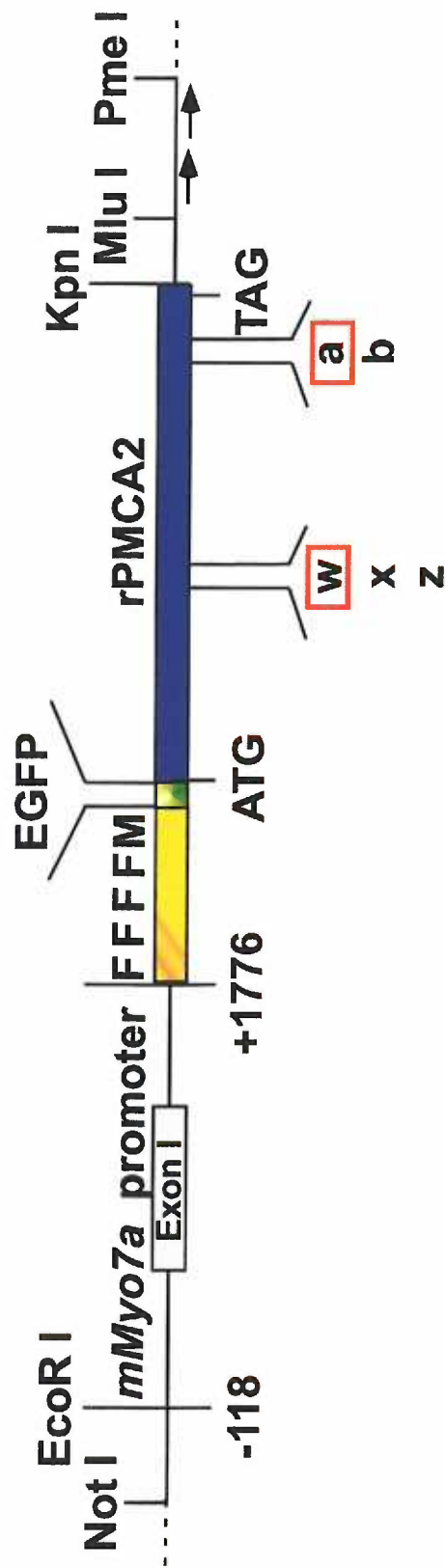
Aim 1. Is PMCA2w/a in mouse hair cells required for hearing and balance? Our goal is to cross *Pmca2* null mice with mice expressing PMCA2w/a only in hair bundles to determine if the deafness and/or vestibular phenotype can be rescued.

We have made a conventional transgenic construct with GFP-tagged PMCA2w/a under the control of the minimal myosin-VIIa promoter (Boeda et al., 2001; Figure 41). Expression and targeting of this construct will be tested by gene gun transfection before oocyte injections.

Aim 2. Is “w” sufficient for hair bundle targeting? Our goal is to demonstrate that “w” is sufficient for dictating apical targeting. A part of this aim will also include identifying the minimal sequence required for apical targeting.

2a. We will assemble EGFP-tagged constructs comprised of PMCA1, PMCA3, or PMCA4 with the “w” insert. These constructs will initially be transfected into tissue culture cells to test for plasma membrane expression. Subsequently, the

Figure 41. PMCA2w/a transgenic construct. Key features of the construct include the minimal *Myo7a* promoter, Flag (F) and myc (M) epitope tags, EGFP, the rat PMCA2 sequence (with "w" and "a" variants at splice sites A and C), and chicken β -globin insulators (to prevent silencing of the transgenic construct). Translation starts at the FFFFM epitope tags.



F = Flag tag

M = Myc tag

→ 250-bp tandem repeat core of chicken β -globin insulator

constructs will be transfected by gene gun into inner-ear epithelia and bundle expression of EGFP will be monitored.

2b. PMCA2w/a constructs with parts of the “w” sequence will be transfected into inner-ear epithelia to locate the minimal sequence required for apical targeting. If a sequence is identified it will be verified by assembling constructs with the “b” form, which should not affect apical expression.

Aim 3. Does PMCA2w/a interact with membrane lipids for localization and regulation? PMCA2w/a is not only targeted to stereocilia, but also focally directed to the tips, the site of maximal Ca^{2+} entry. Our goal is to understand how and why PMCA is concentrated in these areas. Although this aim mostly entails recombinant PMCA2w/a, for *in vivo* experiments we will use bullfrog hair cells, which express PMCA2v/a in their bundles.

3a. Immunoreactivity of PIP_2 , a potent activator of PMCA activity, is abolished by treating bullfrog hair cells with phenylarsine oxide (PAO) (Hirono et al., 2004). We will examine the distribution of PMCA2v/a following PAO treatment.

3b. We will examine the ability of PMCA2w/a or PMCA2v/a fragments to bind acidic phospholipids bound to nitrocellulose membranes (PIP strips), similar to our binding measurements with myosin-1c (Hirono et al., 2004).

3c. Using $^{45}\text{Ca}^{2+}$ flux assays with PMCA2w/a expressing microsomes, we will test the ability of the phospholipids identified in 3b to regulate enzyme activity.

Characterization of Na⁺/H⁺ exchanger 9

Aim 1. Characterize membrane localization of NHE9 in frog and rodent hair cells.

Fluorescent immunolabeling localized NHE9 to bullfrog vestibular hair bundles; however, it is expressed in the bundles and soma of rat auditory and vestibular hair cells. Although the soma labeling appears to be intracellular, the following experiments will determine if NHE9 is expressed on the plasma membrane of hair cells.

1a. To examine surface expression of NHE9 in stereociliary membranes we will analyze surface proteins of isolated hair bundles. Vestibular organs from frog and rat will be subjected to surface biotinylation. Hair bundles will be isolated from the residual maculae and separately immunoprecipitated with anti-NHE9. Surface proteins will be detected on a blot with alkaline phosphatase conjugated avidin.

1b. The plasma membrane is rich with phosphatidylserine, a phospholipid that binds with high affinity to annexin V. We will co-label rat hair cells with fluorescently labeled annexin V to analyze NHE9 membrane localization.

1c. Epitope-tagged NHE6 and NHE9 will be transfected by gene-gun into rat auditory and vestibular organs to examine hair cell localization.

Aim 2. Characterize the cation selectivity of NHE9. In order to have a functional link between bundle H⁺ transport and activity of a candidate transporter, we must show that NHE9 can use K⁺ to transport H⁺.

2a. NHE9 will be expressed in tissue culture cells and H⁺ pumping activity will be measured from microsomal preparations using a ⁸⁶Rb⁺ flux assay. This is similar

to the $^{45}\text{Ca}^{2+}$ flux assay we will use for assaying PMCA activity (PMCA Subaim 3c).

2b. There is an open question as to whether the bundle H^+ transporter can use NMDG^+ as a counterion. To answer this question we will use a fluorescence-based assay to monitor pH change in NHE9 expressing microsomes. This assay was used to determine cation selectivity of NHE8 and relies on the pH indicator pyranine, which has increased fluorescence in alkaline solutions. Therefore, an acidified microsome should have an increase in fluorescence in the presence of NMDG^+ , if this cation can be used for H^+ transport.

2c. We will use our *in vivo* pH assay to show that bundles can extrude H^+ , after acid loading, in the presence of high extracellular K^+ and no Na^+ .

Aim 3. Determine interaction of PMCA and NHE9. Although PMCA and NHE9 interaction is not essential to NHE9 being the bundle H^+ transporter, their localization patterns in frog hair cells was remarkably similar, suggesting that they may interact. Co-immunoprecipitation analyses will be performed on isolated bullfrog hair bundles and residual maculae.

REFERENCES

- Assad, J. A., and Corey, D. P. (1992). An active motor model for adaptation by vertebrate hair cells. *J Neurosci* 12:3291-3309.
- Assad, J. A., Shepherd, G. M. G., and Corey, D. P. (1991). Tip-link integrity and mechanical transduction in vertebrate hair cells. *Neuron* 7:985-994.
- Boeda, B., Weil, D., and Petit, C. (2001). A specific promoter of the sensory cells of the inner ear defined by transgenesis. *Hum Mol Genet* 10:1581-1589.
- Bond, B. R., Ng, L. L., and Schulte, B. A. (1998). Identification of mRNA transcripts and immunohistochemical localization of Na/H exchanger isoforms in gerbil inner ear. *Hear Res* 123:1-9.
- Brett, C. L., Donowitz, M., and Rao, R. (2005a). Evolutionary origins of eukaryotic sodium/proton exchangers. *Am J Physiol Cell Physiol* 288:C223-39.
- Brett, C. L., Tukaye, D. N., Mukherjee, S., and Rao, R. (2005b). The yeast endosomal $\text{Na}^+(\text{K}^+)/\text{H}^+$ exchanger Nhx1 regulates cellular pH to control vesicle trafficking. *Mol Biol Cell* 16:1396-1405.
- Brett, C. L., Wei, Y., Donowitz, M., and Rao, R. (2002). Human $\text{Na}(+)/\text{H}(+)$ exchanger isoform 6 is found in recycling endosomes of cells, not in mitochondria. *Am J Physiol Cell Physiol* 282:C1031-41.
- Brodin, P., Falchetto, R., Vorherr, T., and Carafoli, E. (1992). Identification of two domains which mediate the binding of activating phospholipids to the plasma-membrane Ca^{2+} pump. *Eur J Biochem* 204:939-946.
- Brownell, W. E., Bader, C. R., Bertrand, D., and de Ribaupierre, Y. (1985). Evoked mechanical responses of isolated cochlear outer hair cells. *Science* 227:194-196.

- Bullis, B. L., Li, X., Singh, D. N., Berthiaume, L. G., and Fliegel, L. (2002). Properties of the Na^+/H^+ exchanger protein. Detergent-resistant aggregation and membrane microdistribution. *Eur J Biochem* 269:4887-4895.
- Chalfie, M., and Sulston, J. (1981). Developmental genetics of the mechanosensory neurons of *Caenorhabditis elegans*. *Dev Biol* 82:358-370.
- Chicka, M. C., and Strehler, E. E. (2003). Alternative splicing of the first intracellular loop of plasma membrane Ca^{2+} -ATPase isoform 2 alters its membrane targeting. *J Biol Chem* 278:18464-18470.
- Choquette, D., Hakim, G., Filoteo, A. G., Plishker, G. A., Bostwick, J. R., and Penniston, J. T. (1984). Regulation of plasma membrane Ca^{2+} ATPases by lipids of the phosphatidylinositol cycle. *Biochem Biophys Res Commun* 125:908-915.
- Corey, D. P., Garcia-Anoveros, J., Holt, J. R., Kwan, K. Y., Lin, S. Y., Vollrath, M. A., Amalfitano, A., Cheung, E. L., Derfler, B. H., Duggan, A., Geleoc, G. S., Gray, P. A., Hoffman, M. P., Rehm, H. L., Tamasauskas, D., and Zhang, D. S. (2004). TRPA1 is a candidate for the mechanosensitive transduction channel of vertebrate hair cells. *Nature* 432:723-730.
- Crawford, A. C., Evans, M. G., and Fettiplace, R. (1991). The actions of calcium on the mechano-electrical transducer current of turtle hair cells. *J Physiol (Lond)* 434:369-398.
- Crawford, A. C., and Fettiplace, R. (1985). The mechanical properties of ciliary bundles of turtle cochlear hair cells. *J Physiol (Lond)* 364:359-379.
- Crouch, J. J., and Schulte, B. A. (1995). Expression of plasma membrane Ca-ATPase in the adult and developing gerbil cochlea. *Hear Res* 92:112-119.
- Crouch, J. J., and Schulte, B. A. (1996). Identification and cloning of site C splice variants of plasma membrane Ca-ATPase in the gerbil cochlea. *Hear Res* 101:55-61.

- Crouch, J. J., Sakaguchi, N., Lytle, C., and Schulte, B. A. (1997). Immunohistochemical localization of the Na-K-Cl co-transporter (NKCC1) in the gerbil inner ear. *J Histochem Cytochem* 45:773-778.
- Dallos, P., and Fakler, B. (2002). Prestin, a new type of motor protein. *Nat Rev Mol Cell Biol* 3:104-111.
- Davis, H. (1983). An active process in cochlear mechanics. *Hear Res* 9:79-90.
- Dechesne, C. J., Rabejac, D., and Desmadryl, G. (1994). Development of calretinin immunoreactivity in the mouse inner ear. *J Comp Neurol* 346:517-529.
- Dechesne, C. J., Winsky, L., Kim, H. N., Goping, G., Vu, T. D., Wenthold, R. J., and Jacobowitz, D. M. (1991). Identification and ultrastructural localization of a calretinin-like calcium-binding protein (protein 10) in the guinea pig and rat inner ear. *Brain Res* 560:139-148.
- Delpire, E., Lu, J., England, R., Dull, C., and Thorne, T. (1999). Deafness and imbalance associated with inactivation of the secretory Na-K-2Cl co-transporter. *Nat Genet* 22:192-195.
- DeMarco, S. J., Chicka, M. C., and Strehler, E. E. (2002). Plasma membrane Ca^{2+} ATPase isoform 2b interacts preferentially with Na^+/H^+ exchanger regulatory factor 2 in apical plasma membranes. *J Biol Chem* 277:10506-10511.
- Denk, W., Holt, J. R., Shepherd, G. M., and Corey, D. P. (1995). Calcium imaging of single stereocilia in hair cells: localization of transduction channels at both ends of tip links. *Neuron* 15:1311-1321.
- Di Palma, F., Belyantseva, I. A., Kim, H. J., Vogt, T. F., Kachar, B., and Noben-Trauth, K. (2002). Mutations in Mcoln3 associated with deafness and pigmentation defects in varitint-waddler (Va) mice. *Proc Natl Acad Sci U S A* 99:14994-14999.
- Dou, H., Finberg, K., Cardell, E. L., Lifton, R., and Choo, D. (2003). Mice lacking the B1 subunit of H^+ -ATPase have normal hearing. *Hear Res* 180:76-84.

- Drenckhahn, D., Engel, K., Höfer, D., Merte, C., Tilney, L., and Tilney, M. (1991). Three different actin filament assemblies occur in every hair cell: each contains a specific actin crosslinking protein. *J Cell Biol* 112:641-651.
- Dumont, R. A., Lins, U., Filoteo, A. G., Penniston, J. T., Kachar, B., and Gillespie, P. G. (2001). Plasma membrane Ca^{2+} -ATPase isoform 2a is the PMCA of hair bundles. *J Neurosci* 21:5066-5078.
- Dumont, R. A., and Gillespie, P. G. (2000). Plasma membrane Ca^{2+} -ATPase and hair-cell function. In *Cell and Molecular Biology of the Ear*, Lim, D., ed. (New York: Plenum), pp. 41-54.
- Eatock, R. A., Corey, D. P., and Hudspeth, A. J. (1987). Adaptation of mechanoelectrical transduction in hair cells of the bullfrog's sacculus. *J Neurosci* 7:2821-2836.
- Edmonds, B., Reyes, R., Schwaller, B., and Roberts, W. M. (2000). Calretinin modifies presynaptic calcium signaling in frog saccular hair cells. *Nat Neurosci* 3:786-790.
- Enyedi, A., Elwess, N. L., Filoteo, A. G., Verma, A. K., Paszty, K., and Penniston, J. T. (1997). Protein kinase C phosphorylates the "a" forms of plasma membrane Ca^{2+} pump isoforms 2 and 3 and prevents binding of calmodulin. *J Biol Chem* 272:27525-27528.
- Enyedi, A., Filoteo, A. G., Gardos, G., and Penniston, J. T. (1991). Calmodulin-binding domains from isozymes of the plasma membrane Ca^{2+} pump have different regulatory properties. *J Biol Chem* 266:8952-8956.
- Enyedi, A., Verma, A. K., Filoteo, A. G., and Penniston, J. T. (1993). A highly active 120-kDa truncated mutant of the plasma membrane Ca^{2+} pump. *J Biol Chem* 268:10621-10626.
- Enyedi, A., Verma, A. K., Heim, R., Adamo, H. P., Filoteo, A. G., Strehler, E. E., and Penniston, J. T. (1994). The Ca^{2+} affinity of the plasma membrane Ca^{2+} pump is controlled by alternative splicing. *J Biol Chem* 269:41-43.

- Fain, G. L. (1999). *Molecular and Cellular Physiology of Neurons* (Cambridge, MA: Harvard University Press).
- Fain, G. L. (2003). *Sensory Transduction* (Sunderland, MA: Sinauer Associates).
- Fanning, A. S., and Anderson, J. M. (1999). Protein modules as organizers of membrane structure. *Curr Opin Cell Biol* 11:432-439.
- Furuta, H., Luo, L., Hepler, K., and Ryan, A. F. (1998). Evidence for differential regulation of calcium by outer versus inner hair cells: plasma membrane Ca-ATPase gene expression. *Hear Res* 123:10-26.
- Gillespie, P. G., and Corey, D. P. (1997). Myosin and adaptation by hair cells. *Neuron* 19:955-958.
- Gillespie, P. G., and Gillespie, S. K. (1997). Improved electrophoresis and transfer of picogram amounts of protein with hemoglobin. *Anal Biochem* 246:239-245.
- Gillespie, P. G., and Hudspeth, A. J. (1991). High-purity isolation of bullfrog hair bundles and subcellular and topological localization of constituent proteins. *J Cell Biol* 112:625-640.
- Gillespie, P. G., and Walker, R. G. (2001). Molecular basis of mechanosensory transduction. *Nature* 413:194-202.
- Gillespie, P. G. (1995). Molecular machinery of auditory and vestibular transduction. *Curr Opin Neurobiol* 5:449-455.
- Gillespie, P. G. (2004). Myosin I and adaptation of mechanical transduction by the inner ear. *Philos Trans R Soc Lond B Biol Sci* 359:1945-1951.
- Gong, Z., Son, W., Chung, Y. D., Kim, J., Shin, D. W., McClung, C. A., Lee, Y., Lee, H. W., Chang, D. J., Kaang, B. K., Cho, H., Oh, U., Hirsh, J., Kernan, M. J., and Kim, C. (2004). Two interdependent TRPV channel subunits, inactive and Nanchung, mediate hearing in *Drosophila*. *J Neurosci* 24:9059-9066.

- Goto, S., Oshima, T., Ikeda, K., and Takasaka, T. (1999). Expression and localization of the $\text{Na}^+\text{-H}^+$ exchanger in the guinea pig cochlea. *Hear Res* 128:89-96.
- Goyal, S., Mentone, S., and Aronson, P. S. (2005). Immunolocalization of NHE8 in rat kidney. *Am J Physiol Renal Physiol* 288:F530-8.
- Goyal, S., Vanden Heuvel, G., and Aronson, P. S. (2003). Renal expression of novel $\text{Na}^+\text{/H}^+$ exchanger isoform NHE8. *Am J Physiol Renal Physiol* 284:F467-73.
- Hao, L., Rigaud, J. L., and Inesi, G. (1994). $\text{Ca}^{2+}\text{/H}^+$ countertransport and electrogenicity in proteoliposomes containing erythrocyte plasma membrane Ca-ATPase and exogenous lipids. *J Biol Chem* 269:14268-14275.
- Hemken, P., Guo, X. L., Wang, Z. Q., Zhang, K., and Gluck, S. (1992). Immunologic evidence that vacuolar H^+ ATPases with heterogeneous forms of Mr = 31,000 subunit have different membrane distributions in mammalian kidney. *J Biol Chem* 267:9948-9957.
- Heywood, P., Van de Water, T. R., Hilding, D. A., and Ruben, R. J. (1975). Distribution of microtubules and microfilaments in developing vestibular sensory epithelium of mouse otocysts grown in vitro. *J Cell Sci* 17:171-189.
- Hirono, M., Denis, C. S., Richardson, G. P., and Gillespie, P. G. (2004). Hair cells require phosphatidylinositol 4,5-bisphosphate for mechanical transduction and adaptation. *Neuron* 44:309-320.
- Holt, J. R., Gillespie, S. K., Provance, D. W., Shah, K., Shokat, K. M., Corey, D. P., Mercer, J. A., and Gillespie, P. G. (2002). A chemical-genetic strategy implicates myosin-1c in adaptation by hair cells. *Cell* 108:371-381.
- Howard, J., and Hudspeth, A. J. (1987). Mechanical relaxation of the hair bundle mediates adaptation in mechanoelectrical transduction by the bullfrog's saccular hair cell. *Proc Natl Acad Sci U S A* 84:3064-3068.

- Howard, J., and Hudspeth, A. J. (1988). Compliance of the hair bundle associated with gating of mechanoelectrical transduction channels in the bullfrog's saccular hair cell. *Neuron* 1:189-199.
- Hudspeth, A. J. (1989). How the ear's works work. *Nature* 341:397-404.
- Hudspeth, A. J. (1992). Hair-bundle mechanics and a model for mechanoelectrical transduction by hair cells. *Soc Gen Physiol Ser* 47:357-370.
- Hudspeth, A. J., and Gillespie, P. G. (1994). Pulling springs to tune transduction: adaptation by hair cells. *Neuron* 12:1-9.
- Hudspeth, A. J., and Jacobs, R. (1979). Stereocilia mediate transduction in vertebrate hair cells (auditory system/cilium/vestibular system). *Proc Natl Acad Sci U S A* 76:1506-1509.
- Hudspeth, A. J. (1997). Mechanical amplification of stimuli by hair cells. *Curr Opin Neurobiol* 7:480-486.
- Hung, A. Y., and Sheng, M. (2002). PDZ domains: structural modules for protein complex assembly. *J Biol Chem* 277:5699-5702.
- Ikeda, K., Saito, Y., Nishiyama, A., and Takasaka, T. (1992). Intracellular pH regulation in isolated cochlear outer hair cells of the guinea-pig. *J Physiol* 447:627-648.
- Iwano, T., Yamamoto, A., Omori, K., Akayama, M., Kumazawa, T., and Tashiro, Y. (1989). Quantitative immunocytochemical localization of Na⁺,K⁺-ATPase alpha-subunit in the lateral wall of rat cochlear duct. *J Histochem Cytochem* 37:353-363.
- Jacobs, R. A., and Hudspeth, A. J. (1990). Ultrastructural correlates of mechanoelectrical transduction in hair cells of the bullfrog's internal ear. *Cold Spring Harb Symp Quant Biol* 55:547-561.
- Jaisser, F., and Beggah, A. T. (1999). The nongastric H⁺-K⁺-ATPases: molecular and functional properties. *Am J Physiol* 276:F812-24.

- Kachar, B., Parakkal, M., Kurc, M., Zhao, Y., and Gillespie, P. G. (2000). High-resolution structure of hair-cell tip links. *Proc Natl Acad Sci U S A* 97:13336-13341.
- Karet, F. E., Finberg, K. E., Nelson, R. D., Nayir, A., Mocan, H., Sanjad, S. A., Rodriguez-Soriano, J., Santos, F., Cremers, C. W., Di Pietro, A., Hoffbrand, B. I., Winiarski, J., Bakkaloglu, A., Ozen, S., Dusunsel, R., Goodyer, P., Hulton, S. A., Wu, D. K., Skvorak, A. B., Morton, C. C., Cunningham, M. J., Jha, V., and Lifton, R. P. (1999). Mutations in the gene encoding B1 subunit of H⁺-ATPase cause renal tubular acidosis with sensorineural deafness. *Nat Genet* 21:84-90.
- Kelley, M. W., Ochiai, C. K., and Corwin, J. T. (1992). Maturation of kinocilia in amphibian hair cells: growth and shortening related to kinociliary bulb formation. *Hear Res* 59:108-115.
- Kennedy, H. J., Crawford, A. C., and Fettiplace, R. (2005). Force generation by mammalian hair bundles supports a role in cochlear amplification. *Nature* 433:880-883.
- Kennedy, H. J., Evans, M. G., Crawford, A. C., and Fettiplace, R. (2003). Fast adaptation of mechanoelectrical transducer channels in mammalian cochlear hair cells. *Nat Neurosci* 6:832-836.
- Kim, E., DeMarco, S. J., Marfatia, S. M., Chishti, A. H., Sheng, M., and Strehler, E. E. (1998). Plasma membrane Ca²⁺ ATPase isoform 4b binds to membrane-associated guanylate kinase (MAGUK) proteins via their PDZ (PSD-95/Dlg/ZO-1) domains. *J Biol Chem* 273:1591-1595.
- Kim, J., Chung, Y. D., Park, D. Y., Choi, S., Shin, D. W., Soh, H., Lee, H. W., Son, W., Yim, J., Park, C. S., Kernan, M. J., and Kim, C. (2003). A TRPV family ion channel required for hearing in *Drosophila*. *Nature* 424:81-84.
- Koyama, H., Lewis, E. R., Leverenz, E. L., and Baird, R. A. (1982). Acute seismic sensitivity in the bullfrog ear. *Brain Res* 250:168-172.

- Kozel, P. J., Friedman, R. A., Erway, L. C., Yamoah, E. N., Liu, L. H., Riddle, T., Duffy, J. J., Doetschman, T., Miller, M. L., Cardell, E. L., and Shull, G. E. (1998). Balance and hearing deficits in mice with a null mutation in the gene encoding plasma membrane Ca^{2+} -ATPase isoform 2. *J Biol Chem* 273:18693-18696.
- Lenoir, M. (1998). Promenade 'round the cochlea. www.iurcmontpinsermfr/cric/audition/english/indexhtm
- Liberman, M. C., Gao, J., He, D. Z., Wu, X., Jia, S., and Zuo, J. (2002). Prestin is required for electromotility of the outer hair cell and for the cochlear amplifier. *Nature* 419:300-304.
- Lumpkin, E. A., and Hudspeth, A. J. (1995). Detection of Ca^{2+} entry through mechanosensitive channels localizes the site of mechanoelectrical transduction in hair cells. *Proc Natl Acad Sci U S A* 92:10297-10301.
- Lumpkin, E. A., and Hudspeth, A. J. (1998). Regulation of free Ca^{2+} concentration in hair-cell stereocilia. *J Neurosci* 18:6300-6318.
- Marmo, F., Balsamo, G., and Franco, E. (1983). Calcite in the statoconia of amphibians: a detailed analysis in the frog *Rana esculenta*. *Cell Tissue Res* 233:35-43.
- Martin, P., Bozovic, D., Choe, Y., and Hudspeth, A. J. (2003). Spontaneous oscillation by hair bundles of the bullfrog's sacculus. *J Neurosci* 23:4533-4548.
- Martin, P., and Hudspeth, A. J. (1999). Active hair-bundle movements can amplify a hair cell's response to oscillatory mechanical stimuli. *Proc Natl Acad Sci U S A* 96:14306-14311.
- Meyer, J., Furness, D. N., Zenner, H. P., Hackney, C. M., and Gummer, A. W. (1998). Evidence for opening of hair-cell transducer channels after tip-link loss. *J Neurosci* 18:6748-6756.

- Miyazaki, E., Sakaguchi, M., Wakabayashi, S., Shigekawa, M., and Mihara, K. (2001). NHE6 protein possesses a signal peptide destined for endoplasmic reticulum membrane and localizes in secretory organelles of the cell. *J Biol Chem* 276:49221-49227.
- Montcouquiol, M., Rachel, R. A., Lanford, P. J., Copeland, N. G., Jenkins, N. A., and Kelley, M. W. (2003). Identification of Vangl2 and Scrb1 as planar polarity genes in mammals. *Nature* 423:173-177.
- Mroz, E. A., and Lechene, C. (1993). Extracellular N-methyl-D-glucamine leads to loss of hair-cell sodium, potassium, and chloride. *Hear Res* 70:146-150.
- Nakamura, N., Tanaka, S., Teko, Y., Mitsui, K., and Kanazawa, H. (2005). Four Na⁺/H⁺ exchanger isoforms are distributed to Golgi and post-Golgi compartments and are involved in organelle pH regulation. *J Biol Chem* 280:1561-1572.
- Nauli, S. M., Alenghat, F. J., Luo, Y., Williams, E., Vassilev, P., Li, X., Elia, A. E., Lu, W., Brown, E. M., Quinn, S. J., Ingber, D. E., and Zhou, J. (2003). Polycystins 1 and 2 mediate mechanosensation in the primary cilium of kidney cells. *Nat Genet* 33:129-137.
- Noben-Trauth, K., Zheng, Q. Y., Johnson, K. R., and Nishina, P. M. (1997). mdw: a deafness susceptibility locus that interacts with deaf waddler (dfw). *Genomics* 44:266-272.
- Numata, M., and Orlowski, J. (2001). Molecular cloning and characterization of a novel (Na⁺,K⁺)/H⁺ exchanger localized to the trans-Golgi network. *J Biol Chem* 276:17387-17394.
- Numata, M., Petrecca, K., Lake, N., and Orlowski, J. (1998). Identification of a mitochondrial Na⁺/H⁺ exchanger. *J Biol Chem* 273:6951-6959.

- O'Hagan, R., Chalfie, M., and Goodman, M. B. (2005). The MEC-4 DEG/ENaC channel of *Caenorhabditis elegans* touch receptor neurons transduces mechanical signals. *Nat Neurosci* 8:43-50.
- Orlowski, J., and Grinstein, S. (2004). Diversity of the mammalian sodium/proton exchanger SLC9 gene family. *Pflugers Arch* 447:549-565.
- Orlowski, J., and Grinstein, S. (1997). Na⁺/H⁺ exchangers of mammalian cells. *J Biol Chem* 272:22373-22376.
- Pickles, J. O., Comis, S. D., and Osborne, M. P. (1984). Cross-links between stereocilia in the guinea pig organ of Corti, and their possible relation to sensory transduction. *Hearing Res* 15:103-112.
- Pickles, J. O., and Corey, D. P. (1992). Mechanoelectrical transduction by hair cells. *Trends Neurosci* 15:254-259.
- Puopolo, K., Kumamoto, C., Adachi, I., Magner, R., and Forgac, M. (1992). Differential expression of the "B" subunit of the vacuolar H(+)-ATPase in bovine tissues. *J Biol Chem* 267:3696-3706.
- Rabon, E. C., and Reuben, M. A. (1990). The mechanism and structure of the gastric H,K-ATPase. *Annu Rev Physiol* 52:321-344.
- Reinhardt, T. A., Filoteo, A. G., Penniston, J. T., and Horst, R. L. (2000). Ca(2+)-ATPase protein expression in mammary tissue. *Am J Physiol Cell Physiol* 279:C1595-602.
- Reinhardt, T. A., and Horst, R. L. (1999). Ca²⁺-ATPases and their expression in the mammary gland of pregnant and lactating rats. *Am J Physiol* 276:C796-802.
- Reinhardt, T. A., Lippolis, J. D., Shull, G. E., and Horst, R. L. (2004). Null mutation in the gene encoding plasma membrane Ca²⁺-ATPase isoform 2 impairs calcium transport into milk. *J Biol Chem* 279:42369-42373.

- Ricci, A., Crawford, A. C., and Fettiplace, R. (2003). Tonotopic variation in the conductance of the hair cell mechanotransducer channel. *Neuron* 40:983-990.
- Ricci, A. J., Crawford, A. C., and Fettiplace, R. (2000). Active hair bundle motion linked to fast transducer adaptation in auditory hair cells. *J Neurosci* 20:7131-7142.
- Ricci, A. J., and Fettiplace, R. (1997). The effects of calcium buffering and cyclic AMP on mechano-electrical transduction in turtle auditory hair cells. *J Physiol (Lond)* 501:111-124.
- Ricci, A. J., Wu, Y. C., and Fettiplace, R. (1998). The endogenous calcium buffer and the time course of transducer adaptation in auditory hair cells. *J Neurosci* 18:8261-8277.
- Ricci, A. J., Crawford, A. C., and Fettiplace, R. (2002). Mechanisms of active hair bundle motion in auditory hair cells. *J Neurosci* 22:44-52.
- Rizzolo, L. J. (1999). Polarization of the Na⁺, K(+)-ATPase in epithelia derived from the neuroepithelium. *Int Rev Cytol* 185:195-235.
- Rusch, A., and Thurm, U. (1989). Cupula displacement, hair bundle deflection, and physiological responses in the transparent semicircular canal of young eel. *Pflugers Arch* 413:533-545.
- Rzadzinska, A. K., Schneider, M. E., Davies, C., Riordan, G. P., and Kachar, B. (2004). An actin molecular treadmill and myosins maintain stereocilia functional architecture and self-renewal. *J Cell Biol* 164:887-897.
- Sagne, C., Isambert, M. F., Henry, J. P., and Gasnier, B. (1996). SDS-resistant aggregation of membrane proteins: application to the purification of the vesicular monoamine transporter. *Biochem J* 316:825-831.
- Sakagami, M., Fukazawa, K., Matsunaga, T., Fujita, H., Mori, N., Takumi, T., Ohkubo, H., and Nakanishi, S. (1991). Cellular localization of rat Isk protein in the stria vascularis by immunohistochemical observation. *Hear Res* 56:168-172.

- Sakaguchi, N., Crouch, J. J., Lytle, C., and Schulte, B. A. (1998). Na-K-Cl cotransporter expression in the developing and senescent gerbil cochlea. *Hear Res* 118:114-122.
- Salvador, J. M., Inesi, G., Rigaud, J. L., and Mata, A. M. (1998). Ca^{2+} transport by reconstituted synaptosomal ATPase is associated with H^{+} countertransport and net charge displacement. *J Biol Chem* 273:18230-18234.
- Schneider, M. E., Belyantseva, I. A., Azevedo, R. B., and Kachar, B. (2002). Rapid renewal of auditory hair bundles. *Nature* 418:837-838.
- Schulte, B. A., and Adams, J. C. (1989). Distribution of immunoreactive $\text{Na}^{+},\text{K}^{+}$ -ATPase in gerbil cochlea. *J Histochem Cytochem* 37:127-134.
- Shi, X., Gillespie, P. G., and Nuttall, A. L. (2005). Na^{+} influx triggers bleb formation on inner hair cells. *Am J Physiol Cell Physiol*
- Sidi, S., Friedrich, R. W., and Nicolson, T. (2003). NompC TRP channel required for vertebrate sensory hair cell mechanotransduction. *Science* 301:96-99.
- Siemens, J., Lillo, C., Dumont, R. A., Reynolds, A., Williams, D. S., Gillespie, P. G., and Muller, U. (2004). Cadherin 23 is a component of the tip link in hair-cell stereocilia. *Nature* 428:950-955.
- Sollner, C., Rauch, G. J., Siemens, J., Geisler, R., Schuster, S. C., Muller, U., and Nicolson, T. (2004). Mutations in cadherin 23 affect tip links in zebrafish sensory hair cells. *Nature* 428:955-959.
- Stankovic, K. M., Brown, D., Alper, S. L., and Adams, J. C. (1997). Localization of pH regulating proteins H^{+} -ATPase and $\text{Cl}^{-}/\text{HCO}_3^{-}$ exchanger in the guinea pig inner ear. *Hear Res* 114:21-34.
- Stauffer, T. P., Guerini, D., and Carafoli, E. (1995). Tissue distribution of the four gene products of the plasma membrane Ca^{2+} pump. *J Biol Chem* 270:12184-12190.

- Stopp, P. E. (1983). Effects on guinea pig cochlea from exposure to moderately intense broad-band noise. *Hear Res* 11:55-72.
- Stover, E. H., Borthwick, K. J., Bavalia, C., Eady, N., Fritz, D. M., Rungroj, N., Giersch, A. B., Morton, C. C., Axon, P. R., Akil, I., Al-Sabban, E. A., Baguley, D. M., Bianca, S., Bakkaloglu, A., Bircan, Z., Chauveau, D., Clermont, M. J., Guala, A., Hulton, S. A., Kroes, H., Li Volti, G., Mir, S., Mocan, H., Nayir, A., Ozen, S., Rodriguez Soriano, J., Sanjad, S. A., Tasic, V., Taylor, C. M., Topaloglu, R., Smith, A. N., and Karet, F. E. (2002). Novel ATP6V1B1 and ATP6V0A4 mutations in autosomal recessive distal renal tubular acidosis with new evidence for hearing loss. *J Med Genet* 39:796-803.
- Strassmaier, M., and Gillespie, P. G. (2002). The hair cell's transduction channel. *Curr Opin Neurobiol* 12:380-386.
- Street, V. A., McKee-Johnson, J. W., Fonseca, R. C., Tempel, B. L., and Noben-Trauth, K. (1998). Mutations in a plasma membrane Ca^{2+} -ATPase gene cause deafness in deafwaddler mice. *Nat Genet* 19:390-394.
- Sunose, H., Ikeda, K., Suzuki, M., and Takasaka, T. (1994). Voltage-activated K channel in luminal membrane of marginal cells of stria vascularis dissected from guinea pig. *Hear Res* 80:86-92.
- Takahashi, K., and Kitamura, K. (1999). A point mutation in a plasma membrane $\text{Ca}(2+)$ -ATPase gene causes deafness in Wriggle Mouse Sagami. *Biochem Biophys Res Commun* 261:773-778.
- van Hille, B., Richener, H., Schmid, P., Puettnner, I., Green, J. R., and Bilbe, G. (1994). Heterogeneity of vacuolar $\text{H}(+)$ -ATPase: differential expression of two human subunit B isoforms. *Biochem J* 303:191-198.
- Vetter, D. E., Mann, J. R., Wangemann, P., Liu, J., McLaughlin, K. J., Lesage, F., Marcus, D. C., Lazdunski, M., Heinemann, S. F., and Barhanin, J. (1996). Inner ear defects induced by null mutation of the *isk* gene. *Neuron* 17:1251-1264.

- Walker, R. G., Hudspeth, A. J., and Gillespie, P. G. (1993). Calmodulin and calmodulin-binding proteins in hair bundles. *Proc Natl Acad Sci U S A* 90:2807-2811.
- Walker, R. G., Willingham, A. T., and Zuker, C. S. (2000). A *Drosophila* mechanosensory transduction channel. *Science* 287:2229-2234.
- Wangemann, P. (1995). Comparison of ion transport mechanisms between vestibular dark cells and strial marginal cells. *Hear Res* 90:149-157.
- Wangemann, P. (2002a). K(+) cycling and its regulation in the cochlea and the vestibular labyrinth. *Audiol Neurotol* 7:199-205.
- Wangemann, P. (2002b). K⁺ cycling and the endocochlear potential. *Hear Res* 165:1-9.
- Wangemann, P., Liu, J., and Marcus, D. C. (1995). Ion transport mechanisms responsible for K⁺ secretion and the transepithelial voltage across marginal cells of stria vascularis in vitro. *Hear Res* 84:19-29.
- Wingo, C. S., and Cain, B. D. (1993). The renal H-K-ATPase: physiological significance and role in potassium homeostasis. *Annu Rev Physiol* 55:323-347.
- Wu, Y. C., Ricci, A. J., and Fettiplace, R. (1999). Two components of transducer adaptation in auditory hair cells. *J Neurophysiol* 82:2171-2181.
- Xu, H., Chen, R., and Ghishan, F. K. (2005). Subcloning, localization and expression of the rat intestinal sodium-hydrogen exchanger isoform 8 (NHE-8). *Am J Physiol Gastrointest Liver Physiol*
- Yamoah, E. N., Lumpkin, E. A., Dumont, R. A., Smith, P. J., Hudspeth, A. J., and Gillespie, P. G. (1998). Plasma membrane Ca²⁺-ATPase extrudes Ca²⁺ from hair cell stereocilia. *J Neurosci* 18:610-624.
- Yeoman, M. S., Brezden, B. L., and Benjamin, P. R. (1999). LVA and HVA Ca(2+) currents in ventricular muscle cells of the *Lymnaea* heart. *J Neurophysiol* 82:2428-2440.

- Zhao, Y., Yamoah, E. N., and Gillespie, P. G. (1996). Regeneration of broken tip links and restoration of mechanical transduction in hair cells. *Proc Natl Acad Sci U S A* 93:15469-15474.
- Zheng, J., Shen, W., He, D. Z., Long, K. B., Madison, L. D., and Dallos, P. (2000a). Prestin is the motor protein of cochlear outer hair cells. *Nature* 405:149-155.
- Zheng, L., Sekerkova, G., Vranich, K., Tilney, L. G., Mugnaini, E., and Bartles, J. R. (2000b). The deaf jerker mouse has a mutation in the gene encoding the espin actin-bundling proteins of hair cell stereocilia and lacks espins. *Cell* 102:377-385.
- Zvaritch, E., James, P., Vorherr, T., Falchetto, R., Modyanov, N., and Carafoli, E. (1990). Mapping of functional domains in the plasma membrane Ca^{2+} pump using trypsin proteolysis. *Biochemistry* 29:8070-8076.